UNIVERSITY OF CALIFORNIA

Santa Barbara

Modeling Spatial and Temporal Patterns in Flow and Sediment Transport and Storage in Large, Lowland Rivers

A dissertation submitted in partial satisfaction of the

Requirements for the degree of Doctor of Philosophy

in Environmental Science and Management

by

Michael David Singer

Committee in Charge

Professor Thomas Dunne, Chair

Professor James Frew

Professor Edward Keller

June 2003

This dissertation of Michael David Singer is approved.

_____

Thomas Dunne

_____

James Frew

_____

Edward Keller

June 2003

Modeling Spatial and Temporal Patterns in Flow and Sediment Transport and Storage in Large, Lowland Rivers

ACKNOWLEDGEMENTS

I would like to thank all those who inspired, encouraged, and assisted me over the last six years. Prominent on this list is Tom Dunne, who rescued me from a life of rock grinding and subsequently developed my skills of critique, inquiry, and writing, and supported me tirelessly in many capacities. And thanks to my dissertation committee, who presented me with difficult questions and challenged me to dig deeper. I also want to acknowledge various colleagues who have (informally) taught and influenced me. I want to thank my Santa Barbara lab mates for great discussions, reviews, and for creating a good atmosphere for learning, growing, and having fun: Doug Alsdorf, Andy Ballantine, Trent Biggs, Setenay Bozkurt, Manny Gabet, Daniel Malmon, Simon Mudd, Brad Newton, and Liz Safran. Liz, thanks for giving me the opportunity to work with and learn from you. Thanks also go to my Berkeley colleagues, who let me be a part of their geomorphology group. Notable among these folks is John Stock, who has helped to enrich me with his valuable field insights and to round out my view of geomorphology. Leonard Sklar also deserves acknowledgement for useful conversations about sediment transport. And I owe large dose of gratitude to Bill Dietrich for allowing me to function within the Earth and Planetary Science department at UC Berkeley as a civilized member of the geomorphology group with all the benefits of membership.

I also want to thank the various teachers who have contributed to my edification and to my expertise for producing this document. Thanks go to Uncle Richard and Mr. Krause for fostering my scientific skills, Paul Butler for initiating

my formal education in earth science, Nalini Nadkarni for introducing me to scientific research, and various graduate school professors for getting me up to speed in geology, hydrology, and geomorphology. The standouts include Tanya Atwater, Art Sylvester, Bill Dietrich, and, of course, Tom Dunne. Tom, your small-group courses and evening seminars represent the pinnacle of my educational experience.

I want to thank my family and friends, who have supported me throughout this period, despite not understanding what it is that I do. In addition to all my aunts, uncles, and cousins, I want to specifically thank Mom, Dad, Randy, Earl, and Claudia. Randy, thanks for your statistical assistance. Thank you Charley and Mario, for inadvertently initiating what has become a magical journey. Thanks Jeff for giving me a consistent home-away-from-home during my spells in Santa Barbara.

I also owe my gratitude to various agency, non-profit, and university contacts that facilitated my acquisition of data for, access to, and conversations about the Sacramento basin. These include Koll Buer, Tanya Ehorn, Dwight Russell, Robert Yoha, Pat Huckaby, Jason Schwenkler, Mike Salvador, Pat Schiffer, Al Asquith, Stacy Cepello, Russ Eckman, Ken Dickerson, Jim Edwards, Joel Ferias, Mike Roberts, Greg Golet, Joe Silveira, Marti Ikehara, Eric Larsen, Lisa Micheli, Larry Lee, Karl Malamud-Roam, Bob Meade, John Milliman, Mike Harvey, Allen Molenofsky, Shawn Pike, Lee Price, Bruce Ross, Paul Sankey, Stu Shaner, Dave Schoelhammer, Ed Sing, Larry Smith, Moshen Tavana, Don Twiss, John Elko, James DeStaso, and Jeff Harris.

Finally, I acknowledge the funding I received throughout the years of my Ph.D. from UCSB, the Bren School, NASA, and CALFED. Without these financial resources, none of this would have been possible.

This dissertation is dedicated to the Sacramento River Valley.

"But you did not see the Sacramento Valley as I saw it. Perhaps you never saw a spot of earth so beautiful that the love of it would take you from … [the] mining excitement … of 1849 and cause you to settle down and turn a deaf ear to all the stories of … fortunes made."
Will S. Green

"The banks of the river, something over 20 feet high, were lined on both sides with willows, grape vines, etc. clean down to the water's edge, while upon the banks were tall oaks, sycamore, ash, and cottonwood. Some of those monster trees hung out over the stream, as if to dispute the passage of the advance guard of civilization." **Will S. Green**

"The basins and deltas were characterized by giant tules, said to be ten to fifteen feet high, so that a man on horseback could not be seen in them." **Joseph A. McGowan**

"... we seldom or never were out of sight of game, deer, elk, antelope, and grizzly bear."
John Bidwell

"The year of the Gold Rush ended with heavy rains and floods in the valley, providing evidence that ... Sacramento was located on low land. But it was too late to change the location of the supply base for northern California. Hundreds of thousands of dollars had already been invested in Sacramento and the city was firmly established." **Joseph A. McGowan**

"I came down the river in December, 1852, when the sheet of water covering the country was fifty miles broad." **Lieutenant R.S. Williamson**

"... a large part of this (valley) is undoubtedly barren and unproductive, and must forever remain so. That part that is deemed good soil is inundated annually, not for any great length of time, yet sufficiently long to make it unfit for advantageous settlement." **Lieutenant Charles Wilkes**

"… after the discovery of gold in the Sierra foothills it was but a matter of time until the great potential of this flat-floored topographical oddity was recognized." **Elna Bakker**

"For the better part of the next several generations, embattled farmers and townspeople struggled to get control of their river system so they might live in safety on the Valley floor and put its rich soils to the plow." **Robert Kelley**

"The grass-rich stretches of the great Central Valley are [now], for the most part, lost to orchards and vineyards, cotton and alfalfa fields. Many miles of curving green ribbon along its water courses have been eradicated, replaced by the sterile concrete of flood control and navigation channels." **Elna Bakker**

"No more the long tarrying of floodwaters on the Valley floor for months on end, forming the inland sea; it is a brisk and disciplined passage now to Suisun Bay." **Robert Kelley**

VITA OF MICHAEL DAVID SINGER

June 2003

EDUCATION

University of California, Santa Barbara, CA
Ph.D., Environmental Science and Management, 2003
Advisor: Thomas Dunne

The Evergreen State College, Olympia, WA
B.A. Environmental Science, 1993

Tulane University, New Orleans, LA
Major: Political Science-International Relations

PUBLICATIONS

2003 Singer, M.B. and Dunne, T. Modeling long-term bed-material flux based on stochastic hydrology. In review.
2002 Singer, M.B. and Dunne, T. An empirical-stochastic, event-based model for simulating inflow from a tributary network: Theoretical framework and application to the Sacramento River basin, California. In review.

2001 Singer, M.B. and Dunne, T. Identifying eroding and depositional reaches of valley by analysis of suspended-sediment transport in the Sacramento River, California. *Water Resources Research*, 37(12):3371-3382.

HONORS AND AWARDS

2002	Dissertation Fellowship, *UCSB Graduate Division*
2001	Space Grant Graduate Fellowship, *UCSB Cal Space Institute Center for Excellence*
2001	Grant for Young Geomorphologists, *International Association of Geomorphologists*
2000	Science and Engineering Research Grant, *UCSB Graduate Division*
1999	Dozier Fellowship, *Donald Bren School of Environmental Science and Management*
1999-2001	Dean's Advisory Council Representative, *Donald Bren School of Environmental Science and Management*

FIELDS OF STUDY

Fluvial geomorphology, hydrology, hydroclimatology, sediment transport, restoration science.

ABSTRACT

Modeling Spatial and Temporal Patterns in Flow and Sediment Transport and Storage in Large, Lowland Rivers

by

Michael David Singer

Spatial and temporal patterns of sediment transport and storage control the distribution and condition of aquatic and riparian habitats in large, lowland rivers. These patterns in transport and storage are predicted by coupling hydrology with sediment transport data and models in the Sacramento basin. The predictions are used to assess river rehabilitation strategies that have been proposed to increase the distribution and improve the condition of habitats in the mainstem Sacramento. Empirical time series models of streamflow and suspended sediment concentration are developed to assess historical patterns in suspended sediment transport and storage since the construction of major dams. A model of stochastic hydrology is created to predict inflow to the mainstem from major tributaries based on basin-wide hydroclimatology. The model is applied to the Sacramento to simulate pre- and post-dam flow, detect bed level change, and assess the viability of riparian forest restoration. A method is devised for computing spatial and temporal patterns of bed-material transport and storage by combining stochastic hydrology with sediment transport equations calibrated to data from the Sacramento basin. This method is used to assess the impact of three major river rehabilitation strategies: gravel

augmentation to benefit salmonid spawning habitat, levee setbacks to re-create floodplain corridors, and flow alteration to restore an array of disrupted geomorphic processes and environmental cues. The models of suspended sediment transport suggest the influence of humans and tectonics on spatial storage patterns. The stochastic hydrology model corroborates predicted erosion in one river reach that may be undergoing bed degradation, and it suggests that riparian forest restoration is not viable at one floodplain location without flow alteration. The method for computing bed-material transport predicts large divergences, or imbalances, in sediment storage throughout the Sacramento River. These imbalances in bed-material storage are generally reduced following the implementation of three river rehabilitation strategies. The models may be applied by agencies and managers to anticipate the first-order impacts of large-scale river rehabilitation over a period of decades.

TABLE OF CONTENTS

LIST OF FIGURES

LIST OF TABLES

INTRODUCTION

The probability distribution of sediment transport throughout a river channel network is primarily forced by the spatial and temporal variability in streamflow, sediment supply, and sediment grain sizes in the riverbed. The magnitude and frequency of sediment delivery to and transport through a river channel, in turn, control spatial and temporal patterns of sediment storage. Sediment transport and storage patterns in river reaches generally dictate the spatial distribution (e.g. locations of suitable spawning substrate) and condition (e.g. frequency of nutrient-rich overbank flows) of riverine aquatic and riparian habitats. These processes are the subject of fluvial geomorphology, which therefore has something to contribute to the problem of conserving and rehabilitating riverine habitats. In particular, modeling the variability in the factors that force sediment transport may be used to assess spatial and temporal patterns in bed mobility, erosion and deposition, and their relevance to conditions of riverine habitat throughout a fluvial system. The purpose of this dissertation is to: 1) develop modeling capability for analyzing decadal patterns in sediment transport and storage resulting from the variability in the factors that force sediment transport and 2) model the influence of major rehabilitation strategies that have been proposed to improve the state of riverine habitats.

Species in aquatic and riparian habitats have adapted over millennia to the relationship between flow, sediment movement, and its organization in riverbeds, banks, and floodplains. However, physical conditions along large, lowland fluvial systems have been so altered by river valley development in the last century that

native species in aquatic and riparian habitats have not been able to adapt. Mineral extraction, gravel and sand mining, agricultural 'reclamation' of floodplains, and dam and levee construction have degraded habitats for native species and contributed to their decline.

Public opinion has recently placed more value on aquatic and riparian habitats relative to other activities in channels and floodplains. Governments have begun to fund large-scale 'restoration' projects along major waterways including the Sacramento River in California, the Kissimmee River in Florida, and the Lower Danube River in Romania, to rehabilitate riverine ecosystems by manipulating the physical forcing conditions so that they more closely resemble their former state. Proposed measures for large-scale rehabilitation involve: flow alteration below dams, removal or setting back of flood levees, rescaling channels to new flood regimes, augmenting the supply of selected sediment grain sizes, and reestablishing native vegetation on floodplains. It is hoped that these strategies will recreate the physical conditions necessary for the revival and sustainability of aquatic and riparian habitats and the species they support. However, there are few analytical tools currently available for assessing various management strategies.

Current practice in implementing physical rehabilitation strategies relies on design modeling approaches that use steady-state hydrologic regimes and sediment supplies and thus predict deterministic outcomes. Implemented projects are monitored to determine success or failure and to guide future implementation plans in other river locations. However, there are currently no developed methods for

assessing the risk of outcomes resulting from a particular strategy or combination of strategies throughout a fluvial system before they are actually implemented.

In this dissertation I develop a set of practical, analytical tools for assessing spatial and temporal patterns in sediment transport and storage under conditions that are realistically variable. The tools allow calculation of the risk of implementing river rehabilitation strategies. I develop these tools using data from the Sacramento River basin and apply them to predict the likely impact of proposed rehabilitation strategies on habitat conditions throughout the Sacramento River over a period of decades.

I focus on transport and storage of riverbed sediments because they represent the most fundamental physical controls on riverine habitat distribution and condition. The intersection between streamflow and riverbed sediments in the aquatic environment, for example, determines the availability of gravels for salmonid spawning, depth of flow over (and thus the temperature within) a spawning redd, and the presence of fine sediment, which can hamper embryo growth. In the riparian environment, the interplay between floods and bed level controls overbank flow, for example, which moistens and fertilizes floodplains for vegetation recruitment, exchanges nutrients, and generally sustains riparian habitats.

I develop a stochastic model of streamflow that drives sediment transport equations calibrated to local bedload transport rates and bed-material grain size distributions to predict magnitude and frequency of sediment transport and storage. Multiple model simulations produce a range of potential output data that can be

statistically analyzed to calculate the probability distribution of expected and extreme conditions. I alter modeling constants within the stochastic framework to reflect proposed management strategies and assess the risk of their potential impact on physical conditions within Sacramento River reaches.

Chapter 1 is an empirical study designed to identify spatial patterns of suspended sediment movement and disposition in the main channels of the Sacramento River basin. The analysis employs time series methods to relate historical streamflow to sediment concentration at a number of gauging stations along the mainstem Sacramento and its tributaries. I use these models to compute suspended sediment transport into and through the mainstem and to identify net suspended sediment storage in ~60 km river reaches for recent decades.

Chapter 2 describes a stochastic hydrology model designed to simulate inflow to the mainstem of a large river from its tributaries. The model enables probabilistic prediction of sediment transport, for example, in response to rehabilitation strategies. It samples historical flood events from tributary gauging stations according to spatial and temporal patterns in these data. It simulates daily inflow to the mainstem from each major tributary. I apply this model to the Sacramento River basin, routing these inflows through the mainstem using standard flood routing software to produce decadal flow hydrographs at mainstem locations. The probability distributions of the routed flows are compared with those of observed flow. I demonstrate the utility of the model with applications in detecting bed level change and assessing riparian vegetation restoration.

Chapter 3 couples the stochastic streamflow model with bed-material flux calculations to assess sediment transport and storage patterns in the Sacramento River over a period of decades. I modify an existing sediment transport equation to incorporate a threshold for sediment transport that may vary by cross section and to predict fractional bed-material transport rates (i.e. rates computed by grain size). I also re-calibrate this equation to bedload datasets from the Sacramento and other fluvial environments. The calibration results in a generalized equation that can be applied to predict transport for any cross section where bed-material grain size distributions are available. I use these models to compute bed-material transport into and through the mainstem and to assess peak and decadal patterns in: 1) bed-material load at cross sections spaced ~60 km apart and 2) net accumulation in the reaches between them.

Chapter 4 uses the methods developed in Chapters 2 and 3 to assess the long-term impact of three rehabilitation strategies on bed-material flux and storage change in the Sacramento River. I examine the impact of flow alteration, gravel augmentation, and flood control levee setbacks on bed-material flux because it is a primary indicator of the distribution and condition of riverine habitats.

CHAPTER 1. IDENTIFYING ERODING AND DEPOSITIONAL REACHES OF VALLEY BY ANALYSIS OF SUSPENDED-SEDIMENT TRANSPORT IN THE SACRAMENTO RIVER, CALIFORNIA

(Portions of this chapter were published in *Water Resources Research*, 37(12):3371-3381, 2001)

Abstract

Spatial patterns in suspended sediment transport and storage along the Sacramento River were assessed by evaluating the suspended sediment budget for the main channel accounting for all tributaries and diversions. Time series analysis was employed to quantify the relationship between streamflow and suspended sediment concentration for gauging stations along the main channel and signature tributaries. Sediment concentration records (of 2 yr duration) were extended using Box-Jenkins transfer function models to calculate annual rates of suspended sediment discharge over a 32 yr period since dam construction on the Sacramento River. The suspended sediment budget was evaluated to identify reaches of net erosion or deposition. The results of the budget suggest the influence of tectonics and anthropogenic channel modification.

Introduction

The morphology of a river is determined by the interaction of water and sediment within a channel network as the river deposits and re-mobilizes sediment along its valley floor. The mass balance resulting from these transport processes indicates the accumulation and removal of sediment, and in turn determines the channel and floodplain morphology, which are reflected in flood conveyance capacity, stability of natural and engineered river courses, and the complexity of river channel and riparian habitat [*Dunne*, 1988; *Kondolf and Wolman*, 1993; *Kondolf*, 1995b; *Kondolf*, 1995a]. This paper reports an empirical investigation of decadal patterns in the disposition of suspended sediment in the channel and valley floor of the Sacramento River system.

In the last 150 years the Sacramento River has been the object of a number of anthropogenic alterations including the delivery of hydraulic mining sediments, the emplacement of an extensive system of flood control levees, and the construction of dams on the mainstem and its tributaries. Although the impact of hydraulic mining sediments is still evident on one Sacramento tributary [*James*, 1991], its effect on the river bed of the lower Sacramento has long since passed [*Meade*, 1982]. However, other human modifications including artificial levees and bank protection, have been shown to have lasting effects on the sediment budget in fluvial systems [*Kesel et al.*, 1992]. The purpose of this study was to construct a suspended sediment budget for the Sacramento River valley over a recent period of decades since dam construction and to identify reaches and causes of net erosion or deposition.

Sources of Data

This study focuses on the analysis of suspended load which is calculated using sediment concentration data collected regularly by the United States Geological Survey (USGS) at their gauging stations. These data are collected, compiled, and processed by standardized procedures outlined in [*Guy and Norman*, 1970] and [*Porterfield*, 1972], and are published as daily mean concentrations in annual USGS Water Resources Data reports.

Suspended load error estimates inherent in USGS data collection and processing procedures have been estimated at 5% for the Colorado River and 20% for the Little Colorado River [*Topping et al.*, 2000]. I acknowledge that there may be a significant amount of uncertainty in these datasets, but they remain the best data available. I utilize USGS suspended sediment concentration and daily discharge data herein to develop time series models at various gauging points and subsequently to analyze decadal patterns in sediment transport.

Relating Discharge to Sediment Concentration

Annual loads of suspended sediment are usually computed from irregular, sparse measurements of sediment concentration, a relationship between concentration and water discharge determined by least-squares regression [*Leopold et al.*, 1964; *Loughran*, 1976], and a longer record of flow. Sediment-rating curves, as the regressions are called, have thus been used for predicting the sparsely-collected

variable, sediment concentration, based on the more frequently recorded one, streamflow. However, for a given value of flow in such a model, sediment concentration values may range over two orders of magnitude (Figure 1.1). Generally, this may be the result of hysteresis, caused by differences in sediment supply or hydraulics between rising and falling discharge, and/or of variability in rainstorm characteristics and drainage basin condition. In any case, the rating curve drastically underestimates many of the highest sediment concentration peaks (those assumed responsible for the majority of suspended sediment transport) and overestimate the sediment concentration of dilute flows, even after bias corrections (e.g. [*Ferguson*, 1986]) are made for the regression parameters.

Most importantly standard sediment-rating curves developed using data collected over a **regular** time interval (e.g. daily data) violate the assumption of independence and identical distributions in statistical regression, because the observed values of a particular variable are related to one another by time. Accordingly, each discharge-sediment concentration data pair will plot close to the previous pair. As a result, the residuals of this type of model will be serially correlated inducing bias in the estimation of regression parameters [*Neter et al.*, 1983]. This fact undermines the efficacy of the sediment-rating curve for assessing annual suspended sediment discharge and for making inferences on modes of sediment transport. Inadequacies of sediment-rating curves have been recognized by previous workers who have attempted to modify, analyze, or re-create them to account for the inconstancy in the relationship between sediment concentration and

discharge [*Heidel*, 1956; *Walling*, 1977; *Ferguson*, 1986; *Marcus*, 1989; *Williams*, 1989].

In addition, the rating curve is a static model that is unable to represent the changing, in-channel conditions of fluvial sediment arising during and between high flows. It is the structure and sequencing of these events that govern sediment transport over a period of decades. Thus, whether making long-term predictions of sediment discharge or attempting to gain insight into in-stream sediment transport processes, shortcomings in the rating curve technique make an alternative approach based on time series preferable where adequate data are available.

Previous applications of time-series analysis to concentration-discharge relationships have included modeling sediment yield [*Sharma et al.*, 1979; *Sharma and Dickinson*, 1980], analyzing the effect of drainage basin characteristics on suspended sediment transport [*Fitzgerald and Karlinger*, 1983; *Lemke*, 1991], and determining dominant variables controlling sediment concentration [*Rodriguez-Iturbe and Nordin*, 1968; *Goodwin and Denton*, 1991]. Employed in the present research context, this family of models (auto-regressive, moving average models, or ARIMA models) recognizes that discharge on a particular day is related to that of the previous day(s) and that sediment concentration is related to discharge on that day and previous days, as well as to previous values of sediment concentration. Such a model structure is consistent with field observations and theories of sediment supply and transport processes [*Lemke*, 1991]. Because time is included in the model structures,

there is no consistent under- or over-prediction as an artifact of hysteresis. Consequently, time-series model residuals are not serially correlated.

Basin Characteristics

The Sacramento River drains the northern part of the Central Valley of California and has a total drainage area of 6.8×10^4 km^2 comprising over one half of the total drainage area into the San Francisco Bay system [*Porterfield*, 1980]. It flows on a subsiding alluvial base that it has deposited as the surrounding mountains have been uplifted [*Bryan*, 1923]. The river drains the 96 km wide x 418 km long Sacramento Valley, a broad, alluvial, structurally-controlled lowland basin between the Sierra Nevada and the Coast Range [*Harwood and Helley*, 1987].

The river flows from its source near Mount Shasta through one structurally-controlled, incised reach (Sacramento Canyon), an entrenched, upland valley reach (hereafter referred to as the Redding Plain), and into another incised reach (Iron Canyon) on a bed of mixed gravel and sand [*Bryan*, 1923]. Downstream of Bend Bridge (Figure 1.2), the river enters the synclinal trough known as the Central Valley, where it assumes the character of an alluvial channel, alternating between active meandering, braided, and straight sections, building bars on an armored bed of coarse and medium gravel with a subarmor layer of coarse and medium sand. The channel lies between discontinuous high floodplain surfaces composed of fine sands, silts, and clays [*Brice*, 1977; *Water Engineering &Technology*, 1990]. Between Bend Bridge and Butte City (Figure 1.2) the riverbed is composed of coarse, medium, and fine

sand layers overlain by lobes of fine and medium gravels. The river becomes rapidly depleted of gravel in the low gradient reach upstream of Colusa (Figure 1.2) and transitions to a completely sandy bed between Knights Landing and Sacramento [*Water Engineering &Technology*, 1990]. Finally the Sacramento River enters the tidal zone at Sacramento [*Goodwin and Denton*, 1991].

The basin contains dams, levees, dikes, and gravel mining operations, which affect the geomorphic character of the river and its floodplain. In the 150 years since the discovery of gold in the Sierra Nevada, the Sacramento River valley has been transformed by agriculture and human settlement, and thus, by radical flood control policies intended to ensure the survival of these floodplain activities. The flood control system was designed to convey water and sediment as efficiently as possible through the mainstem Sacramento River using straightened channels and high levees built upon protected riverbanks to prevent overbank flooding and bank erosion, and therefore, lateral channel migration. To relieve pressure on the channel banks, flood waters overflow into two major flood bypasses, Sutter and Yolo, via a system of weirs which were constructed to convey water into existing lowland flood basins (Figures 1.2 and 1.3). These floodways divert water in high flows and provide multi-use zones of agriculture and habitat in drier seasons.

The Model

The model used in this research is the Box-Jenkins transfer function model (hereafter referred to as BJ), which in this case relates inputs of streamflow to outputs

of sediment concentration. The relationship between discharge and sediment concentration is a unidirectional one that can be modeled by a combination of moving average and autoregressive processes. Sediment concentration at time *t* (days) is a function of discharge on that day and previous days (a moving average process, referred to below as MA), as well as a function of sediment concentration on earlier days (an autoregressive process, referred to below as AR). The moving average terminology is misleading, but it is in common use [*Box and Jenkins*, 1994] and therefore employed here. To illustrate a practical BJ example, a mixed model (i.e. both second order MA **and** AR terms) can be represented in algebraic notation:

$$Cs_t - \delta_1 Cs_{t-1} - \delta_2 Cs_{t-2} = \omega_0 Q_t - \omega_1 Q_{t-1} - \omega_2 Q_{t-2} \qquad (1)$$

where Cs_t is the output sediment concentration at time *t* in days; Q is the input stream discharge at time *t-z* where *z* represents a backwards time lag; δ_r is the AR operating on previous values of sediment concentration where *r* is the order of the AR (in this case r = 2, indicating a second-order AR); and ω_s is the MA operating on current and previous values of discharge where *s* is the order of the MA (in this case s = 2, indicating a second-order MA). Solving for Cs_t gives sediment concentration on a particular day as a function of discharge on that day and the previous two days, as well as of sediment concentration on the previous two days. This same model can be written using the backshift operator notation:

$$(1-\delta_1 B-\delta_2 B^2)Cs_t = (\omega_0 - \omega_1 B - \omega_2 B^2)\,Q_t \qquad (2)$$

In this case, B is the backshift operator such that $B^z Q_t = Q_{t-z}$. The general BJ model then appears as:

$$Cs_t = \frac{\omega(B)}{\delta(B)} Q_{t-d} + e_t \qquad (3)$$

where $\omega(B) = (\omega_0 - \omega_1 B - \omega_2 B^2 - \ldots - \omega_s B^s)$ and $\delta(B) = (1 - \delta_1 B - \delta_2 B^2 - \ldots - \delta_r B^r)$; s and r are the orders of the MA and AR, respectively; ω_s and δ_r are the estimated model parameters; and e_t is a noise process at time t, which is independent of the input and can be represented as an ARIMA process [*Box and Jenkins*, 1994]. The d parameter represents a universal lag between the response of sediment concentration to fluctuations in discharge. The delay parameter d was found to be zero for all stations on the Sacramento, so it will be excluded from further discussion.

The first term on the right side of equation (3) is called the systematic term and contains a transfer function consisting of weighted parameters, which determine the extent to which Cs_t depends on previous Q_t values and previous Cs values. Numerator parameters $\omega(B)$, in this model represent MA, whereas denominator parameters $\delta(B)$, represent AR. If an estimated model results in a strictly autoregressive BJ model (only denominator parameters), sediment concentration on a

given day is predicted as a function of that day's discharge and sediment concentration from previous days. On the other hand, if an estimated model results in a strictly moving average BJ model (only numerator parameters), sediment concentration on a given day is predicted using only discharge values from that day and previous days, irrespective of previous conditions of sediment concentration (no memory). The other term in the BJ model is called the noise term and is modeled independently by an auto-regressive/moving average process similar to that mentioned for the systematic term. The noise term represents the model and measurement errors.

Success in estimating BJ model parameters necessitates that the sediment concentration-discharge data are collected with frequency high enough to capture rising and falling patterns. This frequency is reasonable in large river systems (e.g. Sacramento River) with daily mean concentrations, but in smaller, swifter river systems may require more frequent sampling. In such systems patterns of sediment concentration as a function of discharge may be obscured by daily mean concentration/discharge data. Nevertheless, I have used such data (the best published data) in model development to obtain sediment discharges for tributaries to the Sacramento River. Based on results for these models (see below) these tributaries are large enough to model using daily data.

Model Application

I employed BJ models to extend daily records of sediment concentration at six mainstem gauging stations and four tributary gauging stations (Figure 1.2) in order to calculate annual sediment discharge at each gauging point. I used this information to evaluate the suspended sediment budget in the mainstem Sacramento River in a 32 yr period since construction of Shasta Dam, and subsequently to identify mainstem river reaches of net erosion or deposition.

In this study I am providing a new level of insight into sediment transport in the Sacramento River, in the form of a suspended sediment budget. An earlier total-load budget for the Sacramento River channel [*US Army Corps of Engineers*, 1983] analyzed the effects of a proposed bank protection program on sources of sediment for a 19 yr period. The study utilized a combination of rating curves (i.e. stream discharge v. sediment discharge), a sediment routing model, and a priori assumptions to assess the relative importance of particular sediment sources in the system before and after project implementation. The results of the USACE study will not be compared to the results in this paper because the results of its computed suspended load are not reported independently of the total-load budget results.

Other studies have alluded to a long-term trend (decrease) in sediment discharge in the Sacramento River (e.g. [*Gilbert*, 1917]), but my test for stationarity over the 17 yr period (1963-1979) of continuous record at Sacramento revealed no temporal trend in annual suspended load ($R^2 = 0.095$, $p = 0.229$). This result corroborates that of another study, which found stationarity in the dataset [*Goodwin*, 1982].

Figure 1.4 shows the study reach of the mainstem Sacramento River, the mainstem gauging stations for which annual sediment discharge was calculated (triangles), the mainstem reaches that were evaluated for net erosion or deposition (boxed numbers), and the signature tributaries (defined below and indicated in color) used to calculate sediment discharge into the Sacramento from tributary sources.

Signature Tributaries

Very few continuous suspended sediment records exist for Sacramento River tributaries. Therefore, I estimated the sediment discharge from all tributaries draining a common geologic substrate using a single "signature" tributary. The Sacramento River tributaries flow from four primary geologic units (Figure 1.4, inset): the Modoc plateau, a volcanic lava flow in the northeast; the Sierra Nevada, a granitic batholith in the east; the Coast Range, a mélange of graywacke, shale, limestone, chert, and mafic rocks in the west; and the Trinity Mountains, a collection of granites and metavolcanic rocks in the northwest [*California Dept. of Water Resources*, 1994].

Each of these four units is assumed to represent a distinct sediment discharge signal based on geological substrate properties (relevant even in valley deposits below mountain fronts) and slope. Within each geologic unit the gauging station with the longest continuous record of flow and sediment concentration was designated as a signature station. Explanation of the use of signature stations to model sediment discharge follows (Sediment Budget Calculation).

Temporal Domain

I developed a suspended sediment budget for the water years 1948-1979, using sediment concentration data collected at ten gauging stations (6 mainstem, 4 tributary) between 1977 and 1979. The model for the Sacramento gauging station, however, was developed using 17 yr of continuous sediment concentration data that exist for this station. I first developed BJ models relating sediment concentration to discharge for this period and then simulated annual suspended sediment discharge for each mainstem and signature station over the 32 yr discharge domain common to all stations (i.e. WY 1948-1979). This method ensures the resulting sediment budget is consistent for all stations over the temporal modeling domain.

This 32-year period corresponds to the continuous historical daily hydrological record at the station of Sacramento used here as the hydrological domain of the study (the shortest hydrologic record common to all stations modeled). This period also coincides approximately with the time since the construction of Shasta Dam, the last known major perturbation on the mainstem. Although there have been other engineering projects in the basin since the dam was constructed in1945 (e.g. inter-basin water transfers, in-stream gravel mining, dam construction on tributaries) [*California Dept. of Water Resources*, 1994] their influence on the relationship between sediment concentration and discharge in the main channel is discounted as follows.

An inter-basin water transfer from Trinity River basin, which began in 1963, increased mean annual flow at Bend Bridge by 15%, but has had no significant

impact on flood flows [*California Dept. of Water Resources*, 1994], which dominate the transport of suspended sediment. Although the removal of gravel results in temporary suspension during mining operations, it would have minimal influence on bed material suspendibility by flow over the long-term. Dam construction on tributaries in the Sierra Nevada (e.g. Oroville Dam on Feather River) is assumed to have only a diffuse (or second order) effect on the sediment concentration-discharge relationship at the point of confluence with the Sacramento River because of the following. 1) Sediment yields have been low above Sierra dam sites since the last episode of glacial scour in the Pleistocene (evident in low sedimentation rates into Sierra reservoirs reported by *Dendy and Champion* [1978]). 2) There is significant sediment contribution from tributaries below impoundments which are fed by their own undammed tributaries, and which cross the Sierra foothills and lowlands across valleys containing hydraulic mining tailings, agricultural lands, and other sources of alluvial sediment deposited during the Tertiary and Quaternary periods. It is unlikely that impoundments cause a large reduction in sediment discharge at the point of confluence with the Sacramento River, although they do alter the flow structure. Analyzing sediment discharge data collected before and after the construction of Oroville dam on the Feather River lends credence to my assumption (Figure 1.5). Herein I consider only tributary drainage areas downstream of impoundments to calculate sediment discharge.

BJ Model Estimation Procedure

Since this study is concerned with the application of time series models to sediment budget evaluation, only an outline of time series model building is outlined below. For a more detailed description of algorithms and diagnostics involved in transfer function model estimation, the reader may consult [*Box and Jenkins*, 1994] for the general case and [*Fitzgerald and Karlinger*, 1983; *Lemke*, 1991] for application to sediment concentration.

In order to satisfy assumptions of normality, the original discharge and sediment concentration data were transformed to logarithms because discharge values were highly right-skewed. BJ modeling assumes the process being investigated is stationary. A check of the correlogram of the log-transformed series of both flow and sediment concentration revealed nonstationarity (i.e. their autocorrelations did not die out to white noise with increasing lags). Therefore, differences between the logarithms of successive daily flow values were used as a second transformation to convert the nonstationary series to a stationary one. Using differenced input and output data in (3) signifies that the BJ model predicts changes in sediment concentration based on changes in discharge and previous changes in sediment concentration. The original data can be retrieved at the end of the differencing procedure.

A univariate ARIMA model was then fit to the input series (i.e. log-differenced discharge) with an equation of the form:

$$Q_t^{**} = \Phi_1 Q_{t-1}^{*} + \ldots + \Phi_p Q_{t-p}^{*} + a_t - \theta_1 a_{t-1} - \ldots - \theta_q a_{t-q} \qquad (4)$$

where Q_t^{**} is fitted log-differenced discharge; Φ_p are estimated AR parameters operating on the log-differenced discharge series; a_t is a white noise process of random shocks which induce changes in Q_t^*, and θ_q are estimated MA parameters operating on the white noise process in a moving average model. I used an iterative procedure in MATLAB to determine the best univariate model structure for a range of model orders as measured by the autocorrelation and partial autocorrelation functions (ACF and PCF). A particular model was chosen when the Akaike information criterion (AIC), a measure of the number of model parameters and of the model's fit, was minimized [*Brockwell and Davis*, 1987].

An ARIMA model (5) of the same order was then used to model the output series (i.e. log-differenced sediment concentration). After fitting these ARIMA models separately to the log-differenced discharge and sediment concentration data, the two series of residuals were used for estimating Φ_p and θ_q in (3). [*Vandaele*, 1983] recommends using these prewhitened series for model identification, in order to reflect the true nature of the transfer function model by eliminating all variations in each variable (i.e. log-differenced discharge or sediment concentration) that can be explained by its own past data. These residual data series were then used to estimate the cross-correlation function (CCF), $\rho_{QCs,}$ which is a measure of the serial correlation between the two variables *Cs* and *Q*, for a given lag *k* in time (number of days) as:

$$\rho_{QCs} = \frac{\gamma_{QCs}(k)}{\sigma_Q \sigma_{Cs}} \qquad k = 0, 1, 2, 3, \ldots \tag{5}$$

where $\gamma_{QCs}(k)$ is the cross covariance between Q and Cs at lag $+k$ and σ_Q and σ_{Cs} are the standard deviations of the Q and Cs series, respectively. According to a procedure outlined by *Vandaele* [1983], the cross-correlation function aids in identifying some appropriate moving average and auto-regressive polynomial orders, ω_s and δ_r, for the transfer function in (3).

I used an iterative, prediction error/Maximum Likelihood method in MATLAB's System Identification Toolbox [*Ljung*, 1997] to determine the best model structure for a range of model orders suggested by the Vandaele procedure and to minimize the error term in (3). A particular model was chosen from the group of thirty models with the highest model efficiency [*Pierce*, 1979] based on the lowest AIC [*Brockwell and Davis*, 1987]. When choosing between models of similar AIC values, the simpler model (i.e. one with the fewest parameters) was selected. The residuals from the univariate fits were used only for model identification. Once a model structure was identified, the model parameters, ω_s and δ_r in (3), were estimated using the log-differenced series of discharge and sediment concentration without prewhitening. Since the magnitude of model residuals is not known a priori, the noise term is used only for model estimation and is not used in forecasting because the expected value of the model error is zero [*Gurnell and Fenn*, 1984].

After estimating a bivariate model for a particular station, several diagnostic checks were performed to ensure the suitability of the chosen model to represent the physical system [*Lemke*, 1991]. The autocorrelation of BJ model residuals was plotted to show the absence of serial correlation. The Portmanteau lack-of-fit statistic, which considers groups of residual autocorrelations instead of only individuals, is calculated and must be distributed approximately as chi square if the model is appropriate [*Ljung and Box*, 1978]. The cross correlation between the input series (i.e. univariate model residuals of log-differenced discharge) and the bivariate model residuals was examined to check that two were independent. Model stability was assessed by plotting the roots of the characteristic equation on the unit circle. A histogram of the residuals was also plotted to check for a normal distribution. The efficiency of each model, measured by an R^2 coefficient of determination for time series modeling [*Pierce*, 1979], was determined by employing the estimated model to predict sediment concentration on a separate set of validation data. Figure 1.6 shows an example of model predictions against the observed validation data in a time series.

Sediment Budget Calculation

Once a model for a particular station passed all diagnostic tests, it was employed to obtain sediment concentration values over the discharge domain (32 years). The streamflow and modeled sediment concentration were used to calculate daily sediment discharge, S_{day} (in tons), at each mainstem gauging station and signature tributary as:

$$S_{day} = Q_{day} * Cs_{day} \tag{6}$$

where S_{day} is sediment discharge per day, Q_{day} and Cs_{day} are mean daily discharge and mean daily sediment concentration obtained from the time series analysis, respectively. The S_{day} values for each station were then summed for each water year to obtain S, annual sediment discharge. Annual average sediment discharge, SD for each station was calculated as:

$$\overline{SD} = \frac{\left(\sum_{i=1}^{n} S_i\right)}{n} \tag{7}$$

where n is the number of years of record, and S_i is the sediment discharge for year i.

The annual sediment discharge for each tributary was computed from the signature station within the same geologic unit, scaled by a ratio of the drainage areas below any impoundments. The mainstem sediment discharge into the unnumbered reach (Reach 0) from its upstream end (Shasta Dam in Figure 1.2) is considered to be zero.

Sediment records for diversions were not extended using BJ models because they are discontinuous (diversions only transport sediment during periods of high flow when the diversion is activated) and thus do not lend themselves to a time series

approach. To calculate the sediment efflux from the Sacramento River via major diversions, I used sediment discharge data from the USGS for stations that have it. For one diversion (GCID), I have calculated sediment losses into settling ponds using average dredging estimates provided by the Glen Colusa Irrigation District. For the remaining major diversions (ACID and Corning Canal) below Keswick Dam (Figure 1.2), I have conservatively assumed sediment discharge to be zero.

Annual suspended sediment discharge divergence for each reach was calculated as:

$$S_{Div} = U + T - D - E \tag{8}$$

where S_{Div} is the net sediment divergence for a reach, U is the mainstem sediment discharge contribution to the reach from upstream, T is the sum of the discharge contribution to the reach from tributaries, D is the sediment discharge leaving the reach downstream, and E is the sediment efflux via diversions. A suspended sediment budget was thus evaluated for the reaches between the six gauging stations on the mainstem Sacramento River.

Sediment Budget Results and Discussion

A complete discussion of estimated BJ models is beyond the scope of the present sediment budget analysis, so only main points are mentioned here. Analysis of time series model structures allows for general inferences about the response of

sediment concentration to fluctuations in discharge. Although such inferences could be made by analyzing the raw input data used to develop the models, the BJ model quantifies the relationship objectively with simple computation. In the BJ models estimated using (3), there is a preponderance of moving average parameters (Appendix A), indicating a basin responding primarily to fluctuations in discharge with no memory of previous sediment concentration conditions [*Fitzgerald and Karlinger*, 1983; *Lemke*, 1991]. Furthermore, many of the stations' models contain only one estimated parameter indicating that a change in sediment concentration for a given two-day period is dependent on only the change in discharge for that same period. The models estimated for a few stations have autoregressive terms indicating some persistence in sediment concentration. The R^2 efficiency statistics for all models are very high (Appendix A). Models with more parameters were estimated for all stations, but resulted in no improvement in model efficiency.

The sediment budget results are presented in Figure 1.7 and in Appendix B. Figure 1.7a shows the mainstem sediment discharge results derived from BJ modeling at each mainstem gauging station. Figure 1.7b shows mainstem sediment discharge divergences for each reach after evaluating the sediment budget. The divergences include the BJ modeling errors that were propagated downstream. Unquantifiable errors associated with input data [*Topping et al.*, 2000] are not included. The spatial patterns of erosion and deposition gleaned from the sediment budget results will be discussed in terms of sediment sources and sinks.

The budget of suspended sediment, including the amount of sediment sequestered in the floodplain, was analyzed for the reach of valley upstream from each of six gauging stations on the mainstem Sacramento (Figures 1.2 and 1.4). It is important to distinguish this type of analysis from sediment budgets that make determinations about the state of reaches of river channel.

Evaluating the sediment budget using BJ models reveals net deposition in Reaches 0, 1 and 3, and net erosion in Reaches 2, 4, and 5. The divergences in suspended sediment transport along the mainstem Sacramento River appear to be largely the result of tectonic and human influences.

Deposition in Reach 3

The sediment budget predicts negative divergence in sediment discharge in Reach 3, indicating net deposition (Figure 1.7b). The reach is characterized by a reduction in width from 1830 m to 250 m over its 40 km length, while its upstream section contains wide meanders and large sand bars (Figure 1.3). Gilbert [1917] noted that between Colusa and the Feather River confluence (Figure 1.2), channel capacity of the Sacramento decreased to 10% of its "flood discharge". The reduction in width generally corresponds with two structural features. In Reach 3, the Sacramento River follows the trace of the Willows Fault toward Colusa. The fault dips steeply to the east and crosses the Sacramento 8 km north of the Colusa gauge. Just over 1 km downstream of Colusa the river is diverted 2 km eastward for 13 km to traverse Colusa Dome, a southward plunging anticline which displays over 150 m of

structural relief on basement rocks [*Harwood and Helley*, 1987]. Although Colusa Dome lacks surface expression, the Sacramento's longitudinal profile shows a decrease in gradient upstream [*Water Engineering &Technology*, 1990] indicating some structural influence or differential compaction of the alluvium over the Dome. The interface of the Sacramento River and the Dome also corresponds with fixed thalweg elevations associated with the presence of the resistant Modesto Formation outcrop [*Water Engineering &Technology*, 1990], which was brought to the surface by the Dome. It appears that the river migrated away from the Modesto outcrop, and incised into softer materials and subsequently became confined to a narrow channel by cohesive, clay-rich banks.

The downstream reduction of width causes water to be sequestered in the wide portions of Reach 3 and induces overbank flows and suspended sediment deposition. Sediment is deposited on bars and on the floodplain between setback levees (Figure 1.3), and ~1.1 Mt yr^{-1} (Appendix B) are forced into the floodplain through two flood relief structures which empty into the subsiding Butte Basin (at a rate of ~1.3 mm yr^{-1} [*Ikehara*, 1994]) and Sutter Bypass (Figures 1.2 and 1.3). Colusa is the bottleneck of the Sacramento fluvial system because fluxes of water and sediment are diminished at this station (Figure 1.7b).

Deposition in Reaches 0 and 1

Although sediment discharge increases between Bend Bridge and Hamilton City (Figure 1.7a) the sediment budget predicts net deposition of sediment in Reaches

0 and 1 (Figure 1.7b). Reach 0 winds through the steep Sacramento Canyon (slope = 0.0016) below the Keswick Reservoir before reaching the flatter Redding Plain (slope = 0.0011), where the channel is entrenched into a floodplain dissected by the majority of tributaries in Reach 0. The Sacramento then enters Iron Canyon before entering the Central Valley above Bend Bridge.

The Redding plain shows evidence of deposition in the form of point bars (e.g. below Clear and Cottonwood Creeks), as well as tributary fans. The majority of sediment load input to Reach 0 of the Sacramento, ~0.5 Mt yr^{-1}, originates in Cottonwood Creek (Appendix B). The gauging station used for modeling its sediment load in this study has shown no significant aggradation, but is located ~10 km upstream of its confluence with the Sacramento [*McCaffrey et al.*, 1988]. The difference between the net increase in sediment transport through the reach and the calculation of net accumulation in the reach is due to massive fan deposition at the confluence and gravel mining which removes large amounts of sand as well as the gravel.

Reach 1 occurs entirely within the Central Valley and has a large, contiguous floodplain separated from the Sacramento River only by natural levees (and occasional riprap). Floodflow, although reduced by Shasta Dam, frequently overtops the natural levees composed of finer sands, silts, and clays [*Brice*, 1977; *Water Engineering &Technology*, 1990], and causes extensive overbank sedimentation [*Blodgett*, 1971; 1981]. In addition to vertical accretion, lateral floodplain accretion is apparent in this reach in numerous, large sand bars. Another possible location of

stored sediments is in the channel of this reach, evident in anomalously fine grain sizes in the bed's subpavement surveyed during low water conditions [*Water Engineering &Technology*, 1990]. The combination of reduced flood peaks, high tributary input of sediment, and the reduced gradient in the Central Valley ensure net sediment deposition in these reaches.

Erosion in Reaches 2, 4, and 5

The sediment budget results point to the marked influence of channelization on suspended sediment discharge. The sediment balance at Butte City, Knights Landing, and Sacramento predicts net erosion in these reaches (Figure 1.7b). I have quantified the average erosion of suspended load from these reaches of river by dividing the flux divergence for each reach by the planform area available for erosion (including banks). This yielded approximately 1.2 cm yr^{-1}, 0.4 cm yr^{-1}, and 1.7 cm yr^{-1} for Reaches 2, 4, and 5 respectively.

In the upper part of Reach 2, two major bend cutoffs occurred in 1946, straightening and steepening the channel in the upper part of the reach [*Water Engineering &Technology*, 1990]. Perhaps as a response to the cutoffs, the minimum thalweg elevation at a cross section below Hamilton City decreased by ~91 cm or ~4.4 cm yr^{-1} between 1949 and 1969 [*Water Engineering &Technology*, 1990]. It has been shown on the Mississippi River that a wave of channel degradation, associated with increased slope and stream power, travels upstream following natural or anthropogenic cutoff [*Madden*, 1974; *Biedenharn et al.*, 2000]. Additionally, Brice

[1977] observed less islands and bars in this reach compared to Reach 1. Furthermore, project levees begin at about the halfway point in Reach 2 and there are sections where the river is pinned to the levee (Figure 1.8) leading to locally steep channel gradients and accelerated degradation, as [*Kesel and Yodus*, 1992] showed along the Mississippi River.

Reach 4, between Colusa and Knights Landing, has no tributaries and has a smaller channel capacity, as floodwaters are attenuated by Butte and Sutter Basins upstream of the bottleneck (i.e. Colusa). This reach has locally steep sections and is a channelized, meandering reach with levees built upon the channel banks. The artificial levees have produced confined bends that concentrate erosion at flow deflections [*Brice*, 1977]. Biedenharn, et al. [2000] showed that channel confinement on the Mississippi sends a wave of degradation traveling upstream.

Reach 5 continues the pattern of Reach 4, with leveed bends, but its is further influenced by the input of water and sediment by Feather River/Sutter Bypass, as well as by Fremont and Sacramento Weirs (Figure 1.2). Large floodflows leaving the Sacramento through the flood control weirs in this reach cause rapid variations in water surface slope [*Blodgett and Lucas*, 1988] that are capable of inducing erosion. The predicted 1.7 cm yr^{-1} rate of erosion in Reach 5 is corroborated in an approximate way by gauge height data from Verona (downstream of the Feather River confluence), which show 42 cm of bed degradation between 1965 and 1979 (3.0 cm yr^{-1}) [*Water Engineering &Technology*, 1990]. This local erosion is indicative of systemic erosion in the reach, which presumably attenuates downstream with

sediment input from the Feather. Another source of eroded sediment in this reach is the failed leveed banks in the lower Feather River (below the gauging station used in this study) and in the lower Sacramento, both of which are consistently the subject of reports evaluating potential for repair and improvement (e.g. [*US Army Corps of Engineers*, 1983; *Water Engineering &Technology*, 1990]).

Conclusion

Box-Jenkins transfer functions were employed to model the relationship between stream discharge and sediment concentration. Historical records of suspended load were extended over a 32-year period since dam construction on the Sacramento River to analyze spatial patterns in sediment transport and storage. Suspended sediment discharge was calculated and a sediment budget evaluated for river reaches between six mainstem gauging stations, accounting for their tributaries and diversions. The results of the 32-year sediment budget point to the influence of tectonics and anthropogenic channel modifications on erosion and deposition in the Sacramento Valley.

References

Biedenharn, D.S., C.R. Thorne, and C.C. Watson, Recent morphological evolution of the Lower Mississippi River, *Geomorphology*, *34*, 227-249, 2000.

Blodgett, J.C., Determination of floodflow of the Sacramento River at Butte City, California, January 1970, US Geol. Survey, Menlo Park, CA, 1971.

Blodgett, J.C., Floodflow characteristics of the Sacramento River in the vicinity of Gianella Bridge, Hamilton City, California, US Geol. Survey, Menlo Park, CA, 1981.

Blodgett, J.C., and J.B. Lucas, Profile of Sacramento River, Freeport to Verona, California, Flood of February 1986, US Geol. Survey, Sacramento, 1988.

Box, G., and G. Jenkins, *Time Series Analysis, Forecasting, and Control*, Holden Day, San Francisco, 1994.

Brice, J., Lateral migration of the middle Sacramento River, California, US Geol. Survey, Menlo Pk, CA, 1977.

Brockwell, P., and R. Davis, *Time Series: Theory and Methods*, 519 pp., Springer-Verlag, New York, 1987.

Bryan, K., Geology and groundwater resources of Sacramento Valley, California, US Geol. Survey Water Supp. Paper 495, Wash., D.C., 1923.

California Dept. of Water Resources, Sacramento River bank erosion investigation, Dept. Water Resources, Sacramento, CA, 1994.

Dendy, F.E., and W.A. Champion, Sediment deposition in US reservoirs: Summary of data reported through 1975, USDA, 1978.

Dunne, T., Geomorphologic contributions to flood control planning, in *Flood Geomorphology*, edited by V.R. Baker, R.C. Kochel, and P.C. Patton, pp. 421-438, Wiley & Sons, New York, 1988.

Ferguson, R.I., River loads underestimated by rating curves, *Water Resources Research*, *22* (1), 74-76, 1986.

Fitzgerald, M.G., and M.R. Karlinger, Daily water and sediment discharges from selected rivers of the eastern US: A time series modeling approach, US Geol. Survey Water Supp. Paper 2216, Wash., D.C., 1983.

Gilbert, G.K., Hydraulic-mining debris in the Sierra Nevada, US Geol. Sur., Menlo Park, CA, 1917.

Goodwin, P., Characteristics of sediment transport on the Sacramento River at Sacramento, University of California-Unpublished Report, Berkeley, CA, 1982.

Goodwin, P., and R.A. Denton, Seasonal influences on the sediment transport characteristics of the Sacramento River, California, *Proc. Inst. Civ. Engin., Pt. 2*, *91*, 163-172, 1991.

Gurnell, A.M., and C.R. Fenn, Box-Jenkins transfer function models applied to suspended sediment concentration-discharge relationships in a proglacial stream, *Arctic and Alp. Res.*, *16* (1), 93-106, 1984.

Guy, H.P., and V.W. Norman, Field methods for measurement of fluvial sediment, U.S. Geological Survey, Washington, D.C., 1970.

Harwood, D.S., and E.J. Helley, Late Cenozoic tectonism of the Sacramento Valley, California, US Geol. Survey Prof. Paper 1359, Wash., D.C., 1987.

Heidel, S.G., The progressive lag of sediment concentration with flood waves, *Transactions, Amer. Geophysical Union*, *37* (1), 56-66, 1956.

Ikehara, M.E., Global positioning system surveying to monitor land subsidence in Sacramento Valley, CA, USA, *Hydrological Sciences*, *39* (5), 417-429, 1994.

James, L.A., Incision and morphologic evolution of an alluvial channel recovering from hydraulic mining sediment, *GSA Bull.*, *103*, 723-736, 1991.

Kesel, R.H., E.G. Yodis, and D.J. McCraw, An approximation of the sediment budget of the lower Mississippi River prior to major human modification, *Earth Surface Processes and Landforms*, *17* (7), 711-722, 1992.

Kesel, R.H., and E.G. Yodus, Some effects of human modifications on sand-bed channels in Southwestern Mississippi, USA, *Environ. Geol. Water Sci*, *20* (2), 93-104, 1992.

Kondolf, G.M., Geomorphological stream channel classification in aquatic habitat restoration: uses and limitations, *Aquatic Cons.: Marine & Freshwater Ecosys.*, *5*, 127-141, 1995a.

Kondolf, G.M., Managing bedload sediment in regulated rivers: Examples from California, USA, in *Natural and Anthropogenic Influences in Fluvial*

Geomorphology, edited by J.E. Costa, A.J. Miller, K.W. Potter, and P.R. Wilcock, pp. 239, Amer. Geophysical Union, Wash. D.C., 1995b.

Kondolf, G.M., and M.G. Wolman, The sizes of salmonid spawning gravels, *Water Res. Research*, *29* (7), 2275-2285, 1993.

Lemke, K., Transfer function models of suspended sediment concentration, *Water Resources Research*, *27* (3), 293-305, 1991.

Leopold, L., M.G. Wolman, and J.P. Miller, *Fluvial Processes in Geomorphology*, 522 pp., W.H. Freeman & Co., San Francisco, CA, 1964.

Ljung, G.M., and G.E.P. Box, On a measure of lack of fit in time series models, *Biometrika*, *65* (2), 297-303, 1978.

Ljung, L., System Identification Toolbox User's Guide, Mathworks, Inc., Natick, MA, 1997.

Loughran, R.J., The calculation of suspended-sediment transport from concentration v. discharge curves: Chandler River, N.S.W., *Catena*, *3*, 45-61, 1976.

Madden, E.B., Mississippi River and Tributaries Project, Problems Relating to Changes in Hydraulic Capacity of the Mississippi River, US Army Corps of Engineers, Vicksburg, MS, 1974.

Marcus, A.W., Lag-time routing of suspended sediment concentrations during unsteady flow, *Geol. Soc. Amer. Bull.*, *101*, 644-651, 1989.

McCaffrey, W.F., J.C. Blodgett, and J.L. Thornton, Channel morphology of Cottonwood Creek near Cottonwood, Calif. from 1940 to 1985, US Geol. Survey, 1988.

Meade, R.H., Sources, sinks, and storage of river sediment in the Atlantic drainage of the United States, *J. Geology*, *90*, 235-252, 1982.

Neter, J., W. Wasserman, and M. Kutner, *Applied Linear Regression Models*, 547 pp., Richard D. Irwin, Homewood, IL, 1983.

Pierce, D.A., R^2 measures for time series, *J. Amer. Stat. Ass.*, *74* (368), 901-910, 1979.

Porterfield, G., Computation of fluvial-sediment discharge, U.S. Geological Survey, Washington, D.C., 1972.

Porterfield, G., Sediment transport of streams tributary to San Francisco, San Pablo, and Suisun Bays, California, 1909-66, US Geological Survey WRI 80-64, Menlo Park, 1980.

Rodriguez-Iturbe, I., and C.F. Nordin, Time series analyses of water and sediment discharges, *Hydrol. Sci. Jour.*, *13* (2), 69-84, 1968.

Sharma, T., and W. Dickinson, System model of daily sediment yield, *Water Resources Research*, *16* (3), 501-506, 1980.

Sharma, T.C., W.G.S. Hines, and W.T. Dickinson, Input-output model for runoff-sediment yield processes, *J. Hydrology*, *40*, 299-322, 1979.

Topping, D.J., D.M. Rubin, and J. L.E. Vierra, Colorado River sediment transport 1. Natural sediment supply limitation and the influence of Glen Canyon Dam, *Water Resources Research*, *36* (2), 515-542, 2000.

US Army Corps of Engineers, Sacramento River and tributaries bank protection and erosion control investigation, California, U.S. Army Corps of Engineers, Sacramento, CA, 1983.

Vandaele, W., *Applied Time Series and Box-Jenkins Models*, 417 pp., Academic, San Diego, CA, 1983.

Walling, D.E., Assessing the accuracy of suspended sediment rating curves for a small basin, *Water Resources Research*, *13* (3), 531-538, 1977.

Water Engineering &Technology, Geomorphic analysis of Sacramento River, Water Engineering and Technology, Fort Collins, CO, 1990.

Williams, G.P., Sediment concentration versus water discharge during single hydrologic events in rivers, *J. Hydrology*, *111*, 89-106, 1989.

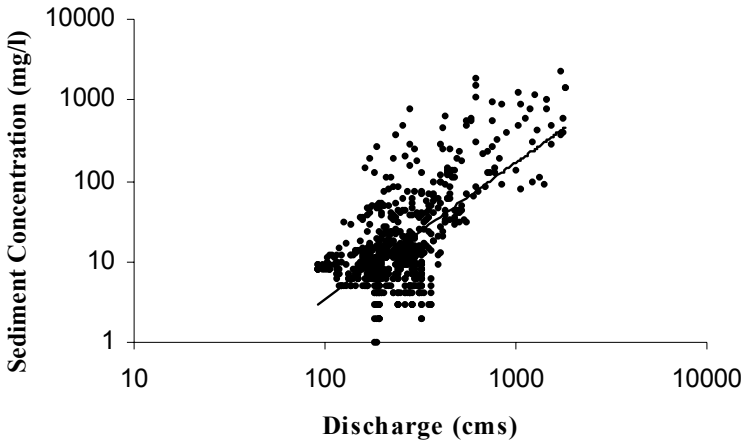

Figure 1.1 Sediment rating curve for Bend Bridge 1977-1980.

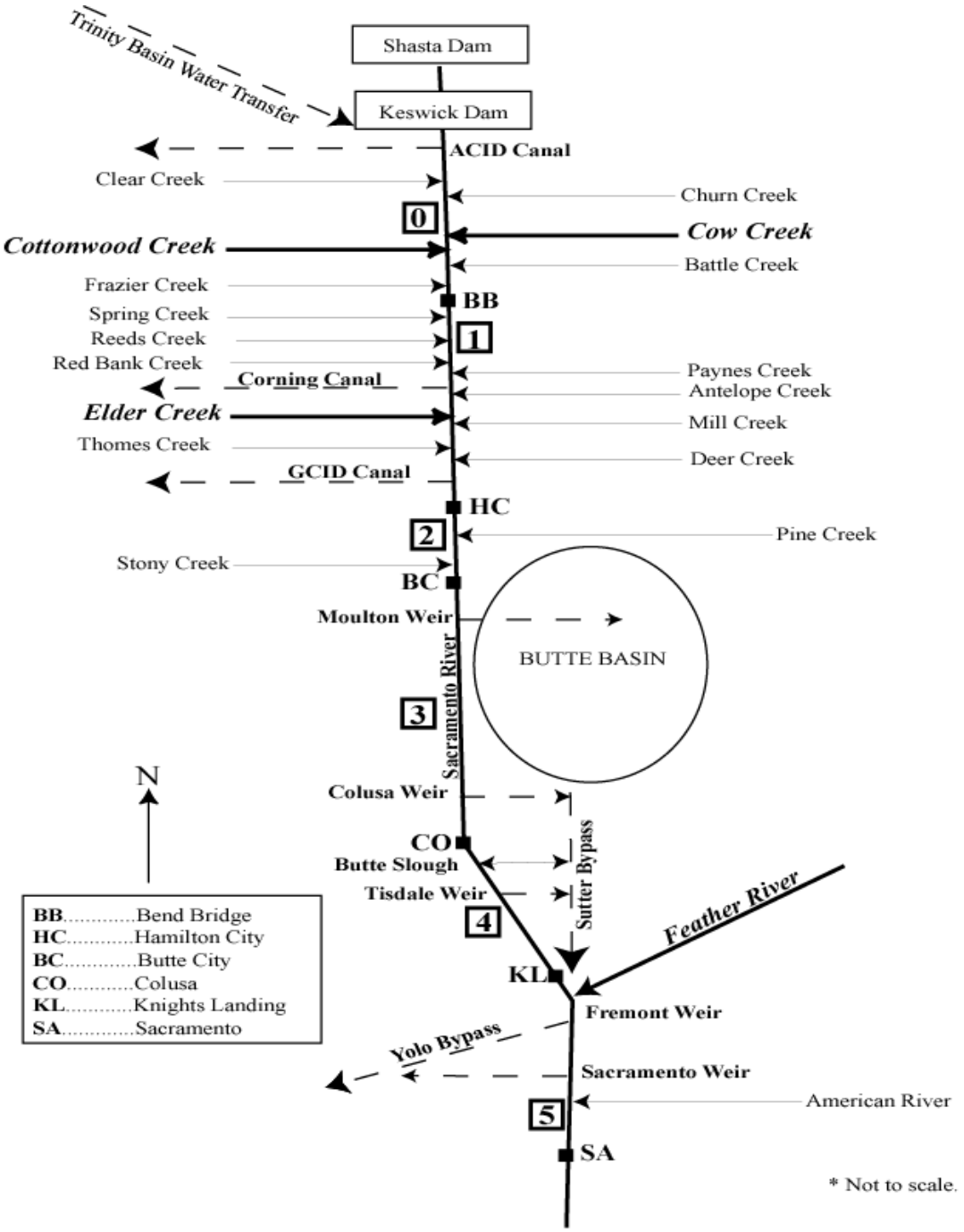

Figure 1.2 Schematic of tributaries, diversions, and bypasses along the Sacramento River's main channel. Project levees (not shown) begin between Hamilton City and Butte City. Artificial channels are depicted with dashed lines and natural channels with solid lines. Gauging station names are abbreviated in bold caps. Reaches used for analysis are represented by boxed numbers.

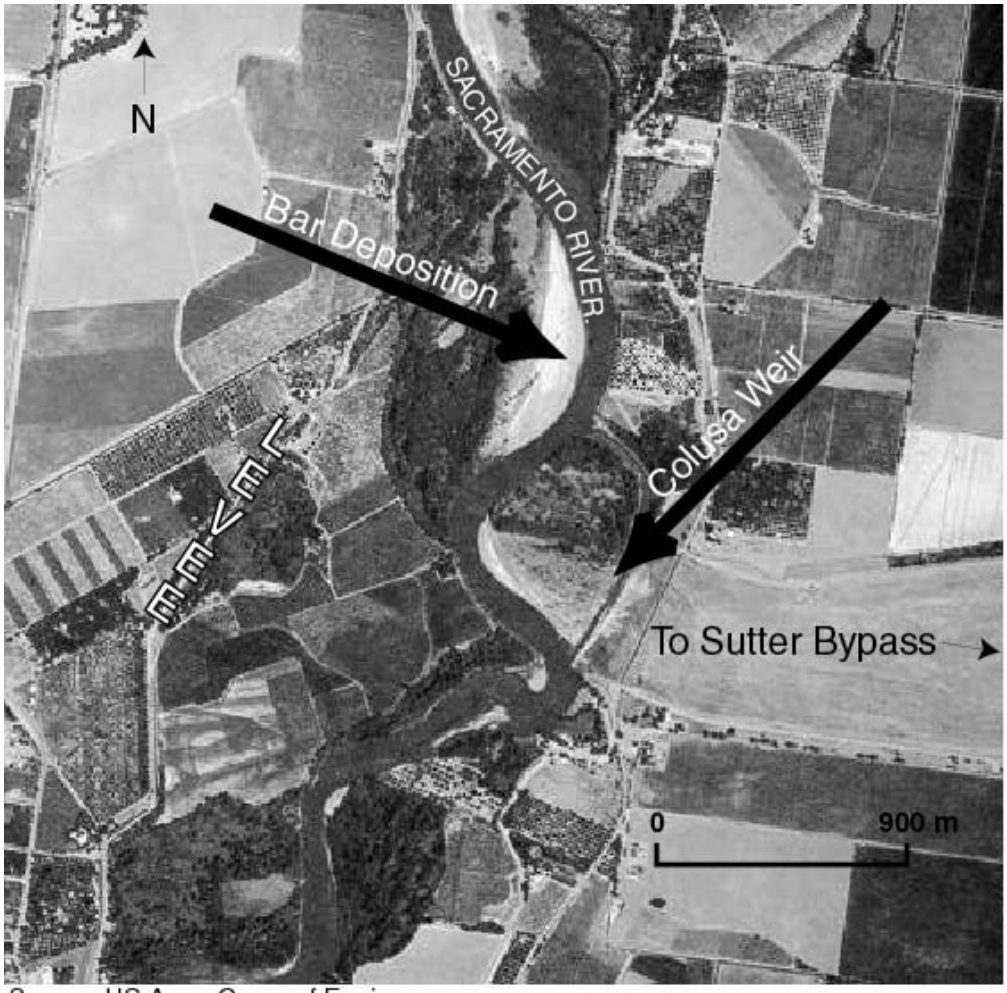

Source: US Army Corps of Engineers

Figure 1.3 Aerial photograph showing Colusa Weir overflow to Sutter Bypass and point bar deposition in the wide reach-of-valley upstream (Reach 3).

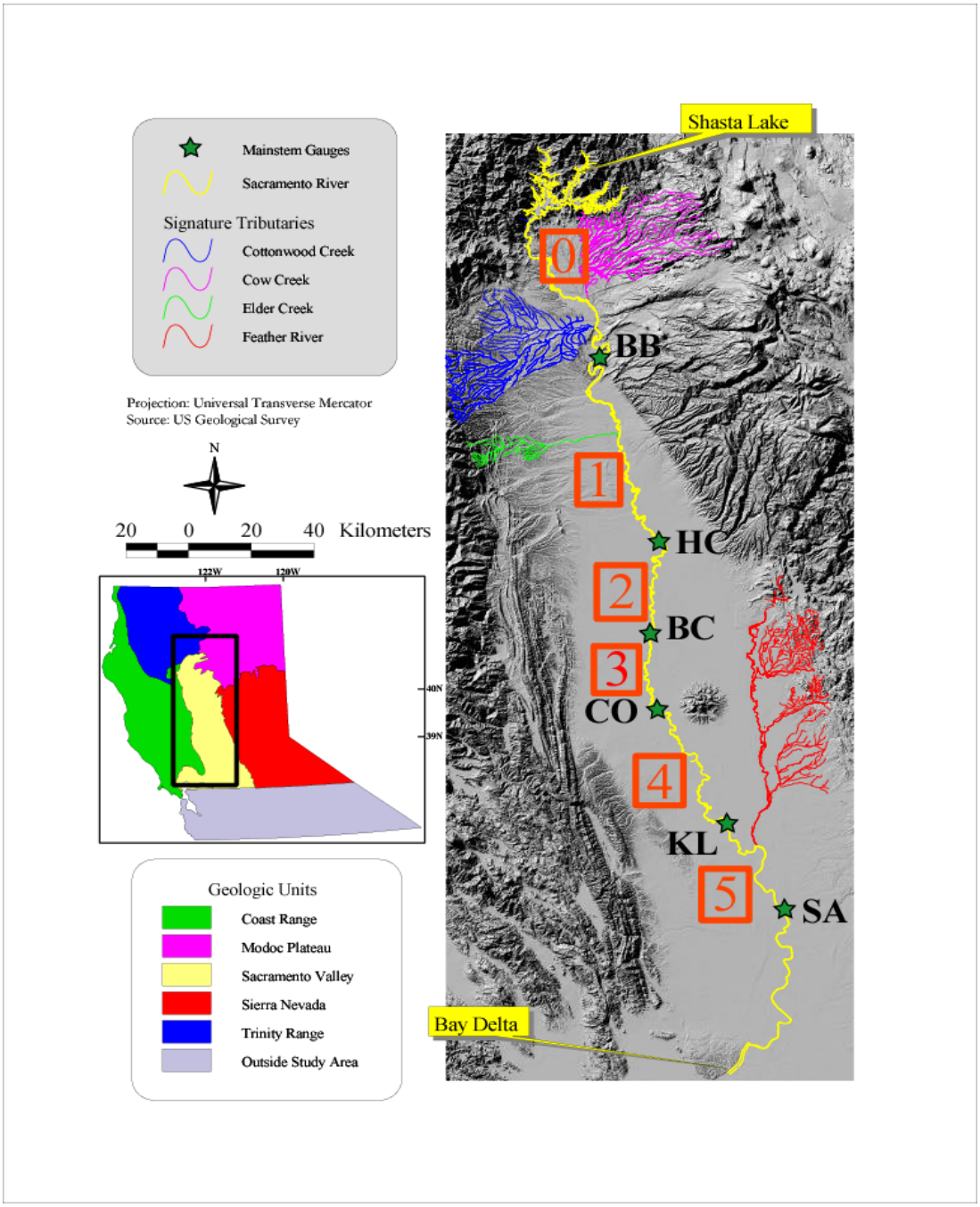

Figure 1.4 The Sacramento River Valley map shows the six gauging stations (triangles) used in this study, the signature tributaries (color-coded) and the five reaches (boxed red numbers). The inset shows geologic units (color-coded) from which signature tributaries were selected. Abbreviations for sampling stations are given in Figure 1.2.

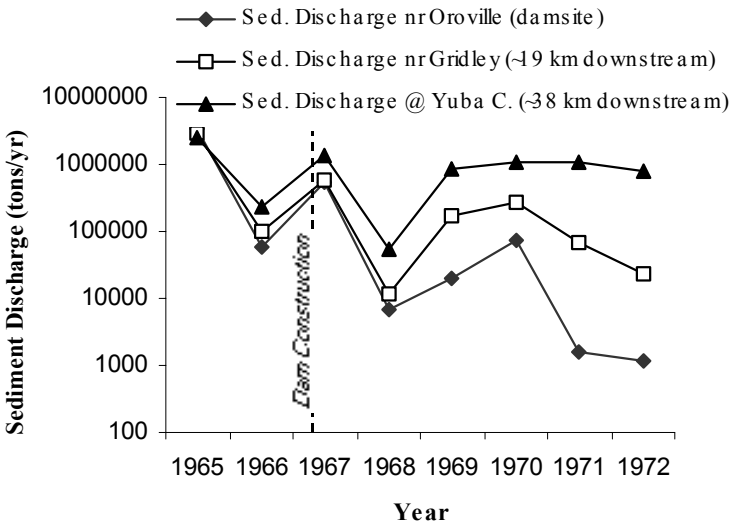

Figure 1.5 The annual sediment discharge before and after the construction of Oroville Dam on the Feather River, demonstrating that the dam has had minimal influence on the sediment discharge near the Feather's confluence with the Sacramento.

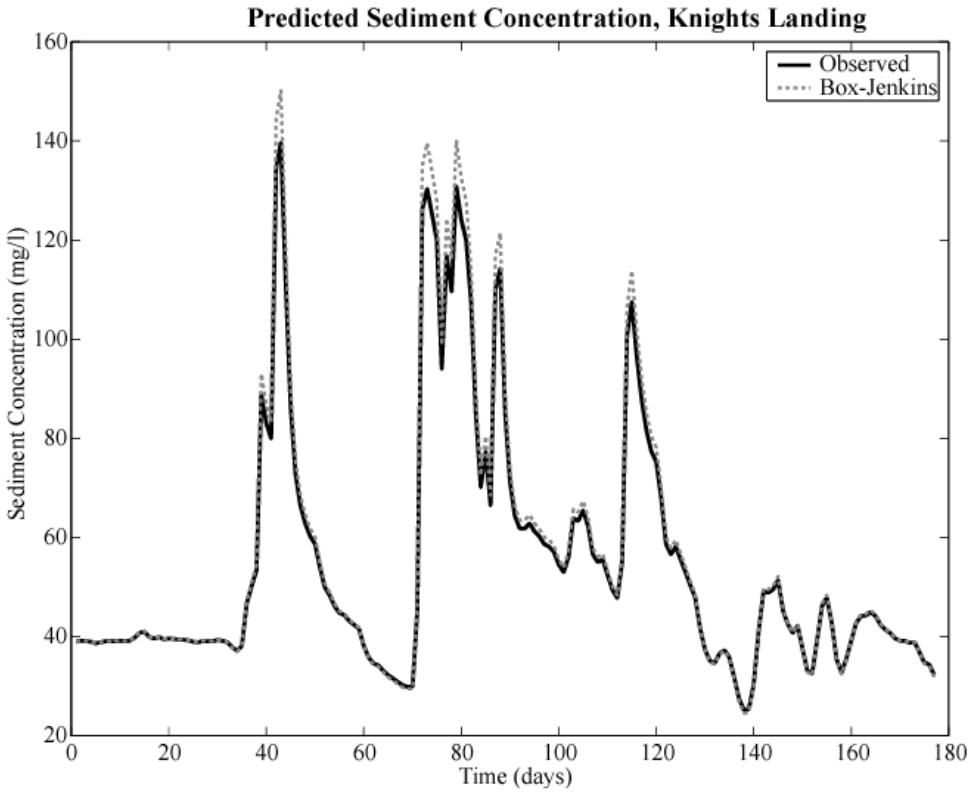

Figure 1.6 An example of BJ model predictions against observed daily values of sediment concentration from a validation dataset (not used in model estimation) at the Knights Landing gauging station.

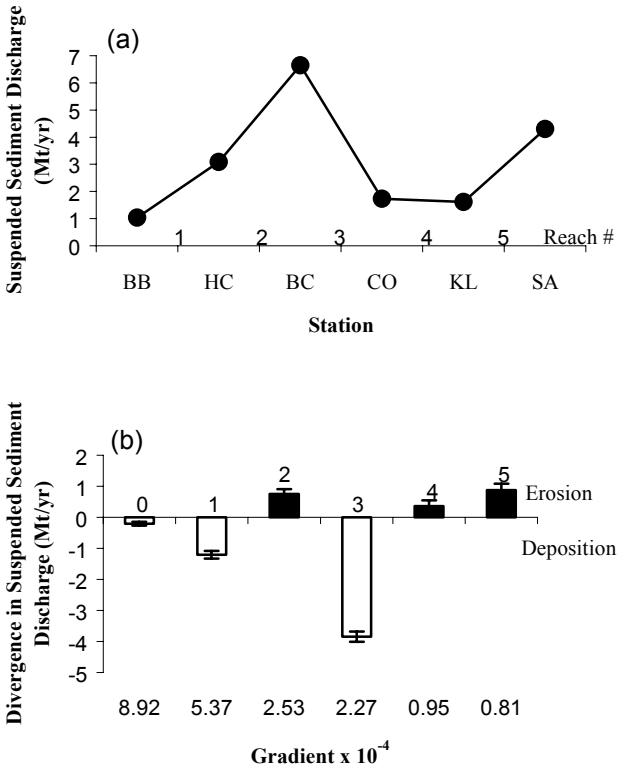

Figure 1.7 (a) Mean annual sediment flux computed by BJ modeling in millions of tons per year for the six mainstem gaging stations, which are denoted on the abscissa by their station abbreviations. The numbers below the curves are the river reach numbers. (b) Sediment flux divergence based on the sediment balance for each reach with the reach gradient on the abscissa. Reach numbers are labeled on the top of each bar.

Source: US Army Corps of Engineers

Figure 1.8 Aerial photograph showing main channel pinned to west levee (arrow) in Reach 2. Levees on the west bank cut off the Sacramento from Colusa Basin to the west and force overflow into Butte Basin to the east.

CHAPTER 2. AN EMPIRICAL-STOCHASTIC, EVENT-BASED MODEL FOR SIMULATING INFLOW FROM A TRIBUTARY NETWORK: THEORETICAL FRAMEWORK AND APPLICATION TO THE SACRAMENTO RIVER BASIN, CALIFORNIA

(Submitted)

Abstract

A stochastic model of streamflow was developed to simulate inflow to a large river from a network of gauged tributaries. The model uses historical streamflow data from major tributary gauges near their confluence with the mainstem and combines them stochastically to represent spatial and temporal patterns in flood events. It incorporates seasonality, event basis, and correlation in flood occurrence and flood peak magnitude between basins. The model produces synchronous tributary inflow hydrographs, which when combined and routed, preserve mainstem hydrograph characteristics, including peak, volume, shape, duration, and timing. The paper verifies the model using daily streamflow data from primary tributary and mainstem gauges in the Sacramento River basin, California. Simulations can be used in flood routing models to predict flow at ungauged mainstem locations, to assess risk in fluvial systems, to calculate sediment budgets, to assess the role of streamflow in habitat functioning, and to detect bed level change.

Introduction

For a number of purposes [estimation of flood risk; sediment transport and routing; prediction of inundation regimes of floodplain vegetation; and effects of flow regulation on all of the above], it would be useful to know about the probability distributions of flood hydrograph characteristics, including their peak, volume, shape, duration, and timing. It would also be useful to analyze these aspects of flood hydrographs on large rivers at locations other than major mainstem gauging stations, and to examine the effects of certain engineering modifications on flood characteristics. The commonly used flood-frequency curve, derived from the annual maximum series of a single realization of one n-year peak flow series, does not yield as much information as could be gleaned from treating the empirical record as a sample of all other possible realizations. I propose to view the flood record in this latter fashion to derive from it some of the flood-regime characteristics useful for multiple purposes, including traditional design needs in flood control and zoning as well as research and management needs relevant to ecosystem functions.

There is currently a separation of responsibilities for the analysis of floods in lowland river systems. Some hydrologists are concerned mainly with floods as hazards that need to be designed for and others view floods as agents of ecosystem maintenance that are essential for aquatic and riparian biodiversity [*National Research Council*, 2001]. Flood control engineers and planners are generally interested in large flood peaks to assess flood risk and design flood control [*US Army*

Corps of Engineers, 1992]. Ecologists and geomorphologists are interested in a range of floods, including those below the zero-damage stage, that transport sediments of differing caliber, inundate and scour floodplains, and maintain riparian plant communities [*Junk et al.*, 1989; *Church and Hassan*, 1992; *Poff et al.*, 1997; *McLean et al.*, 1999; *Tockner et al.*, 2000]. The two groups have different sets of methods for analyzing floods (c.f. [*National Research Council*, 1988; *Richter et al.*, 1996]). Therefore, there is use for a single model that treats the spectrum of floods, from instantaneous flood peaks used in flood control design to hydrograph characteristics (e.g. shape, duration) that affect riparian and aquatic ecosystems [*Richards et al.*, 2002]. Such a model would simulate sequences of floods as decadal hydrographs that could be analyzed statistically or used as input to a variety of other models. The word 'flood' is used to here to describe not only the large, damaging peaks that flood control systems are designed to convey, but the time series of discrete flow events slightly above and below bankfull discharge.

In Part 1 of this paper, I develop the theoretical framework of a model for simulating the statistical properties of the full range of flow hydrographs that affect flood control, the sediment transport budget, and various riparian processes. In Part 2, I apply this model to the Sacramento River basin in California to verify its predictive capability, and I discuss its application in: (1) simulating flow at ungauged mainstem locations; (2) assessing risk in fluvial systems; and (3) detecting bed level change.

1. Theoretical Framework

Background

Previous Work on Streamflow Simulation

Streamflow simulation is the generation of synthetic discharge data over a regular time interval (e.g. days) in a river basin for use in long-range planning and development [*Fiering*, 1967]. Methods of simulating streamflow vary depending on the quantity and quality of empirical data available for a particular basin in both time and space. The two groups of these methods are: 1) those that model the hydrologic processes by which rainfall becomes streamflow (hereafter called process-based); and 2) those that model streamflow based entirely on historical datasets of streamflow (hereafter called empirical).

Process-based methods tend to be applied in small river basins where flow data are sparse, and tend to use rainfall-runoff models to simulate streamflow (see [*Beven*, 2000] for a discussion of the differences in data-based versus physically-based rainfall-runoff models). Process-based streamflow simulations in large river basins have combined rainfall-runoff models for subbasins [*Burnash et al.*, 1973], and have linked surface properties to climate models via soil-vegetation-atmosphere transfer methods [*Nijssen and Lettenmaier*, 1997].

Empirical methods tend to be applied in river basins that have been subjected to intensive data collection campaigns. Streamflow simulation by empiricism extends historical flow records from individual gauges by analyzing the seasonal autocorrelation structure of the data. These data can be treated using parametric (e.g.

[*Salas et al.*, 1982; *Vecchia*, 1985]) or nonparametric methods (e.g. [*Sharma et al.*, 1997]), or by correlation with a nearby long-term gauge (e.g. [*Matalas and Jacobs*, 1964; *Hirsch*, 1982; *Moog and Whiting*, 1999]). Historical streamflow records can also be interpolated by disaggregation. This involves simulating seasonal flow at one temporal level using data from a higher temporal level (e.g. simulating monthly flow from disaggregated annual flow data) [*Valencia and Schaake*, 1973; *Lane*, 1993].

Empirical methods of streamflow simulation attempt to preserve the statistical properties of the historical data when simulating data at a particular gauge. For example, mean annual flow should be approximately the same for observed and simulated data. However, the spatial structure and timing of flow delivery from a network of gauging stations to the mainstem have been largely ignored. If these factors were incorporated into a streamflow simulation model on the basin scale, one could predict the statistical structure of mainstem hydrology based on the spatial and temporal patterns of inflow from its tributaries. The model could be used to simulate hydrographs at any mainstem location by routing simulated tributary inflows through the main channel by standard procedures (e.g. [*Brunner and Bonner*, 1994]).

Modeling Strategy

In this paper I develop an empirical-stochastic model (hereafter referred to as HYDROCARLO) for simulating synchronous, event-based streamflow from major tributaries, in river basins where flood control and water supply concerns have dictated long and spatially extensive streamflow gauging programs.

Spatial and temporal variability of inflow from major tributaries is the principal control on stream discharge in large river channels. Such variability results largely from rainstorm magnitude, duration, and trajectory, rates of snowmelt, and from differential rates in runoff generation based on tributary basin characteristics (e.g. slope, elevation, vegetation). My goal is to simulate streamflow from a basin-wide network of tributaries as sequences of flood events, by preserving seasonal oscillations in flow magnitude, flow duration, inter-storm period duration, and the synchronicity in flood occurrence and flood peak magnitude, as they are reflected in historical records. The stochastic flow model would yield an infinite number of realistic simulations in the form of synchronous hydrographs from the tributary gauging network, which could be combined or routed to produce mainstem hydrographs that are based on plausible patterns of tributary inflow.

Stochastic Approach

I conceptualize an idealized large river basin as a mainstem with (say) six major tributaries, each of which has a streamflow gauge near the confluence (Figure 2.1). The main channel has a gauge (labeled 0 in Figure 2.1) to monitor streamflow entering the reach from upstream and a gauge to monitor streamflow at the basin outlet. Each gauge has recorded mean daily streamflow for fifty years.

A purely empirical approach to streamflow simulation would route contemporaneous measured inflow from all tributary gauging stations in the network through the main channel to reproduce the 50-years of historical record at the basin outlet. This deterministic modeling strategy allows for only one outcome based on

the historical record, and does not represent the variable nature of flow delivery to the main channel. Following the recommendations of other workers (e.g. [*Hirschboeck*, 1988, pp.39-42]), I have opted for a stochastic approach to modeling tributary inflow, in order to represent the potential variability (and thus the uncertainty in predicting) storm magnitude, frequency, duration, and trajectory, and in snowpack, melt rate, and tributary basin characteristics and condition.

The theory of stochastic processes acknowledges that some physical processes cannot be modeled accurately based on available data and existing theories, rooted in first principles. The theory instead relies on the use of probability to represent uncertainties in the theory. Stochastic modeling of hydrologic data extends back at least as far as the application of creating longer streamflow series by sampling at random from annual historical series for a given location [*Sudler*, 1927]. Its methods later became more formalized using statistical theories to develop autoregressive models for monthly rainfall data [*Hannan*, 1955]. Since that time, stochastic statistical theory has been applied to empirical streamflow simulation primarily to synthetically extend the historical record of annual maximum series at a particular gauging point (e.g. [*Stedinger and Taylor*, 1982]), and to generate synthetic series for ungauged basins using regional parameters (e.g. [*Benson and Matalas*, 1967]).

I use HYDROCARLO as a stochastic seasonal flood generator at a network of streamflow gauging points. Each gauge can be thought of as a valve that is opened when a flood occurs (solid arrows in Figure 2.1). During inter-storm periods, the valve at a gauging station never closes completely, but instead "leaks" with a flow

magnitude equivalent to the baseflow discharge (dashed arrows in Figure 2.1). There are numerous combinations of uncertain variables (e.g. rainstorm trajectory, tributary basin condition) that could induce flood conditions at some gauges while leaving others unaffected. Figure 2.1 illustrates the effect of a seasonal storm (e.g. a frontal rainstorm in winter) on a trajectory through the southern portion of the idealized basin, inducing flood conditions at Gauges 3, 4, 5, and 6, but leaving Gauges 0, 1, and 2 unaffected. In the development of HYDROCARLO I have accounted for the numerous possible combinations of season, storm characteristics, and drainage basin conditions that could affect streamflow at all tributary gauges in a basin. Lacking the data or understanding to model these factors explicitly, I represent them in HYDROCARLO by stochastically drawing upon historical flood data from tributary gauges, which reflect seasonal storm patterns, the frequency of storms at each gauge, and the correlation in storm conditions between gauges.

Model Initialization

HYDROCARLO's fundamental features are: 1) seasonality; 2) basis on flood events; and 3) basinwide synchronicity. Each will be discussed separately in terms of model initialization (Figure 2.2).

Seasonality

Seasonal controls on discharge differ by geographic region and these differences are detectable in annual hydrographs. For example, in some river basins

discharge hydrographs are influenced by large frontal rainstorms in the winter (e.g. Sacramento River in California). Others receive the majority of their precipitation from a summer monsoon (e.g. Narmada River in India). The predominant flood pulses of other basins result from the melting of snow and glaciers in the spring (e.g. Copper River in Alaska). Distinct seasonal flood hydrographs are produced in each climatic setting [*Hirschboeck*, 1988]. Specifically, in addition to seasonally varying flood peak magnitude, there are seasonal controls on the probability of flood event occurrence (e.g. floods are less frequent in a dry season), the length of inter-storm periods, and the magnitude of baseflow.

I parameterize these seasonal discharge attributes in HYDROCARLO with user-defined seasons for a given set of input data. The model uses the seasonal definitions to separate flood events and inter-storm periods, and to calculate event probability and baseflow magnitude. For example, a flow series with wet winters and dry summers would be separated into two hydrologic series from which flood events would be extracted and stored in matrices (Figures 2.2 and 2.3). The flood event probability and baseflow discharge would also be calculated for each season, according to a procedure described in the subsequent section.

Event Basis

My intention is to simulate decades-long hydrographs at tributary gauging points using combinations of recorded flood events from the historical flow record at each gauge (i.e. sequences of discharge days above a threshold value). I call this

threshold the baseline discharge, and obtain it using the LOWESS smoothing procedure [*Cleveland*, 1979]. I use LOWESS to obtain a smoothed curve for each seasonal hydrologic series at each gauge, and then calculate the mean of that curve and call it baseline discharge (Figures 2.2 and 2.4). Figure 2.4 shows a collection of wet season events that have been patched together to calculate the baseline discharge. I ignore the magnitude of flows below the baseline discharge because they are insignificant to sediment transport, flood dike stability, and most aspects of river restoration.

After determining the baseline discharge for each seasonal flow series, I discretize continuous sequences of flood days (i.e. those above the baseline discharge) into flood events of varying magnitude and duration (Figure 2.4). I store each historic flood event as a column vector in a flood event matrix (Figure 2.3) in rank order of flood peak magnitude. I define event probability for each flow series at each gauging station by dividing the number of days in the partial duration flood series (i.e. those above the baseline discharge) by the total number of days in the flow record.

In addition to the flood event matrix for each gauge, a matrix of inter-storm periods is generated at the gauge with the longest record. This matrix is seasonally composed of inter-storm period lengths (i.e. sequences of days below the seasonal baseline discharge), which represent the range of inter-arrival times that could occur in the basin over the long term.

Correlation in Events

There is no continuous field of streamflow as a function of distance between two nearby gauges, as can be assumed for rainfall in point process models (e.g. [*Rodriguez-Iturbe et al.*, 1987]), because each streamflow gauge makes measurements of flow that is fed through a discrete tributary basin. However, nearby tributary basins that have similar characteristics (e.g. drainage area, slope, land use, vegetation) are likely to produce similar, synchronous streamflow near their confluences with the main channel, if there are no orographic effects that consistently cause more rainfall to occur in one basin over the other. However, there are conceptual problems with developing a model that represents this type of relationship as something other than totally similar or totally random. For this purpose, I combine a stochastic approach with empiricism based on historical flood records.

In HYDROCARLO I represent two types of spatial and temporal correlation in flood events between gauges. First, I account for correlation in flood event occurrence via the event probability at each gauge. This correlation arises because two gauges located in close proximity are likely to have flood conditions induced by the same storms in a particular season and a similar number of flood days and thus, similar seasonal event probabilities. Conversely, gauges furthest from each other are likely to have different seasonal event probabilities because prevailing storm trajectories may favor rainfall in one tributary basin over another. For example, Figure 2.1 illustrates a southerly storm trajectory that might consistently cause rainfall in the tributary basin of Gauge 5 and consistently cause low rainfall in the basin of

Gauge 2. One could imagine orographic and other localized effects that could induce similar conditions. These effects would be reflected in the number of flood days and thus the event probabilities for each season at these stations (hereafter referred to as seasonal event probabilities).

Second, I account for correlation in flood peak magnitude between gauges for synchronous flood events (i.e. events that are measured at two or more gauges on the same day). This correlation arises from regional storm cells that generate consistent spatial patterns of rainfall over a basin. These patterns, in turn, induce flood peaks of similar rank order at each gauge, whether or not these peaks occur simultaneously at each gauge. Thus, I expect synchronous floods at nearby gauging stations to have similar flood event ranks (i.e. of relative magnitude). For example, if the winter frontal storm in Figure 2.1 caused the tenth magnitude event (column 10 in the wet season flood matrix) at Gauge 3, it is reasonable to assume that Gauge 5 would have an event ranking similar but not necessarily equal to 10. I sought to maintain this spatial correlation in flood peak ranking in HYDROCARLO, while retaining the maximum amount of randomness in event selection. Therefore, I assess correlation in all flood peaks (i.e. not only annual maxima) from synchronous events recorded at gauges at opposite ends of a river basin. Figure 2.5 illustrates how the model extracts all synchronous flood events using data from two widely separated tributary gauges in the Sacramento River basin. HYDROCARLO stores the flood peaks from these events at each gauge and calculates the cross correlation between their peak discharges, which I call the across-basin correlation, *ABC*, calculated as:

$$ABC_{05} = \frac{\gamma_{05}}{\sigma_0 \sigma_5} \tag{1}$$

where γ_{05} is the covariance in synchronous flood peaks between Gauges 0 and 5 (Figure 2.1), for example, and σ_0 and σ_5 are the standard deviations in flood peaks at Gauges 0 and 5, respectively. I calculate *ABC* specifically for widely separated gauges in order to characterize the spatial correlation for the basin as a whole, according to the presumed least correlated gauges in the network.

I use *ABC* to develop a system of relative flood selection in HYDROCARLO. I divide column vectors in seasonal flood event matrices (Figure 2.3) into a number of bins that is determined according to *ABC* (e.g. one bin for $ABC \leq 0.25$, two bins for $0.25 < ABC \leq 0.50$, three bins for $0.50 < ABC \leq 0.75$, four bins for $0.75 < ABC \leq 1.00$). To illustrate the process of relative flood selection, suppose there were 18 flood events (i.e. 18 column vectors) in the wet season flood event matrix for each gauge in the idealized basin (Figure 2.1), and the *ABC* (i.e. between gauges 0 and 5) was 0.72. The seasonal flood matrix for each gauge in the basin would be divided into three bins, each containing 6 flood events (Figure 2.3).

The number of bins into which floods are divided indicates the degree to which flood event magnitude is related for gauges in the basin. A river basin with high probability of disparity in event magnitude between gauges for synchronous events would have a low *ABC,* and one with a low probability of disparity would have a high *ABC*. The bins represent a narrowing of the flood event selection pool

according to the influence of basinwide storms. If there were a preponderance of basinwide storms in a particular basin that induced similar flood ranks at the most distant tributary gauges, *ABC* would be large. If, on the other hand, most storms occurred in isolated regions of the basin, *ABC* would be small because flood ranks at the most distant gauges would be less correlated. Generally, river basins with higher across-basin correlation are likely to be small, homogenous (in topography and vegetation), or commonly affected by basinwide storms or snowmelt. River basins with lower across-basin correlation would include those that are very large, heterogeneous, or that have a number of climatic zones accessed by different tributaries.

Model Operation

Random numbers are generated in HYDROCARLO to determine flood occurrence at each gauge and to select flood events from each gauge, when they occur. Flood events and inter-storm periods are simulated in the various seasons and stored in a simulation matrix for each gauge (Figure 2.3). This simulation matrix can be aggregated into a decadal hydrograph at each gauge. Reference to Figure 2.2 may clarify the following detailed discussion of model operation.

HYDROCARLO first generates a random number between zero and one (RN1 in Figure 2.2), and compares it to the seasonal event probability for each gauge. If RN1 is greater than a gauge's seasonal event probability, then no event will occur at the gauge. If RN1 is less than or equal to the seasonal event probability, an event

will occur at this gauge. HYDROCARLO then randomly selects one bin out of the bin structure specified by the *ABC*, from which all synchronous floods will be chosen. The model generates another random number (an integer between 1 and the number of event columns in that bin) to select flood events at each gauge (i.e. each gauge where a synchronous event occurs). For example, assuming the *ABC* were 0.72 for the idealized basin at the depicted point in time (Figure 2.1), if Bin Two were selected randomly, then flood events at Gauges 3, 4, 5, and 6 would be selected at random from event ranks 7-12 of their respective flood event matrices (Figure 2.3).

The historical daily streamflow for the selected event at each gauge is then entered into the simulation matrix as a column vector (like Figure 2.3). In this empirical-stochastic approach, there may be multiple events of varying duration occurring at different gauges simultaneously. I have defined the length of an event period as the duration (in days) of the longest event selected for that period. Therefore, when an event for a gauge terminates before the end of the event period, HYDROCARLO resets the discharge for that gauge to the seasonal baseline discharge until the end of the event period (i.e. until the longest flood event among the tributaries is complete). Similarly if no event occurs at a particular gauge for an event period, the appropriate column in its simulation matrix will contain seasonal baseline discharge for the duration of the event period. Discharge at all gauges never falls below the seasonal baseline discharge. At the completion of the event period, HYDROCARLO generates a new RN1 to compare with event probabilities at all

gauges and the selection procedure repeats (Figure 2.2). HYDROCARLO creates a new column in the simulation matrix for each event period.

If no event is selected at *any* gauge for an event period (i.e. RN1 is greater than the event probability at all gauges), HYDROCARLO selects an event period duration by randomly choosing a column from the seasonal matrix of inter-storm periods. In simulation, the model assembles, in each gauge's simulation matrix, a column of inter-storm days whose length equals the duration of the selected inter-storm period (Figure 2.3), and whose values are equal to the seasonal baseline discharge for that gauge.

As the model proceeds through event periods, the simulation matrix at each gauge grows with the selection of flood events punctuated by inter-storm periods in alternating user-defined seasons (Figure 2.3). Because of its employment in a stochastic model, the user definition of season length is not followed exactly. For example, if there are ten days remaining in the wet season and an eleven-day flood event is selected from the wet season flood matrix, this event will complete its 11-day progression before the model switches to the dry season matrix for flood selection.

Once a simulation is complete, the simulation matrix assembled at each gauging point can be concatenated to form a hydrograph with length equal to that of the simulation. These synchronous hydrographs at each gauge can then be routed through the mainstem with a flow routing package that allows for lateral inputs (e.g. HEC-RAS). I describe this in part two of this paper.

2. Model Application

Basis for Application

There are two purposes to this part of the paper. First, I validate the capability of HYDROCARLO to simulate hydrographs on the mainstem Sacramento River in California, using mean daily streamflow data from the United States Geological Survey for primary Sacramento tributaries. I: 1) simulate inflow hydrographs at primary tributary junctions; 2) route simulated tributary inflow through the mainstem Sacramento; 3) construct probability distributions of flow characteristics from simulated, mainstem hydrographs; and 4) compare these distributions with probability distributions derived from independent historical data for the same locations. Second, I discuss how HYDROCARLO can be applied for practical purposes in multiple-use river basins.

There have been several quantitative streamflow studies in the Sacramento River Basin. Previous work has mostly focused on evaluating the sensitivity of streamflow to climate change. This has been accomplished empirically by relating streamflow to temperature [*Risbey and Entekhabi*, 1996] and by predicting monthly and seasonal runoff with the aid of a water balance model [*Gleick*, 1987]. Process-based methods have been used in the Sacramento to model runoff using temperature estimates from general circulation models in medium-sized test basins [*Lettenmaier and Gan*, 1990], and to evaluate the impact of warming on the State Water Project [*Lettenmaier and Sheer*, 1991]. Other studies have aimed to extend historical streamflow records on the Sacramento over millennial time scales using isotopic

analysis on fossil bivalves [*Ingram et al.*, 1996] and to investigate climatic changes over centuries using tree ring analysis [*Earle and Gritts*, 1986].

One area of study absent from this list involves fully utilizing the abundant streamflow dataset available for the Sacramento River basin within a streamflow simulation model that represents recent hydroclimatology as spatial and temporal patterns of daily tributary inflow to the mainstem. I fill this void by applying HYDROCARLO to the Sacramento data to simulate the range of potential flood events that could occur in the basin. To reiterate, I use the word 'flood' here to describe not only the largest peaks that flood control systems are designed to convey, but also [i.e. I also include the events that are far above bankfull] the time series of discrete high-flow events slightly above and below bankfull discharge. I am simulating complete floods that are relevant to flood control engineers, ecologists, and geomorphologists.

Sacramento River Basin

Geographical Background

The Sacramento River drains the northern part of the Central Valley of California and has a total drainage area of 6.8×10^4 km^2 comprising over one half of the total drainage area into San Francisco Bay. It flows from its source near Mount Shasta, 600 km south to its confluence with the San Joaquin River, where the two rivers form the Sacramento-San Joaquin-San Francisco Bay-Delta. The Sacramento flows for approximately 400 km within its low gradient valley (mean slope ~0.0002).

Its tributaries rise from the Coast Ranges in the west, the Trinity Mountains in the northwest, the Modoc Plateau in the northeast, and the Sierra Nevada in the east.

The Sacramento is a rare large river in that its channel capacity gradually decreases in the downstream direction between the Butte Creek and Feather River confluences (Figure 2.6), leading prehistorically to extensive floodplain inundation [*Gilbert*, 1917; *Kelley*, 1998]. The advent of permanent human settlement into this flood regime led to the Sacramento Valley Flood Control Project, a system of flood control levees, weirs, and bypasses built between 1917 and 1929 [*Water Engineering &Technology*, 1990], designed to convey flood waters through the Sacramento River and adjacent floodways. To relieve pressure on the channel banks, high flows are diverted into Sutter and Yolo bypasses via five major weirs. The flood control system was bolstered between 1943 and 1970 with the construction of a number of dams, including Shasta Dam on the Sacramento River.

Sacramento Hydroclimatology

The Sacramento Valley has a Mediterranean climate with mostly dry summers and wet winters dominated by large frontal rainstorms in the winter with occasional snowmelt floods in the spring. Annual precipitation in the basin ranges from 25 cm in the southern part of the valley to 250 cm in the mountains to the north and east with more than 80% of precipitation occurring between November and March [*Jones et al.*, 1972].

The majority of the flood flow at the basin outlet originates in the mountainous portions of tributary basins, and not in the Sacramento lowland [*Thompson*, 1960]. Moderate sized floods can be generated from melting snowpack in the Sierra Nevada, but major floods in the Sacramento River under present conditions of flood control are generated by rain on melting snow during winter [*Thompson*, 1960].

Many tributaries flow into the Sacramento (Figure 2.6), including the large American and Feather Rivers that drain the Sierra Nevada. Discharge contribution from Coast Range tributaries is limited because they have drier climates, and many are controlled by impoundments or captured by a system of irrigation canals that run parallel to the Sacramento River. The northern perennial streams rise from the Trinity Mountains to the northwest and the Modoc Plateau to the northeast.

In this paper I apply HYDROCARLO to the mainstem Sacramento River south from Keswick (below Shasta Dam) to the town of Freeport (south of Sacramento), using data from primary tributaries near their confluence with the mainstem (Figure 2.6). I define primary tributaries in this basin as those which have drainage area of at least 300 km^2 and at least 10 years of continuous daily streamflow data. My drainage area threshold of 300 km^2 is approximately one half of one percent of the total drainage area for the study area (5.2×10^4 km^2). The total study area was calculated by subtracting drainage area disconnected from the mainstem Sacramento by engineering structures from the drainage area at Freeport. The majority of daily flow records from Sacramento tributaries span several decades, so I have chosen 10

years as a time scale representative of the hydroclimatological correlation in flow records between gauges. Therefore, I used only flow records from stations that had records of at least 10 years. Two creeks that fit my drainage area criterion, Pine Creek (536 km^2) and Burch Creek (412 km^2), were omitted from this analysis due to lack of streamflow records.

Figure 2.6 shows the primary tributaries and the gauges used in this study for historical flood selection and Table 2.1 shows statistics on each primary tributary. The primary tributaries used in this study comprise more than 90% of the study area. I included additional tributaries in my simulations to account for the ungauged drainage area, the specifics of which are discussed below.

Regional Parameterization

Regional parameterizations of seasonality, event basis, and correlation in events are outlined below. However, I make an additional modification to hydrologic datasets that are influenced by major dams on the following tributaries: Sacramento River at Keswick, the Feather River, the American River, and Clear Creek. I discarded hydrologic data that were recorded during the period of reservoir filling (using information provided by the United States Bureau of Reclamation and the California Department of Water Resources), a period that was not representative of natural or regulated flow conditions. I divided the remaining data at these gauges into pre- and post-dam hydrologic series. Stony Creek also has upstream impoundments

(Table 2.1), but the historical record at the gauge employed in this study was not operational in the pre-dam era.

Seasonality

I subdivided pre- and post-dam Sacramento basin hydrologic series into two distinct flood seasons: a wet season (November 1 - May 31), and a dry season (June 1 - October 31). I considered dividing the flood record into three seasons to represent the snowmelt period in the Sierra Nevada as a separate season. I inspected plots of February-March and April-May flow data for each of 20 years recorded at Feather River in the pre-dam era and could not detect obvious differences in the populations of flood events between them (e.g. flood duration, baseline discharge). The lack of a distinct snowmelt flood signal may be due to its attenuation over significant travel distance from the melting snow and the mixing of melt water with rain-derived floodwater from foothill tributaries. Therefore, I conservatively assume that there is no distinct hydrograph expression in the snowmelt season for Sierra tributaries, and by extension, for the Sacramento Basin as a whole, and therefore I model the basin with one wet and one dry season. I recognize the limitations of a user-defined approach to representing seasonality in my model, but have not as yet developed a more rigorously objective approach. However, my approach is no more inappropriate for defining seasons than traditional flood frequency techniques of segregating mixed flood populations by their generating mechanisms (c.f. [*Hirschboeck*, 1987]).

Event Basis

At each gauge I determined the baseline discharge and calculated the event probability on any given day, for each hydrologic series (i.e. pre-dam wet season, post-dam wet season, pre-dam dry season, etc.) according to the procedure described in Part 1 of this paper. Table 2.2 shows the seasonal baseline discharge calculated for pre- and post-dam simulations at each tributary gauge.

The process of defining the baseline discharge and calculating event probabilities provides some insight into the differences between wet and dry seasons in pre- and post-dam hydrologic regimes. For example, since dams were constructed on impounded tributaries (e.g. Feather River, American River), the baseline discharge and the event probability at these gauges have increased in the dry season and decreased in the wet season to serve irrigation and flood control (Table 2.2).

Correlation in Events

I calculated seasonal *ABC* for pre-dam simulations using data from Bend Bridge and American River for 1905-1942, and for post-dam simulations using data from Keswick and American River over the years 1964-1997. I used the following criteria to determine the number of bins into which the flood matrices were divided: one bin for $\rho <= 0.25$, two bins for $0.25 < \rho < 0.50$, three bins for $0.50 < \rho < 0.75$, four bins for $0.75 < \rho < 1.00$. The pre-dam result is an *ABC* of 0.79 and the post-dam result is an *ABC* of 0.78. Table 2.2 contains the seasonal initialization parameters,

baseline discharge and event probability, for each gauge in pre- and post-dam simulations, respectively.

High *ABC* for both pre- and post-dam series signifies that the Sacramento River Basin is affected by regional storms that increase discharge in many tributary basins within a 24-hour period (historical data are mean daily discharge). This interpretation is corroborated by inspection of National Climatic Data Center historical precipitation maps (http://lwf.ncdc.noaa.gov/oa/ncdc.html) for storm days, which portray high daily rainfall totals over most of the basin.

Model Verification

I check to see whether simulated hydrographs from simulations (i.e. 50 n-year runs of the model) routed through the mainstem are statistically similar to historical data for these locations. Verifying HYDROCARLO at a gauge located some distance downstream from tributary confluences (e.g. at the basin outlet) requires explicit flood routing to account for channel dimensions, the velocity of flowing water, overbank flow storage and losses, diversion weirs, and channel characteristics such as roughness. I used the flow routing package, HEC-RAS to model these factors [*Brunner and Bonner*, 1994]. The cross-sectional data for the lower Sacramento were extracted from a US Army Corps of Engineers (USACE) bathymetric survey from 1997 and those for the upper Sacramento from a 2001 California Department of Water Resources (CDWR) bathymetric survey. Hydraulic roughness values for the channel and adjacent floodplain were obtained from calibrations by USACE and

CDWR for their respective datasets. Locations and dimensions of diversion weirs were obtained from US Geologic Survey 1:24,000 topographic maps and from CDWR.

I represented the Sacramento River within HEC-RAS geometrically as a single channel with ~1000 cross-sections spaced ~0.4 km apart. Dimensions and locations of major flood diversion weirs were included in the modeling as lateral spill weirs according to standard HEC-RAS procedures [*Brunner and Bonner*, 1994]. The flow over Moulton, Colusa, and Tisdale weirs was routed into Sutter Bypass east of the Sacramento, where it was added to the tributary inflow from Butte Creek and Feather River. Flow over Fremont and Sacramento Weirs is routed to Yolo Bypass, which drains back to the Sacramento River outside of my model space. Whereas each of the other weirs is operationally passive, Sacramento Weir has 48 gates that are opened and closed by the USACE and CDWR according to a complex set of rules [*US Army Corps of Engineers*, 1998]; *R. Eckman*, CDWR, pers. comm.]. However, to simplify my HEC-RAS modeling, I represent Sacramento Weir as a passive weir with elevation equal to that at the bottom of the gates. I recognize that this may introduce consistent bias to flows routed downstream of this weir, but could devise no better modeling strategy for this weir given the complexity of the flood control system.

I ran HEC-RAS with unsteady lateral inflow on a daily step (with an hourly computational time step) using hydrographs stochastically generated by HYDROCARLO at each primary tributary. I analyzed flood frequency statistics for

the routed flows and compared them to frequency statistics for completely independent historical streamflow records at gauges near the basin outlet. In pre- and post-dam simulations I verified the model's ability to simulate the central tendency and distribution of the following hydrograph characteristics: 1) annual maximum flood peak; 2) mean annual flood; 3) total annual flood volume; 4) mean annual flood duration; 5) mean annual duration of hydrograph recession (i.e. drawdown from flood peak to baseline discharge); and 6) mean annual interarrival time. Annual peaks were calculated by selecting the maximum discharge of each year for both historical and simulated data. Mean annual flow, flood volume, flood duration, and hydrograph recession were calculated for the partial duration series above the wet-season baseline discharge from all upstream gauges added together.

Pre-Dam

In pre-dam simulations I verified HYDROCARLO at Verona using data from 1929-1943 (the entire pre-dam period of record at this gauge). Verona is the only mainstem gauge near the basin outlet and upstream of the delta with historical streamflow records that extend prior to dam construction. The pre-dam simulations in the model were run using data from the following gauges: Antelope Creek, Bend Bridge, Butte Creek, Deer Creek, Elder Creek, Mill Creek, Feather River, Stony Creek, and Thomes Creek (Figure 2.6). The pre-dam inflow data for tributaries upstream of Bend Bridge amounted to less than 10 years of daily data so I replaced these upstream tributaries with the gauging records from Bend Bridge itself (52 years

of pre-dam data). I included tributary input from Cow and Cottonwood Creeks in HYDROCARLO simulations to account for the ungauged drainage area discussed previously.

Post-Dam

For the post-dam scenario, I verified HYDROCARLO at Verona and Freeport (Figure 2.6) using data from the period following major dam construction in the basin (i.e. 1970-2000). The post-dam simulations in HYDROCARLO were run using data from the following gauges: American River, Antelope Creek, Battle Creek, Butte Creek, Clear Creek, Cottonwood Creek, Cow Creek, Deer Creek, Elder Creek, Feather River, Keswick, Mill Creek, Stony Creek, Thomes Creek (Figure 2.6). I included tributary input from American River (pre-dam) in HYDROCARLO simulations to account for ungauged drainage area that is unaffected by impoundments.

Verification Results

Numerous flow properties can be decomposed from any hydrograph, whether it is recorded or simulated. I have chosen six properties to verify HYDROCARLO's ability to simulate hydrographs that represent historical flood peak, duration, shape, and timing. However, this is by no means an exhaustive list of flow properties that can be extracted from HYDROCARLO's hydrographs. Although I have taken efforts to verify that HYDROCARLO predicts historical flow characteristics well on the

mainstem, the model is (like the flood frequency curve itself) essentially unverifiable. However, it is possible to validate the utility of the model in repeated applications to decision-making in which it is found to be useful. In general, my simulations accurately describe the flow conditions recorded during the pre- and post-dam eras. From them I calculated a range and central tendency of all simulations for each era (Figures 2.7, 2.8, 2.9, and 2.10).

Annual Peak, Mean Annual Flow, and Flood Volume

Figures 2.7 and 2.8 show the results of three probability checks on pre- and post-dam hydrographs generated by HYDROCARLO at Verona and Freeport, respectively. Each depicts the historical data as crosshairs and the simulations as dots, all plotted on Log Pearson III probability paper. The dark line in each plot represents the median value of all simulations and the dashed lines represent their range.

The historical flood peaks at Verona (Figure 2.7a) bound the simulated range of annual maximum peaks at the lowest and highest exceedence probabilities. The lower bound of simulated peaks at the highest exceedence probability, or the flow most frequently exceeded, is set to the value of combined, routed wet season baseline discharge from all tributaries, which is slightly higher than the lowest historical annual peak. However, this is not a concern because HYDROCARLO was developed to simulate flows above baseline discharge. At the lowest exceedence probability, the simulated flood peak at Verona is asymptotic to 2178 cms in the pre-dam era (Figure

2.7a) and 2614 cms in the post-dam era (Figure 2.7d). These values represent the thresholds of flood flow, above which flow spills over Fremont Weir. The weir constrains the variability of annual-maximum flows upwards of 2000 cms to a narrow range. This is the reason that the simulated range (i.e. the uncertainty) does not increase at the lowest exceedence probabilities, as would be expected in flood frequency curve for a river reach devoid of flood control weirs. It is noteworthy that pre-dam peaks of flow within the leveed channel at Verona (or Freeport) are lower than post-dam ones and this matter is discussed below. Otherwise, pre- and post-dam simulated flood peaks bound the historical data and illustrate the potential range of variability, especially for flows of intermediate frequencies that transport most sediment [*Singer and Dunne*, 2001] and drive important ecological processes [*Mahoney and Rood*, 1998; *Milhous*, 1998; *Pitlick and Van Steeter*, 1998; *Johnson*, 2000]. There are no pre-dam historical data at Freeport, but I simulated pre-dam flows at this location (Figure 2.8a-c). Again, the annual historical post-dam peaks are bracketed by post-dam simulations from HYDROCARLO that were routed via HEC-RAS.

Mean annual flow simulations at Verona bound pre- and post-dam historical data for all but the highest exceedence probability (Figures 2.7b and e). It appears that mean annual flow at Verona has increased slightly in the post-dam era concomitant with the increase in annual peaks, and my simulations reflect that change. Historical mean annual post-dam flow at Freeport is also well predicted by HYDROCARLO simulations (Figure 2.8e). There is a larger simulated range for the

lowest exceedence probabilities at Freeport, perhaps due to the lesser effect its upstream weir has on flow in the main channel (Sacramento Weir has less than 1/3 the spill capacity of Fremont Weir).

Flood volumes appear to have changed very little between the pre- and post-dam eras (Figure 2.7c and f), except that the longer record in the post-dam era has sampled larger flood volumes at the lowest exceedence probabilities, thereby better reflecting the flow variability. In general, simulated data from HYDROCARLO are biased upwards of the historical data (exceedence probability > 0.6) in the post-dam era for both Verona (Figure 2.7c and f) and Freeport (Figure 2.8c and f). This is probably due to my lack of accounting for water diverted out of the Sacramento for irrigation (e.g. via the Glen-Colusa Irrigation District Canal). The effect of these withdrawals would be significant in drought years. I currently do not have the data to accurately simulate diverted flow volumes. Otherwise, my simulations bracket all historical data at Verona and Freeport.

Flood Duration, Drawdown, and Interarrival Time

Figures 2.9 and 2.10 show the results of three more probability checks on pre- and post-dam hydrographs generated by HYDROCARLO at Verona and Freeport, respectively. The symbols are the same as Figures 2.7 and 2.8.

Flood duration at Verona appears to have changed very little between the pre- and post-dam eras and my simulations bracket the historical data in both cases (Figure 2.9a and d), as well as for Freeport (Figure 2.10d). Drawdown duration

describes the shape of the falling limb in comparison with the entire flood duration. In the Sacramento River, the rising limb of the hydrograph tends to be very short in duration [*Singer and Dunne*, 2001]. Thus the plots of drawdown duration look very similar to those of entire flood duration (c.f. Figures 2.9b and e with Figure 2.9a and d), and again my simulations bracket the historical data. The lack of major changes in flood duration and drawdown between eras is probably due to the similar effect of flood attenuation by upstream flood control dams in the post-dam era and upstream floodplains in the pre-dam one. It is not clear why my simulations of pre-dam drawdown at Freeport (Figure 2.10b) produce much lower pre-dam durations than post-dam ones, but it may be the combinded result of reservoir and weir operations (Figure 2.10e). Interarrival times appear to have increased slightly between eras (c.f. Figures 2.9c and f), perhaps due to the effects of flood control in damping out the smallest flood peaks. This effect is replicated between my pre- and post-dam simulations at Freeport (Figures 2.10c and f).

Discussion

HYDROCARLO is a single tool that can be used in conjunction with flow routing models to analyze a spectrum of floods and flow properties for analyses in engineering, geomorphology, and ecology. With numerous simulations HYDROCARLO is capable of producing representative estimates of flow properties that may be used for simulating flow at mainstem locations for which there are no gauging records, for assessing risk in a fluvial system, and for detecting bed level

change. The model was developed to perform simulation using historical data from the Sacramento basin, but may be adapted to reflect the hydroclimates of other basins, as well as to represent unrecorded events in a particular basin.

Simulating Flow at Ungauged Mainstem Locations

Estimates of flow properties at ungauged mainstem locations are required for a number of purposes. In engineering applications, point estimates of peak flow and total annual flow volume may be needed to design flood control levees and diversion structures. Estimates of sediment transport and hydrograph fluctuation may be important in determining the operational capacity and longevity of such engineering works. In geomorphic applications, local flow estimates are required to assess thresholds for sediment transport, to route sediment through river reaches, and to model sediment concentration, floodplain inundation, and floodplain sedimentation. In ecological applications, local estimates of instream flow and overbank flow may be required to assess quality of fish and benthic habitat and inundation regimes of riparian habitats, respectively. Estimates of sediment transport may also be required to calculate the frequency of flushing flows and general habitat disturbance. Rates of drawdown may be needed to test whether riparian seedlings in a particular area could viably germinate and establish themselves on floodplains.

In the absence of detailed hydrographs at particular locations, estimates of flow properties are generally transferred from the closest streamflow gauge, which might be tens of river kilometers away and possess very different hydraulic

conditions from the site in question. HYDROCARLO can provide flow estimates at the relevant locations for a variety of at-a-point analyses.

Assessing Risk in a Fluvial System

The concept of risk has been used to describe hazard, expected loss, or the probability of an outcome [*US Army Corps of Engineers*, 1992]. Risk analysis is currently used in design and maintenance of flood control levees [*National Research Council*, 2000] and in design of dam and storage facilities [*Federal Energy Regulatory Commission*, 1993]. Analysis of potential outcomes has utility in applications of sediment transport and the restoration of aquatic and riparian habitats, which are generally sensitive to various hydrograph components including magnitude, frequency, timing, duration, and rate of change [*Poff et al.*, 1997].

For example, in order for riparian cottonwood seedlings to successfully germinate and recruit they require a flood pulse sufficient to wet the floodplain surface for seed deposition [*Mahoney and Rood*, 1998]. Once this flood peak occurs, seedling survival depends on drawdown rate, such that saturated sites are exposed for seedling establishment and growing roots maintain contact with the capillary fringe on the water surface. Although cottonwood roots grow anywhere from 0.5-1.0 cm/day, a maximum survivable rate of water-table decline is approximately 2.5 cm/day [*Mahoney and Rood*, 1998]. Existing methods for analyzing flow at ungauged locations are limited and often involve the use of pressure transducers to infer stage over a single flood season (J. Stella, UC Berkeley, pers. comm.). Such a

strategy provides little guidance in evaluating the likelihood of a particular flood to occur in the season of riparian seedling germination, because the historical record is relatively short.

HYDROCARLO may be used to assess whether hydrologic conditions for a particular place are suitable for the establishment and recruitment of cottonwoods. It may also be used to evaluate the probability of successful cottonwood recruitment. For example, posit a potential cottonwood recruitment site north of Tehama ~3 km downstream of Elder Creek confluence (Figure 2.6). I simulated annual stage peaks and stage decline rates for this location between April and May (the period April though mid-June was identified as the cottonwood germination season in the nearby San Joaquin River basin, J. Stella, UC Berkeley, pers. comm.) using pre- and post-dam flow regimes. Figure 2.11a shows that under the pre-dam flow regime, the stage necessary to access the floodplain (68.7 m) was exceeded approximately 30% of the time, whereas it is rarely if ever exceeded in the post-dam flow regime (Figure 2.11c). The implication is that the current flow regime is not viable for the establishment of cottonwood seedlings. Figure 2.11b shows that in the pre-dam flow regime the maximum drawdown rate of 2.5 cm/day is exceeded approximately 10% of the time. In the post-dam flow regime, however, the maximum drawdown rate is exceeded approximately 45% of the time (Figure 2.11d) during the critical period of seedling root growth [*Mahoney and Rood*, 1998]. The implication here is that the current flow regime is not conducive to the establishment of cottonwoods and may be a severe limit on their subsequent growth. Although this is a preliminary result requiring more

rigorous analysis of local cottonwoods, it is clear that some type of flow alteration would be necessary to restore cottonwood stands in this floodplain location.

HYDROCARLO can be used to provide a range of boundary conditions for analyses of sediment transport and routing, floodplain inundation and sedimentation, and the relationship between streamflow and habitat functioning. It may be used to predict potential outcomes to numerous modifications in large fluvial systems. However, a complete discussion of HYDROCARLO's utility in these applications is beyond the scope of this paper. Generally, HYDROCARLO simulates numerous potential flow outcomes that can enhance flood frequency analysis by predicting the range and central tendency of various flow properties at each plotting position.

Using HYDROCARLO to Detect Bed Level Change

The use of HYDROCARLO simulations within HEC-RAS has led to new insights into the relationship between flood control structures and bed level in the Lower Sacramento River. The following discussion illustrates how the application of a stochastic model to a fluvial system highlighted a decadal change in the fluvial system.

Evidence

The Sacramento flood control system was designed to shunt flow above certain thresholds through weirs into bypasses that eventually drain to the San Francisco-Sacramento-San Joaquin Bay-Delta. Thus as flow from upstream increases

(above the threshold for flow over the weir), there should be ever larger increases in flow over the weir compared with flow increases through the mainstem downstream of the weir. Since flow in the mainstem is published as mean daily discharge, smaller and smaller increments of flow increase at a mainstem gauge downstream would tend to be asymptotic to a particular value of discharge. The flood frequency (of annual maximum peak flows) at a gauging station downstream of the flood weir can thus be thought of as asymptotic to the discharge at which increasing flow from upstream would cause no increase at that gauge. This asymptote should be more or less steady through time, as long as there are no modifications to the flood control system, significant changes in roughness, or bed level changes. If the channel bed were to erode significantly, the connection between mainstem channel flow and flow passing over the weir would be altered. Larger discharges would reach the downstream gauge causing the asymptote to shift upward. Figure 2.12 illustrates how bed level changes could alter flood levels and change the functioning of the flood control system. With increased channel bed erosion the flow depth at which the weir is overtopped increases, and higher peak flows pass downstream through the main channel.

Inspection of pre- and post-dam historical flood peaks at Verona shows larger flows in the post-dam era than in the pre-dam one (crosshairs in Figures 2.7a and d). However, this seems counterintuitive given that dams have been operated to control the largest flood peaks. Working under this assumption alone, one could only surmise that the pre-dam historical period represented in this analysis was one of anomalously low flood peaks compared to the post-dam one. My pre-dam

simulations from HYDROCARLO, however, utilized high flood flows from each tributary and especially at the upstream boundary condition of Bend Bridge. But these higher discharge boundary conditions did not elevate mainstem flood peaks at Verona beyond those of the historical data for the lowest exceedence probabilities, because they were shunted out of the model space in HEC-RAS simulations via Fremont Weir upstream of the gauge. Other possibilities for the higher flood peak asymptote in the post-dam era include alterations to the flood control system, significant change in roughness, and bed level change. There have been no major alterations to the flood control system [*US Army Corps of Engineers*, 1998] and I assume that roughness has only undergone minor changes. I used HYDROCARLO in conjunction with HEC-RAS to investigate bed level change in the lower Sacramento River.

A previous study documented erosion on the bed in the Sacramento River between Knights Landing and Sacramento [*Water Engineering &Technology*, 1990] and I calculated an average erosion rate for this reach of 1.7 $cmyr^{-1}$ for the time period 1948-1979 from the sediment transport budget [*Singer and Dunne*, 2001]. Here, I use HYDROCARLO to examine whether changes in the flood peak asymptote are consistent with annual channel-bed erosion in the reach.

Procedure

I simulated 50 fourteen-year model runs (pre-dam) and 50 thirty-year model runs (post-dam) to identify the asymptote at Verona for each era. Then I selected one

simulation in each era that is asymptotic to the highest simulated peak flow and saved its boundary conditions (i.e. inflow hydrographs) in HEC-RAS. Next I ran more HEC-RAS simulations with these same inflow hydrographs while adjusting the elevation of Fremont Weir (rather than adjusting the bed elevation at each cross-section) until the simulated asymptote equaled that of the historical data (i.e. pre-dam peak = 2178 cms and post-dam peak = 2614 cms). In other words, I zeroed HEC-RAS, so that historical data and simulations for each era had a common datum (or in this case, a common elevation for Fremont Weir). Once the asymptotes matched, I re-ran all the simulations for each era and used the resulting simulations for model verification (Model Verification).

Erosion Rate

Since simulations for both eras were zeroed, I could calculate the difference in the elevation of Fremont Weir between them. I divided this elevation difference by the number of years between the eras to arrive at an average annual erosion rate for this reach of river in intervening period. This result is 1.9 cm yr^{-1} (79 cm between the first year of each era, 1929 and 1970), which is close to the 1.7 cm yr^{-1} rate for the period 1948-1979, independently predicted in my analysis of suspended sediment transport [*Singer and Dunne*, 2001]. This erosion trend is corroborated by flow data from the Fremont Weir Spill. Figure 2.13 shows that from 1955 to 1975 there was a progressive change in the partitioning of water between the main channel and the flow over the weir. For example the weir spill diminished from ~4300 cms between

1955 and 1957 to ~1000 cms between 1973 and 1975 for a mainstem flow of ~1850 cms at Verona. Likewise mainstem flow at Verona increased from ~1600 cms between 1949-51 to ~1850 cms between 1973-75 for Fremont Weir spill of ~1000 cms. Although there are clearly episodes of erosion and deposition in this reach, there is an apparent trend of erosion that persisted over 25 years. Over this same period there is a weakly increasing trend in combined annual peak discharge from Fremont Weir spill and Verona (R^2 = 0.31 and p = 0.222), indicating that changes in the partitioning of water between the weir and the mainstem are not due to diminished flood flow.

Figure 2.14 shows a frequency plot of pre-dam and post-dam historical flood peaks (open circles) and one simulation with a zeroed asymptote (plusses). Each asymptote has a label that corresponds to the highest peak flow for the bed elevation of that era. I then altered the elevation of Fremont Weir for flood-routing simulations, assuming the constant bed erosion rate. The upper panel shows how boundary conditions from a pre-dam simulation (beginning in 1929) would look after being routed through the river channel of the post-dam era (beginning in 1970). Remarkably, routing high pre-dam flows through the post-dam channel (i.e. with lowered bed level equal to that of the post-dam era) produces peak discharges asymptotic to the approximately the same peak flow that was recorded in the post-dam era (~2500 cms). If the erosion trend were to continue into the future, the same flood-frequency regime in the tributaries and upper mainstem would pass progressively larger floods to the lower Sacramento (Figure 2.14, lower panel).

Implications

These results have implications for flood control in the lower Sacramento. First, flood control dams have had very little impact on the largest peak flows in the leveed channel of the lower Sacramento River. I have demonstrated by normalizing flow for changes in bed elevation, that peak flows in the post-dam era are approximately the same as those in the pre-dam era. In other words, flood control dams in the Sacramento basin do not diminish the largest peak floods traveling through the channel of the lower river. The *[US Army Corps of Engineers, 1998]* documented that flows discharged from Shasta Dam take 62 hours to reach Verona. As a result, high flows may be released from Shasta prior to the arrival of a large, swift rainstorm in the lower Sacramento Valley. Such a rainstorm may cause increased flood discharges from the lower Feather River basin, for example, to arrive at its confluence with the Sacramento concurrent with the high flow release from Shasta. This inefficiency in flood control would be inherent in any basin where flood control dams are located at the outer edges of a large valley, and where large and swift storms are generated in the lower part of the basin.

Second, although channel capacity increases with incision, there is nevertheless an increase in flood risk for areas outside the levees of the lower Sacramento. Incision can expose unprotected and permeable banks (i.e. below riprap and levees), and weaken aged levee materials. Flow from the main channel can seep under or through porous levee materials and emerge from the floodplain outside the

levee. Perched water tables and evidence of boils and piping have been reported outside the East Levee along Pocket Road in the City of Sacramento in the reach between Verona and Freeport (M. Salvador, CDWR, pers. comm.). Incision can also focus shear stress at the toe of riprap or a levee, and weaken the engineering structure by undercutting its toe. Such a scenario could eventually lead to levee break and catastrophic flooding in a populated area.

Adapting HYDROCARLO

The streamflow simulation model is applicable to large river basins for which streamflow data are spatially and temporally abundant. The predictive power of HYDROCARLO is increased by the length of synchronous records for each major tributary in a basin and by records that represent the entire range of flood events that could occur at a particular station. The model may be adapted for a particular river basin by altering the across-basin correlation and/or the number of bins. If the modeler determined that *ABC* were particularly high between the most distant gauges, but assumed there was some reason other than basinwide storms for correlation between these gauges, then this information should be used to assess across-basin correlation. For example, in a large river basin that spans a wide range of latitude, flood event ranks at the two most distant gauges might lie along an east-west axis, and therefore be correlated according to latitude. In this case, across-basin correlation should be tested between flood peaks from gauging stations furthest from each other in the north-south direction, instead of those furthest in absolute distance.

The number of bins used in HYDROCARLO is set using *ABC*, a measure assumed to represent the relationship between all gauges in the basin. This assumption may be relaxed to account for local relationships between gauges by varying the number of bins used. For example, if across-basin correlation were low (< 0.25) between the most distant gauges, but it was assumed that correlation was higher between some gauges in the network, one bin for flood event selection over the entire basin would be insufficient to represent this relationship. To rectify this problem, the modeler could test for correlation between each gauge and every other gauge in the basin to develop a system of look-up tables containing differing numbers of bins. For example, if the correlations in synchronous flood peaks (1) between Gauge 3 and Gauges 4, 5, and 6, were 0.4, 0.6, and 0.8, respectively, flood events would be chosen at Gauges 4, 5, and 6 from two, three, and four bins, respectively (Figure 2.1). The number of bins for each correlation range (and the correlation ranges themselves) could also be altered to reflect more complexity in a particular river basin.

HYDROCARLO's predictive capability could be improved by augmenting historical streamflow records with synthetic hydrographs for extreme floods using data from ancillary sources. This has been recommended to better capture hydrologic trends and the statistical distribution of natural phenomena [*National Research Council*, 1991; *Archer*, 1999]. Flood event selection at any tributary is limited at the upper end of the distribution (i.e. at the lowest exceedence probability) by the largest flood event of record. Field evidence has demonstrated, however, that events larger

than those recorded have likely occurred in the past, and such events are likely to occur again in the future [*Baker et al.*, 2002]. Therefore, theoretical hydrographs constructed for such floods should be added to the historical record from which HYDROCARLO selects events, in order to widen the range of possible flood events and represent potential events that have not been recorded. Estimates of peak flow can be made by a variety of paleohydrological proxies including tree ring analysis, palynology, fluvial deposits, and surveys of tributary channel dimensions. These techniques provide guidance in creating theoretical hydrographs that represent extreme flood conditions in a particular river system. However, the technique for adding these large floods to the flood matrix (Figure 2.3) with the appropriate frequency requires further research.

Conclusion

The HYDROCARLO stochastic streamflow generator stochastically represents spatio-temporal patterns in tributary inflow by incorporating the seasonality in flow and the correlation in flood event occurrence and flood peak magnitude that are reflected in historical streamflow records. It produces simulated sets of synchronous tributary inflow to a large river. I applied the model to the Sacramento River Basin, utilizing tributary gauges to simulate mainstem hydrology. I conducted preliminary verification of the model by comparing the frequency of various hydrograph characteristics from the simulated series with those from historical records at mainstem gauging points for pre- and post-dam flow scenarios.

The model produces output that can be used for numerous applications including simulating flows at ungauged mainstem locations, assessing flood risk, characterizing the flooding regimes in ways that are relevant for ecosystem functioning, and detecting bed level change. HYDROCARLO may be adapted for different hydroclimates and its predictive capability could be improved by incorporating synthetic hydrographs of unrecorded extreme floods at tributary gauges.

References

Archer, D., Practical application of historical flood information to flood estimation, in *Hydrological Extremes: Understanding, Predicting, Mitigating*, edited by L. Gottschalk, J.C. Olivry, D. Reed, and D. Rosbjerg, pp. 191-199, IAHS, Wallingford, UK, 1999.

Baker, V.R., R.H. Webb, and P.K. House, The scientific and societal value of paleoflood hydrology, in *Ancient Floods Modern Hazards*, edited by P.K. House, R.H. Webb, V.R. Baker, and D.R. Levish, pp. 1-19, American Geophys. Union, Washington, D.C., 2002.

Benson, M.A., and N.C. Matalas, Synthetic hydrology based on regional statistical parameters, *Water Resources Research*, *3* (4), 931-935, 1967.

Beven, K.J., *Rainfall-Runoff Modelling, A Primer*, 360 pp., J. Wiley & Sons, Chichester, 2000.

Brunner, G.W., and V. Bonner, HEC river analysis system (HEC-RAS), Hydrologic Engineering Center, Davis, CA, 1994.

Burnash, R.J.C., R.L. Ferral, and R.A. McGuire, *A generalized streamflow simulation system: Conceptual modeling for digital computers*, 204 pp., National Weather Service, Sacramento, CA, 1973.

Church, M., and M.A. Hassan, Size and distance of travel of unconstrained clasts on a streambed, *Water Res. Research*, *28* (1), 299-303, 1992.

Cleveland, W.S., Robust locally weighted regression and smoothing scatterplots, *J. Amer. Stat. Assoc.*, *74*, 829-836, 1979.

Earle, C.J., and H.C. Gritts, Reconstructing riverflow in the Sacramento basin since 1560, Laboratory of Tree-Ring Research, Tucson, AZ, 1986.

Federal Energy Regulatory Commission, Engineering Guidelines for the Evaluation of Hydropower Projects, FERC, Washington, D.C., 1993.

Fiering, M.B., *Streamflow Synthesis*, 139 pp., Harvard Univ. Press, Cambridge, MA, 1967.

Gilbert, G.K., Hydraulic-mining debris in the Sierra Nevada, US Geol. Sur., Menlo Park, CA, 1917.

Gleick, P.H., The development and testing of a water balance model for climate impact assessment: Modeling the Sacramento basin, *Water Resources Research*, *23* (6), 1049-1061, 1987.

Hannan, E.J., A test for singularities in Sydney rainfall, *Aust. J. Phys.*, *8* (2), 289-297, 1955.

Hirsch, R.M., A comparison of four streamflow record extension techniques, *Water Resources Research*, *18* (4), 1081-1089, 1982.

Hirschboeck, K.K., Hydroclimatically-defined mixed distributions in partial duration flood series, in *International Symposium on Flood Frequency and Risk Analyses*, edited by V.P. Singh, pp. 199-212, D. Reidel Pub. Co., Baton Rouse, LA, 1987.

Hirschboeck, K.K., Flood hydroclimatology, in *Flood Geomorphology*, edited by V.R. Baker, R.C. Kochel, and P.C. Patton, pp. 27-49, J. Wiley & Sons, New York, 1988.

Ingram, B.L., J.C. Ingle, and M.E. Conrad, A 2000 yr record of Sacramento-San Joaquin river inflow to San Francisco Bay estuary, California, *Geology*, *24* (4), 331-334, 1996.

Johnson, W.C., Tree recruitment and survival in rivers: influence of hydrological processes, *Hydrological Processes*, *14*, 3051-3074, 2000.

Jones, B.L., N.L. Hawley, and J.R. Crippen, Sediment transport in the Western tributaries of the Sacramento River, California, US Geol. Survey, Washington, D.C., 1972.

Junk, W.J., P.B. Bayley, and R.E. Sparks, The flood pulse concept, in *International Large River Symposium*, edited by D.P. Doge, pp. 110-127, Can. Fish. Aquatic Science Special Publ., 1989.

Kelley, R., *Battling the Inland Sea*, 395 pp., University of California Press, Berkeley, CA, 1998.

Lane, W.L., Aggregation and disaggregration modelling, in *Stochastic Hydrology and its Use in Water Resources Systems Simulation and Optimization*, edited by J.B. Marco, R. Harboe, and J.D. Salas, pp. 97-116, Kluwer Academic Pub., Dordrecht, The Netherlands, 1993.

Lettenmaier, D.P., and T.Y. Gan, Hydrologic sensitivities of the Sacramento-San Joaquin River basin, California, to global warming, *Water Res. Res.*, *26* (1), 69-86, 1990.

Lettenmaier, D.P., and D.P. Sheer, Climatic sensitivity of California water resources, *J. Water Resources Planning and Mngmt.*, *117* (1), 108-125, 1991.

Mahoney, J.M., and S.B. Rood, Streamflow requirements for cottonwood seedling recruitment-An integrative model, *Wetlands*, *18* (4), 634-645, 1998.

Matalas, N.C., and B.A. Jacobs, A correlation procedure for augmenting hydrologic data, US Geol. Survey Prof. Paper 434-E, Menlo Park, CA, 1964.

McLean, D.G., M. Church, and B. Tassone, Sediment transport along lower Fraser River 1. Measurements and hydraulic computations, *Water Resources Research*, *35* (8), 2533-2548, 1999.

Milhous, R.T., Modelling of instream flow needs: the link between sediment and aquatic habitat, *Regulated Rivers: Res & Mngmt*, *14*, 79-94, 1998.

Moog, D.B., and P.J. Whiting, Streamflow record extension using power transformations and application to sediment transport, *Water Resources Research*, *35* (1), 243-254, 1999.

National Research Council, *Estimating Probabilities of Extreme Floods: Methods and Recommended Research*, 141 pp., National Academy Press, Washington, D.C., 1988.

National Research Council, *Opportunities in the Hydrologic Sciences*, 348 pp., National Academy Press, Washington, D.C., 1991.

National Research Council, *Risk Analysis and Uncertainty in Flood Damage Reduction Studies*, 202 pp., National Academy Press, Washington, D.C., 2000.

National Research Council, *Future Roles and Opportunities for the U.S. Geological Survey*, 179 pp., National Academy Press, Washington, D.C., 2001.

Nijssen, B., and D.P. Lettenmaier, Streamflow simulation for continental-scale river basins, *Water Res. Research*, *33* (4), 711-724, 1997.

Pitlick, J., and M.M. Van Steeter, Geomorphology and endangered fish habitats in the upper Colorado River. 2. Linking sediment transport to habitat maintenance, *Water Resources Research*, *34* (2), 303-316, 1998.

Poff, N.L., J.D. Allan, M.B. Bain, J.R. Karr, K.L. Prestegaard, B.D. Richter, R.E. Sparks, and J.C. Stromberg, The natural flow regime, *Biosci.*, *47* (11), 769-784, 1997.

Richards, K., J. Brasington, and F. Hughes, Geomorphic dynamics of floodplains: ecological implications and a potential modelling strategy, *Freshwater Bio.*, *47*, 559-579, 2002.

Richter, B.D., J.V. Baumgartner, J. Powell, and D.P. Braun, A method for assessing hydrologic alteration within ecosystems, *Conserv. Bio.*, *10* (4), 1163-1174, 1996.

Risbey, J.S., and D. Entekhabi, Observed Sacramento Basin streamflow response to precipitation and temperature changes and its relevance to climate impact studies, *J. Hydrology*, *184*, 209-223, 1996.

Rodriguez-Iturbe, I., D.R. Cox, and V. Isham, Some models for rainfall based on stochastic point processes, *Proc. R. Soc. Lond.*, *A410*, 269-288, 1987.

Salas, J.D., D.C. Boes, and R.A. Smith, Estimation of ARMA models with seasonal parameters, *Water Resources Research*, *18* (4), 1006-1010, 1982.

Sharma, A., D.G. Tarboton, and U. Lall, Streamflow simulation: A nonparametric approach, *Water Resources Research*, *33* (2), 291-308, 1997.

Singer, M.B., and T. Dunne, Identifying eroding and depositional reaches of valley by analysis of suspended-sediment transport in the Sacramento River, California, *Water Resources Research*, *37* (12), 3371-3381, 2001.

Stedinger, J.R., and M.R. Taylor, Synthetic streamflow generation: 1. Model verification and validation, *Water Resources Research*, *18* (4), 909-918, 1982.

Sudler, C.E., Storage required for the regulation of streamflow, *Am. Soc. Civil Engrs. Trans.*, *91*, 622-, 1927.

Thompson, K., Historical flooding in the Sacramento Valley, *Pacific Historical Review*, *29*, 349-360, 1960.

Tockner, K., F. Malard, and J.V. Ward, An extension of the flood pulse concept, *Hydrological Processes*, *14*, 2861-2883, 2000.

US Army Corps of Engineers, Guidelines for Risk and Uncertatinty Analysis in Water Resources Planning, Water Resources Support Center, Fort Belvoir, VA, 1992.

US Army Corps of Engineers, Post-Flood Assessment for 1983, 1986, 1995, and 1997, Central Valley, California, Sacramento District, Sacramento, CA, 1998.

Valencia, R.D., and J.C. Schaake, Disaggregation processes in stochastic hydrology, *Water Resources Research*, *9* (3), 580-585, 1973.

Vecchia, A.V., Periodic autoregressive-moving-average (PARMA) modeling with applications to water resources, *Water Resources Bull.*, *21* (5), 721-730, 1985.

Water Engineering &Technology, Geomorphic analysis of Sacramento River, Water Engineering and Technology, Fort Collins, CO, 1990.

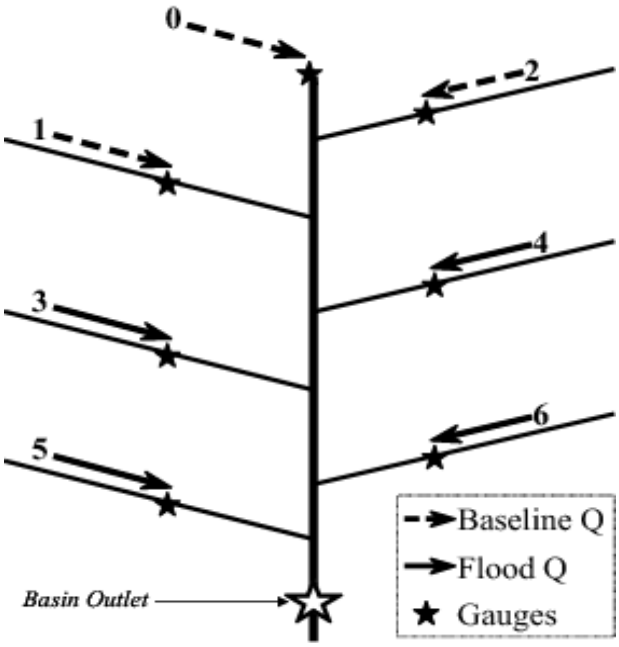

Figure 2.1 An idealized depiction of a drainage basin highlighting a network of tributary gauges upstream of the basin outlet. The figure shows one example of a range of possible rainstorms. In this case, the winter frontal rainstorm is inducing flood conditions at Gauges 3-6, while Gauges 0-2 are unaffected.

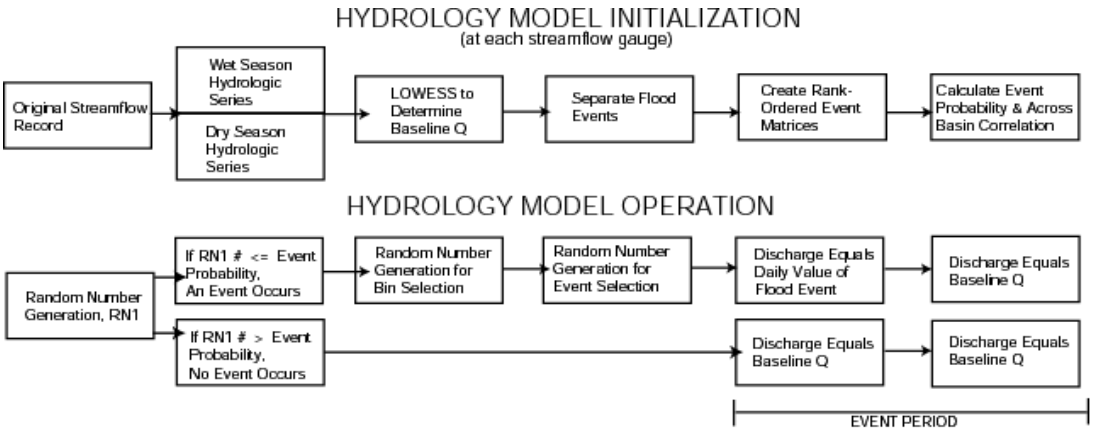

Figure 2.2 Flow chart shows important steps in model initialization which occur at each gauge, and model operation which occurs for all gauges simultaneously. RN1 (in Model Operation) corresponds to the random number generated at the beginning of each event period and is compared to the event probability at all gauges.

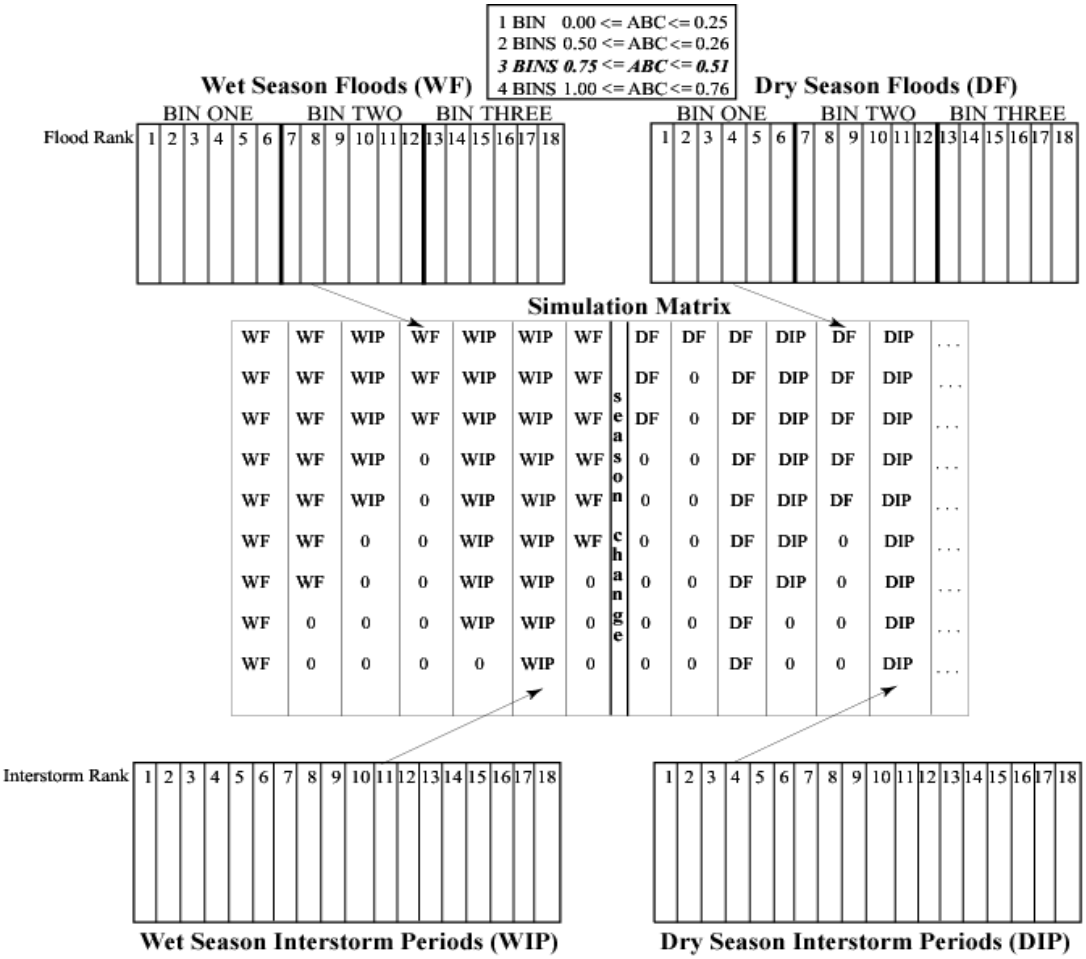

Figure 2.3 Diagram describes assemblage of the simulation matrix at each tributary gauge. Wet season flood events (WF) and interstorm periods (WIP) of varying lengths are chosen at random from their rank-ordered matrices and used as columns in the simulation matrix. Each column represents an event, which includes a column of discharge whose length is equal to the event's duration. Once wet season days are exhausted (45 days for this example), the simulation matrix is assembled using random selections from dry season flood and interstorm period matrices, until dry season days are exhausted. This continues for the duration of the simulation. HYDROCARLO divides seasonal flood matrices into a number of bins that narrow flood selection based on the influence of regional storms on flood flow at gauges across the basin. The floods are placed into the matrix by rank of their peaks and the across-basin correlation, ABC, is calculated to determine the number of bins to use. In this idealized case, ABC = 0.72.

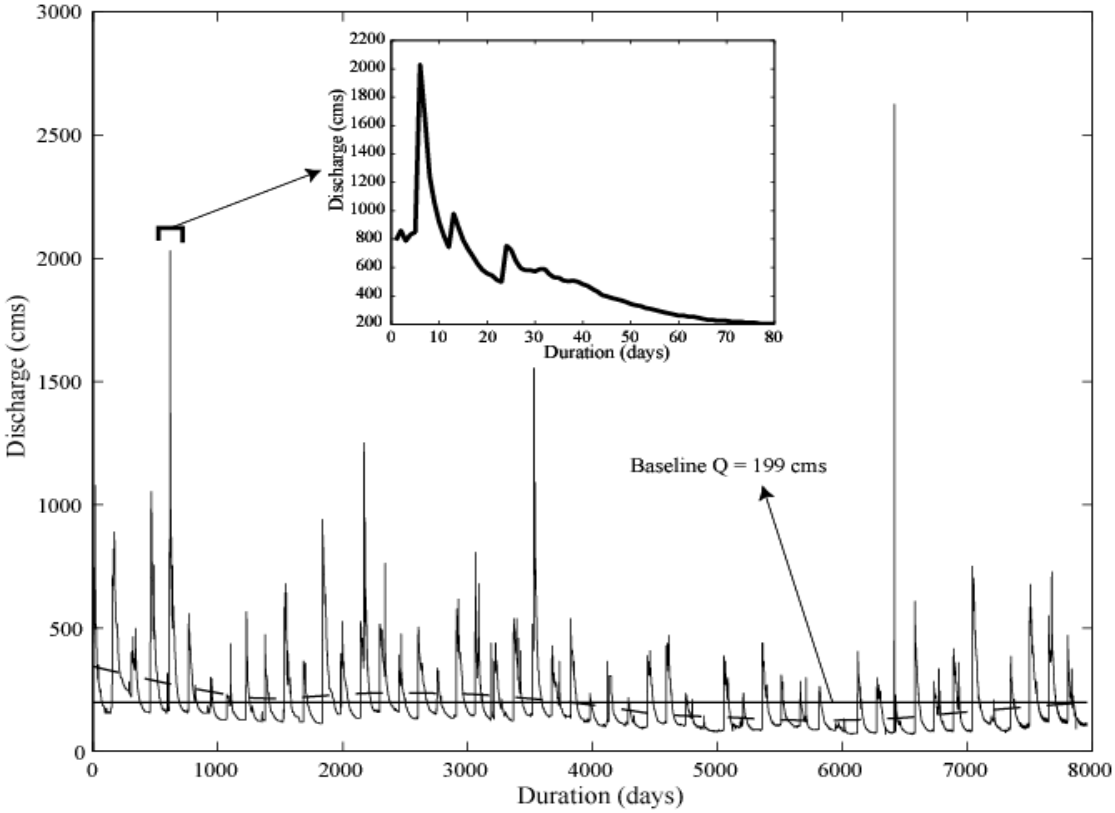

Figure 2.4 An example of baseline discharge calculation for the dry season flood series from Bend Bridge on the Sacramento River. The plot consists of a patchwork of all flood days in the dry season over a 49-year period. A smooth LOWESS curve is first fitted to the data (dashed line) and then its mean is calculated and called the baseline Q (labeled). Baseline Q is the threshold for a flood event. Discharge days above the threshold are considered flood days and those below the threshold are considered interstorm periods. Baseline Q is calculated separately for each seasonal series. Inset shows how individual flood events are separated using the baseline Q.

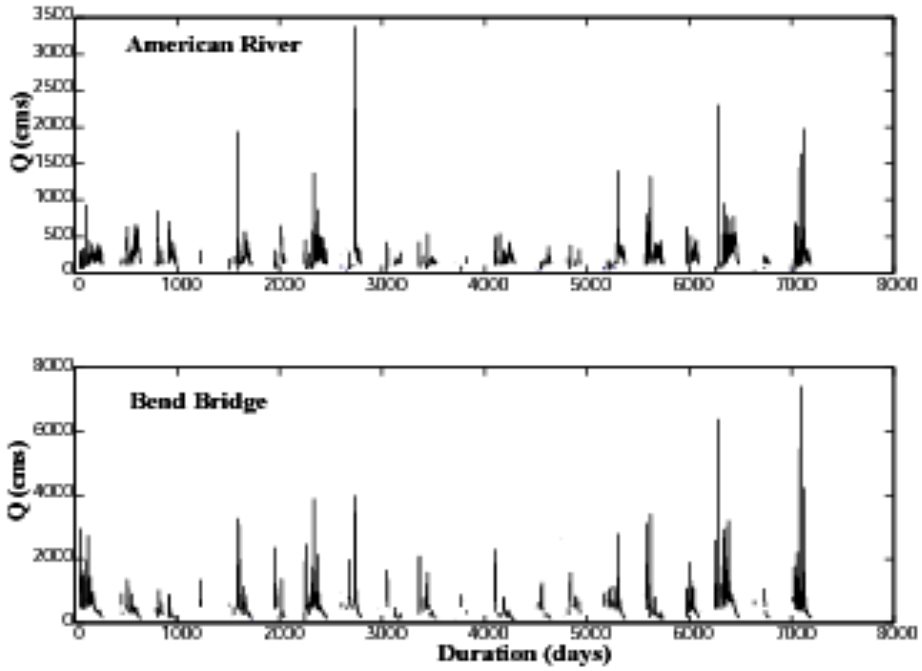

Figure 2.5 An example of how I test for across-basin correlation in synchronous flood peaks. The figure shows a twenty-year period of synchronous floods at the two most distant gauges on Sacramento River inflow gauges: American River and Sacramento River at Bend Bridge. HYDROCARLO then extracts flood peaks from each synchronous flood and calculates their correlation.

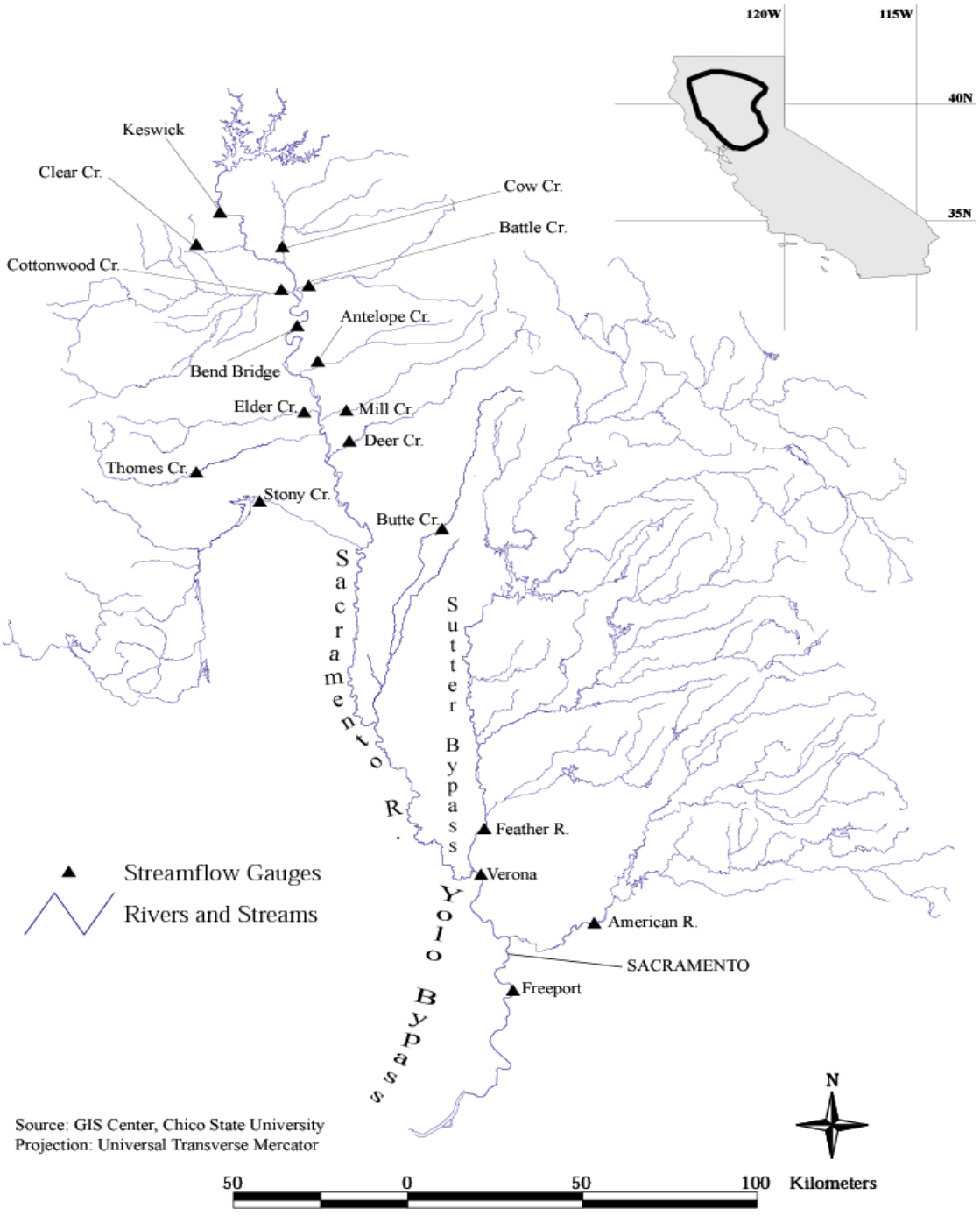

Figure 2.6 Map of Sacramento River drainage basin showing primary tributaries, gauges, flood bypasses, and reservoirs (not labeled). Flood diversion weirs are not depicted. Note: Butte Creek does not actually join the Sacramento at its depicted confluence, but instead drains into a slough, which flows east directly into Sutter Bypass. Sutter Bypass flows south, where it ultimately joins the Sacramento River at the Feather River confluence.

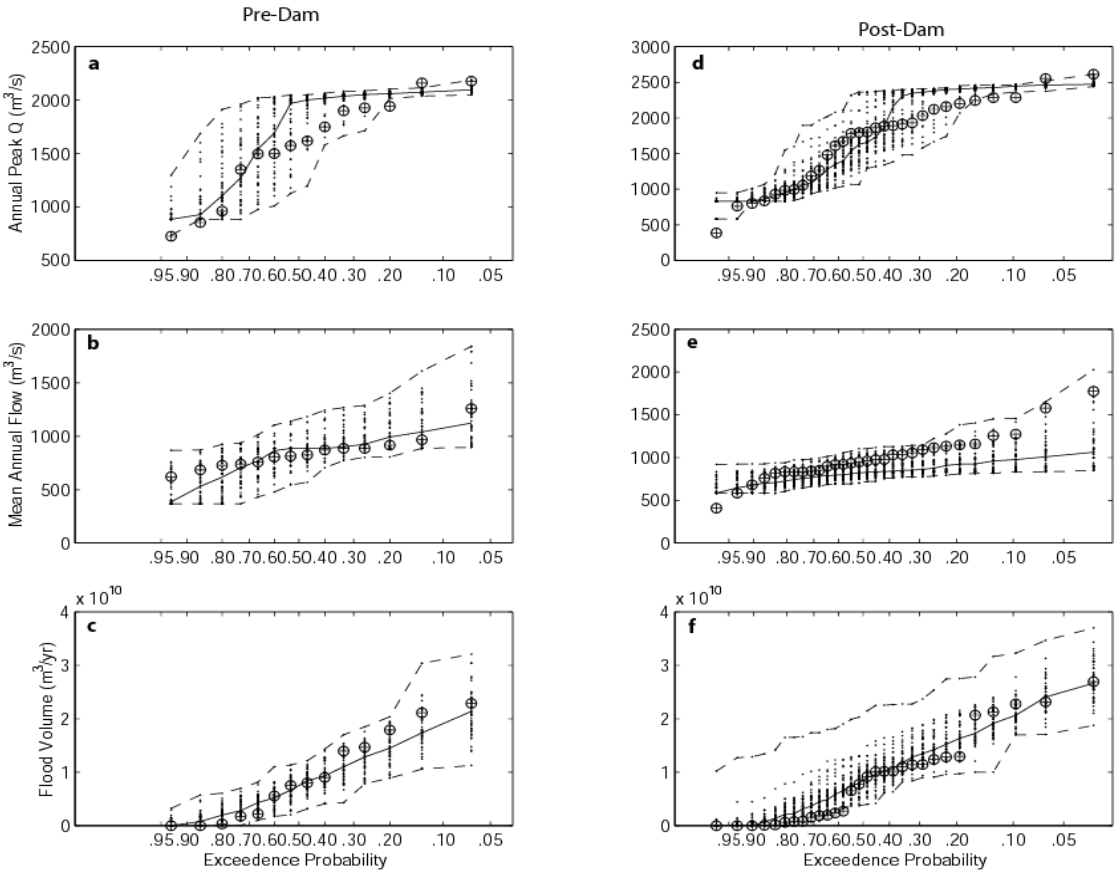

Figure 2.7 Pre-dam cumulative probability plots (Log Pearson III) of a) annual maximum flood peaks, b) mean annual flow above wet season baseline discharge, and c) flood volume (above wet season baseline discharge). Figure 2.7 (d, e and f) contains the same information for the post-dam simulations. Data for the verification gauge at Verona are shown as crosshairs and the simulated series from 50 pre-dam HYDROCARLO simulations are shown as dots. Dashed lines represent the simulation ranges and solid lines represent the median value of simulations, or central tendency.

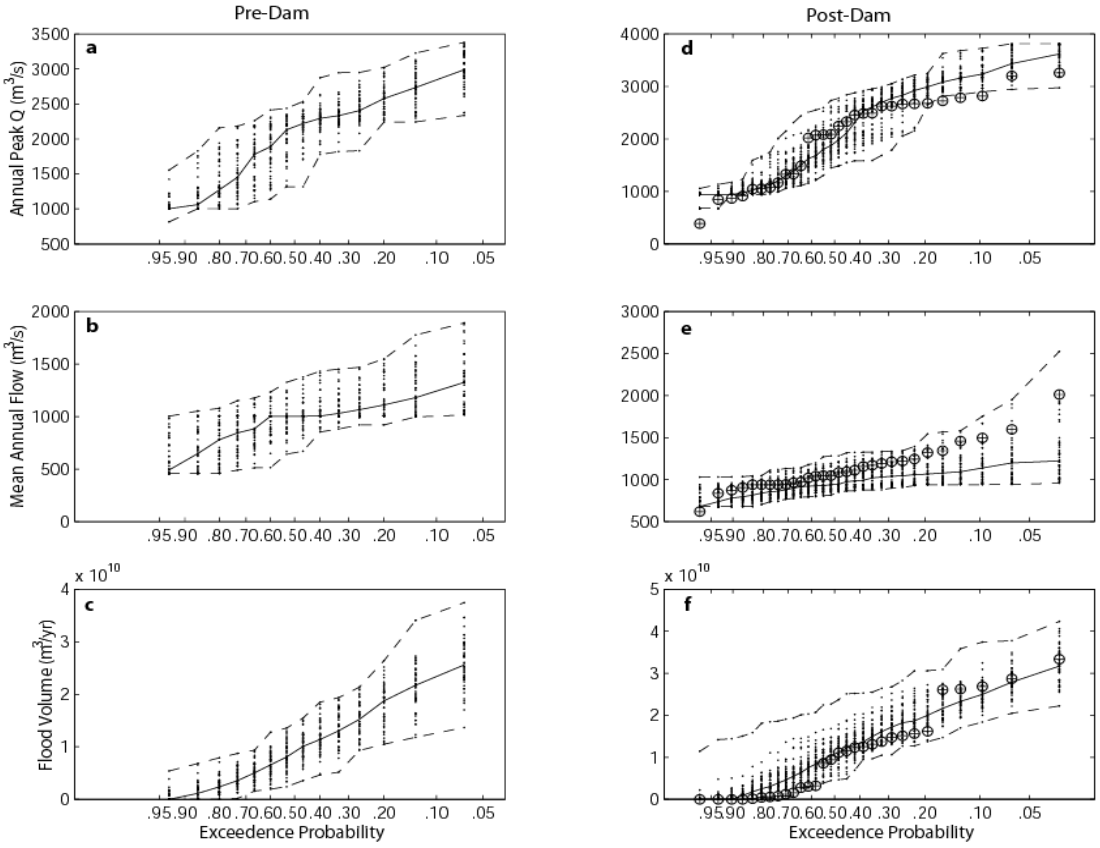

Figure 2.8 Pre-dam cumulative probability plots (Log Pearson III) of a) annual maximum flood peaks, b) mean annual flow above wet season baseline discharge, and c) flood volume (above wet season baseline discharge). Figure 2.9 (d, e and f) contains the same information for the post-dam simulations. Data for the verification gauge at Freeport (post-dam only) are shown as crosshairs and the simulated series from 50 pre-dam HYDROCARLO simulations are shown as dots. Dashed lines represent the simulation ranges and solid lines represent the median value of simulations, or central tendency.

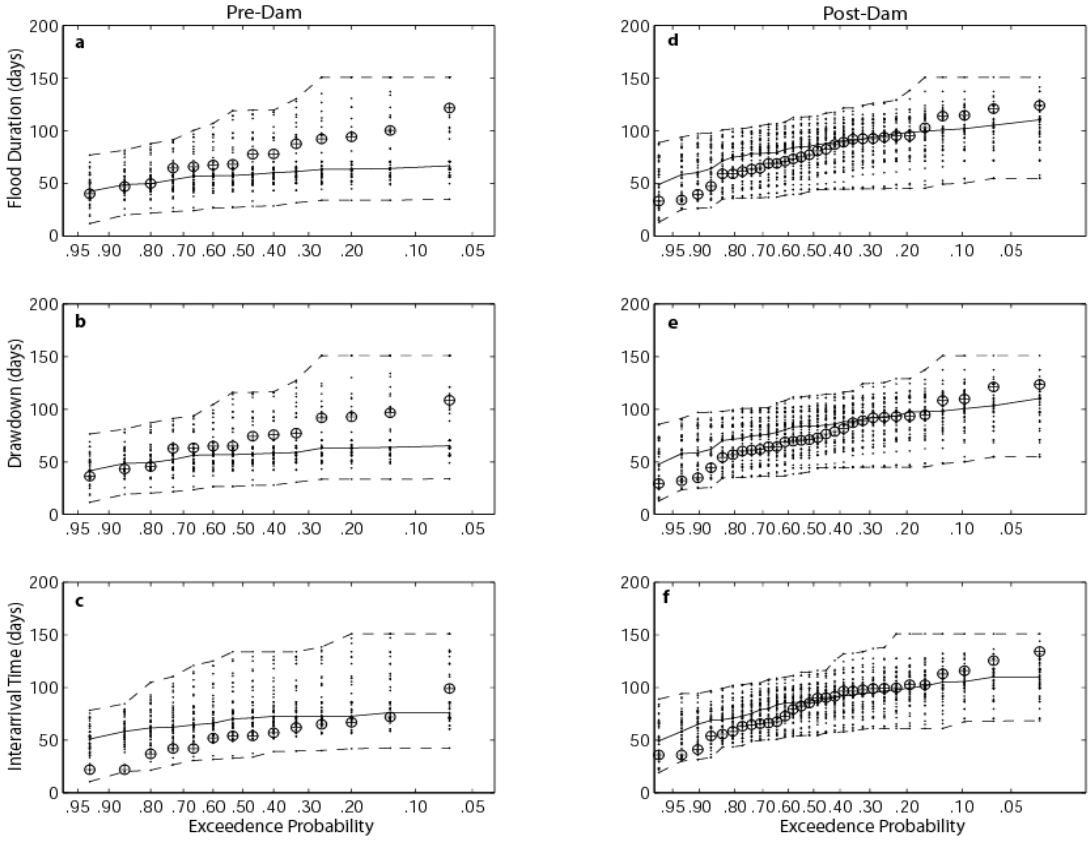

Figure 2.9 Pre-dam cumulative probability plots (Log Pearson III) of a) mean flood duration, b) mean drawdown duration from flood peak to wet season baseline discharge; and c) mean interarrival time. Figure 2.8 (d, e, and f) contains the same information for post-dam simulations. Data for the validation gauge at Verona are shown as crosshairs and the simulated series from 50 pre-dam HYDROCARLO simulations are shown as dots. Dashed lines represent the simulation ranges and solid lines represent the median value of simulations, or central tendency.

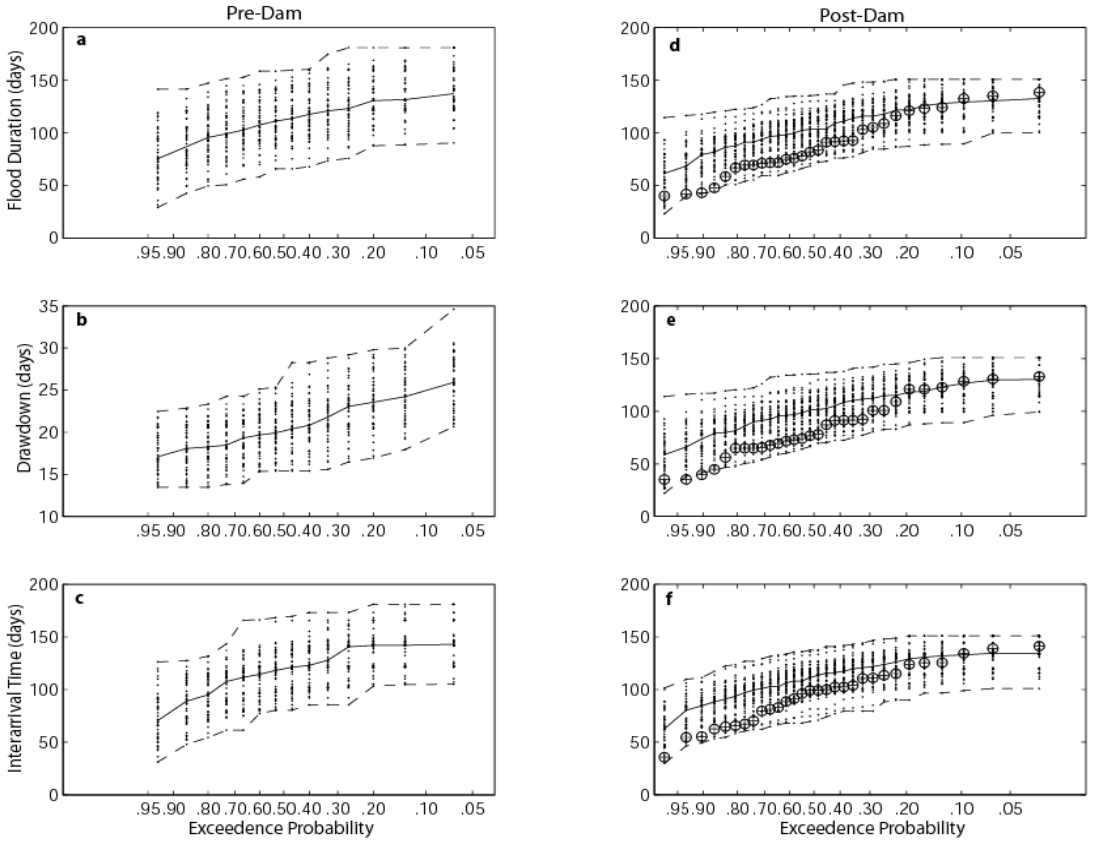

Figure 2.10 Pre-dam cumulative probability plots (Log Pearson III) of a) mean flood duration, b) mean drawdown duration from flood peak to wet season baseline discharge; and c) mean interarrival time. Figure 2.10 (d, e, and f) contains the same information for post-dam simulations. Data for the validation gauge at Freeport (post-dam only) are shown as crosshairs and the simulated series from 50 pre-dam HYDROCARLO simulations are shown as dots. Dashed lines represent the simulation ranges and solid lines represent the median value of simulations, or central tendency.

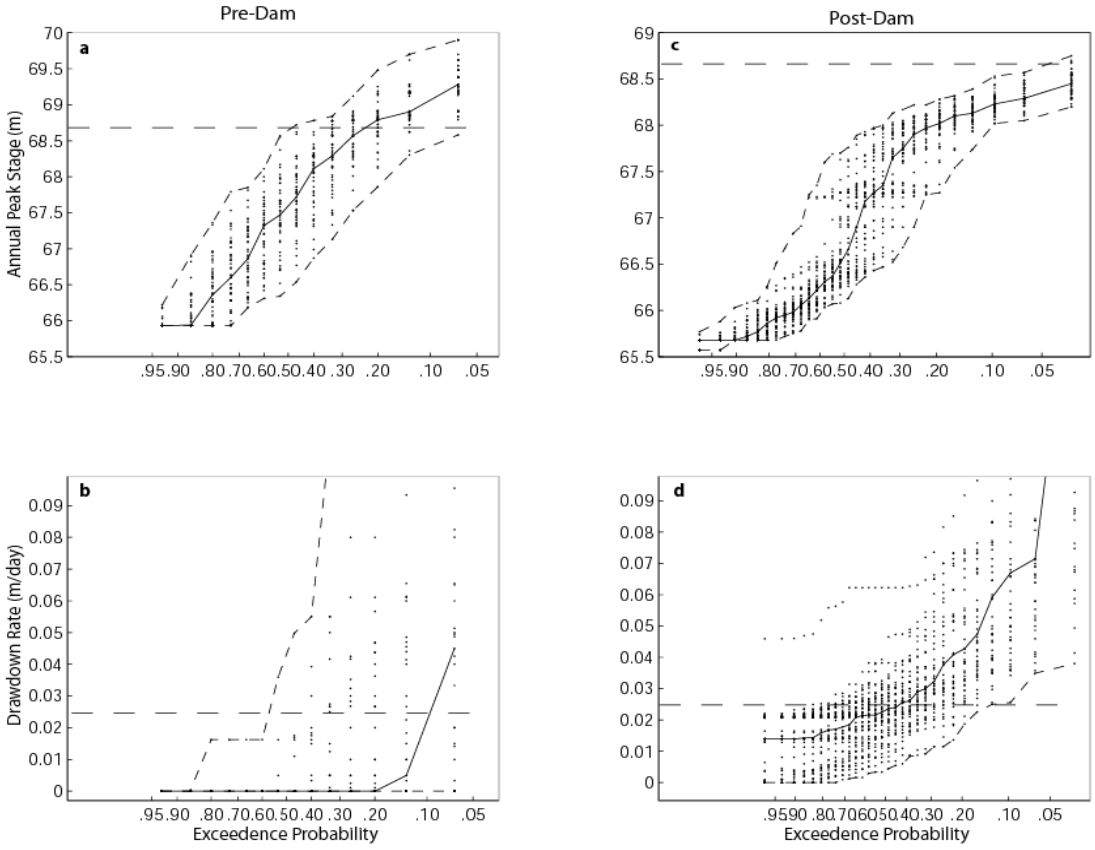

Figure 2.11 Annual peak stage at Tehama (below the Elder Creek confluence) in the pre-dam era (a) and post-dam era (c). Dashed line represents the stage necessary to access the floodplain. Mean rate of drawdown at the same site is shown for the pre-dam (b) and post-dam (d) eras. The dashed lines here represent the maximum survivable rate of 2.5 cm/day of cottonwood seedlings (Mahoney and Rood, 1998). The plots illustrate the effect of dam operations on flow conditions necessary for cottonwood establishment and recruitment.

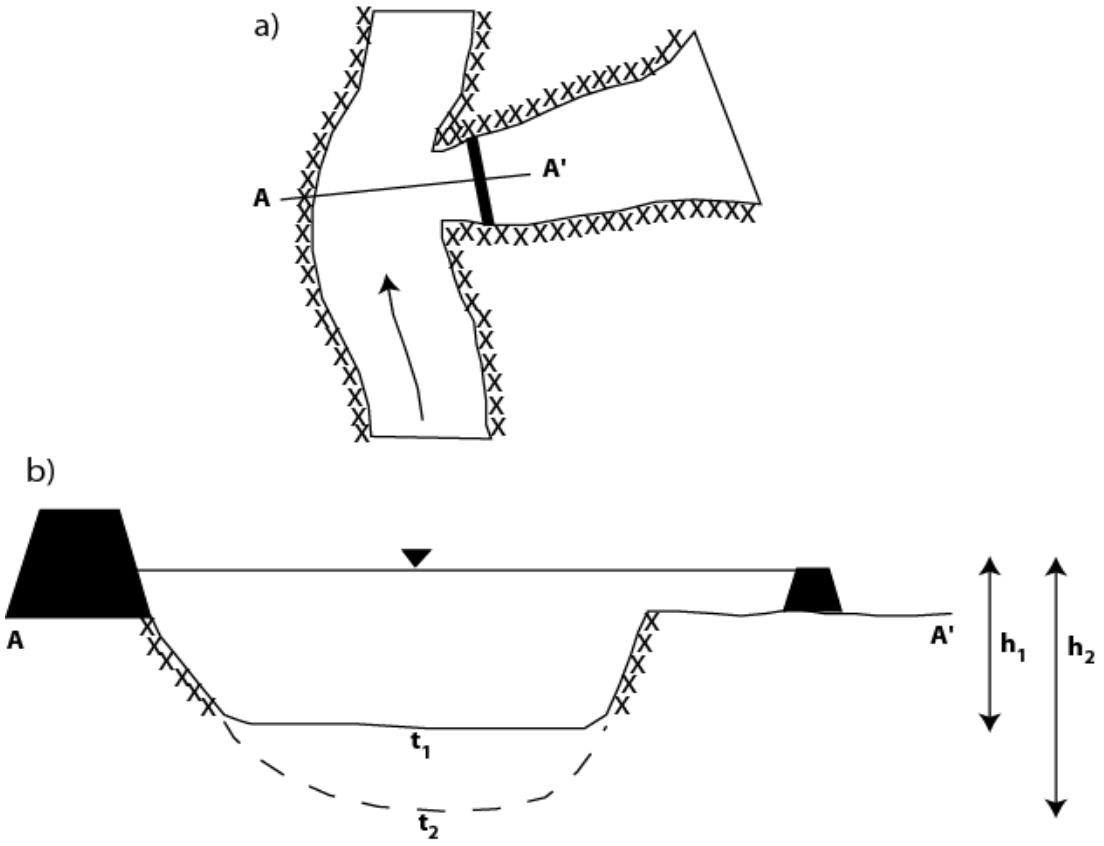

Figure 2.12 Schematic showing a) planform view of leveed main channel reach with a flood weir leading to a bypass and b) cross-sectional view of how flood control system could become impaired by incision of the channel bed. Bed levels before (t_1) and after (t_2) erosion. Water levels necessary to overtop the weir before (h_1) and after (h_2) incision.

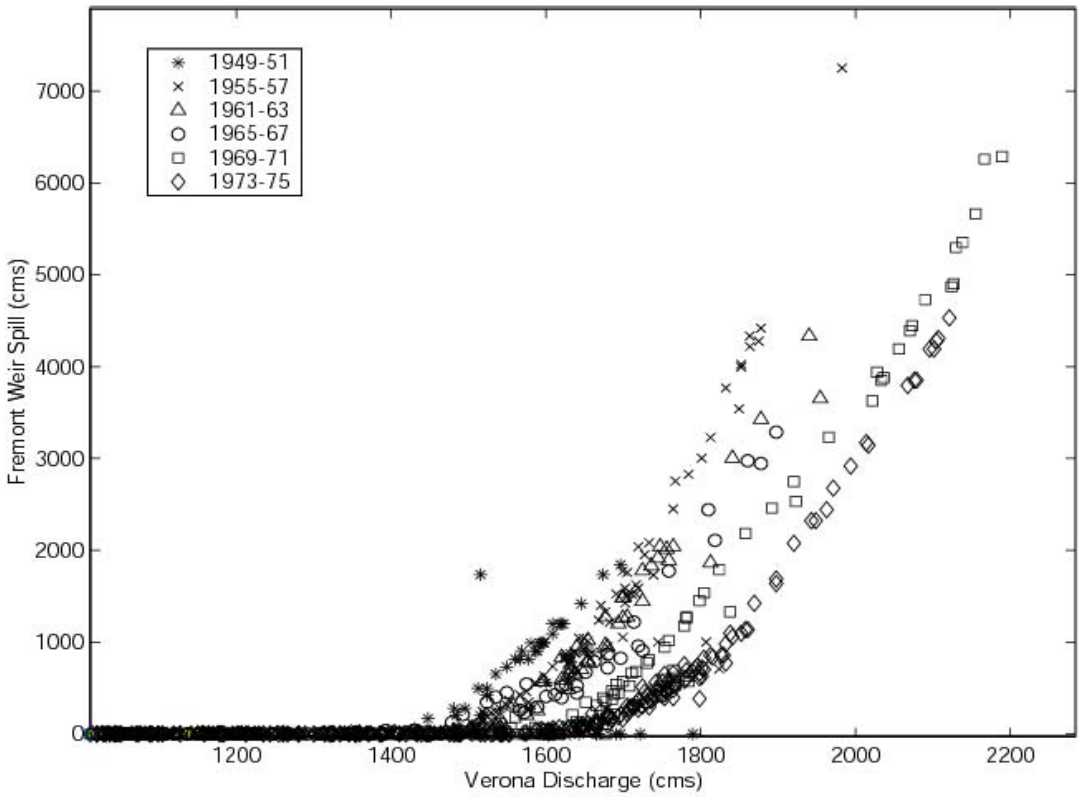

Figure 2.13 Plot showing declining flow over Fremont Weir compared with flow at Verona on the mainstem downstream of the weir from 1949-1975.

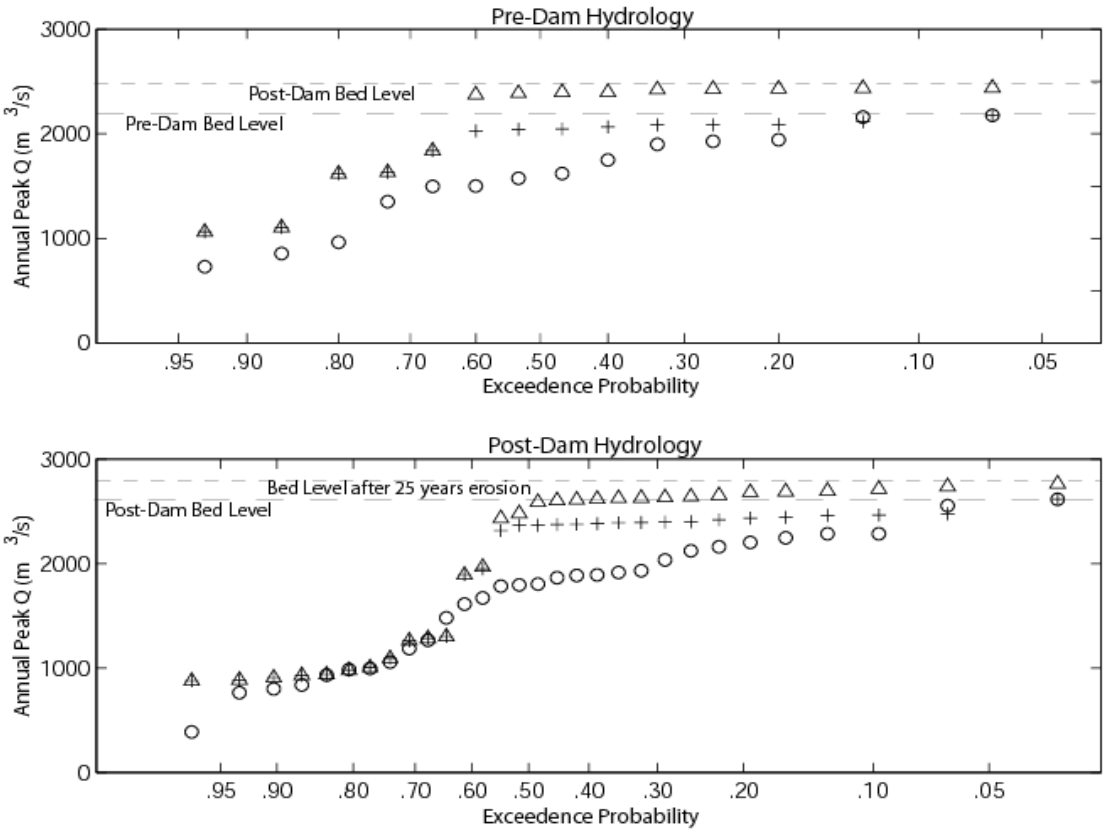

Figure 2.14 Plot shows zeroed simulations (plusses) for pre-dam (upper panel) and post-dam (lower panel) hydrology at Verona. Open circles are historical data. Triangles (upper panel) are how simulated pre-dam data would look at the post-dam bed level beside which Fremont Weir would be 0.79 m higher. Triangles in the lower panel show how erosion continued at calculated rate for 25 years would affect flow at Verona.

Table 2.1 Tributary Basin Characteristics

Basin Name	USGS Station #	D.A. (km^2)	Years of Q Data	Mean Q	Max Q	Dam
American River	11446500	5014	1904-1997	106	3738	X
Antelope Creek	11379000	319	1940-1982	1	161	
Battle Creek	11376550	925	1940-1996	14	309	
Sacamento R. @ Bend Br.	11377100	23051	1891-1999	340	7392	X
Butte Creek	11390000	380	1930-1999	12	753	
Clear Creek	11372000	591	1940-1999	8	428	X
Cottonwood Creek	11376000	2401	1940-1999	25	1538	
Cow Creek	11374000	1101	1949-1999	20	920	
Deer Creek	11383500	544	1920-1999	9	569	
Elder Creek	11380500	352	1949-1969	3	237	
Feather River	11425000	15335	1943-1983	245	8863	X
Sacamento R. @ Keswick	11370500	16752	1938-1999	267	4531	X
Mill Creek	11381500	339	1928-2000	9	408	
Stony Creek	11388000	1911	1955-1990	15	680	X
Thomes Creek	11382000	526	1920-1996	8	844	

Table 2.1 Information on major tributaries used in the study. These include the US Geological Survey gauging station number, drainage area, years of data available, the mean annual flood, the maximum mean daily flood, and the presence or absence of a major upstream dam.

Table 2.2 Model Initialization Parameters

Basin Name	Wet Event Prob.	Dry Event Prob.	Wet Baseline Q (cms)	Dry Baseline Q (cms)	Floods/Bin (Wet)	Floods/Bin (Dry)
Pre-Dam Simulations, *ABC* = 0.79						
American River	0.316	0.314	118	92	54	15
Antelope Creek	0.236	0.261	6	2	68	16
Bend Bridge	0.306	0.296	445	199	72	18
Butte Creek	0.298	0.309	15	7	88	25
Deer Creek	0.286	0.261	12	5	111	27
Elder Creek	0.258	0.219	5	0.6	30	7
Feather River	0.317	0.276	292	124	23	7
Mill Creek	0.285	0.354	10	7	134	29
Stony Creek	0.17	0.349	22	8	25	14
Thomes Creek	0.299	0.249	12	3	107	27
Post-Dam Simulations, *ABC* = 0.78						
American River	0.282	0.383	108	97	20	26
Antelope Creek	0.236	0.314	6	2	68	26
Battle Creek	0.337	0.334	17	9	94	26
Butte Creek	0.298	0.309	15	7	89	26
Clear Creek	0.171	0.213	7	2	45	18
Cottonwood Creek	0.263	0.289	38	7	66	23
Cow Creek	0.252	0.260	29	5	98	21
Deer Creek	0.286	0.261	12	5	110	27
Elder Creek	0.258	0.219	5	0.6	30	7
Feather River	0.262	0.465	283	142	8	6
Keswick	0.251	0.487	259	293	26	23
Mill Creek	0.285	0.354	10	7	134	29
Stony Creek	0.17	0.349	22	8	25	14
Thomes Creek	0.299	0.249	12	3	107	26

Table 2.2 Event probabilities, baseline discharge, and number of floods/bin for each season in pre- and post-dam simulations.

CHAPTER 3. MODELING DECADAL BED-MATERIAL SEDIMENT FLUX BASED ON STOCHASTIC HYDROLOGY

(Submitted)

Abstract

This paper reports estimates of decadal bed-material sediment flux and net storage obtained by driving sediment transport calculations with a stochastic hydrology model. The resulting estimates represent the whole distribution of sediment flux based on the natural variability in channel characteristics (gradient, width, and bed grain size), and the magnitude, duration, and interarrival time of flood events. The paper describes a procedure for calibrating common sediment transport formulae to the bed-material grain-size distribution at a cross section. The procedure is applied to the Sacramento River basin to compute estimates of annual total and annual peak bed-material discharges into and through the mainstem over a thirty-year period. Simple mainstem bed-material budgets are evaluated to identify reaches in states of net accumulation or scour. Simulations highlight large imbalances in sediment storage throughout the Sacramento River, which can be explained by a combination of local hydraulics and bed material grain size distributions.

Introduction

Bed-material flux is the transport of sediment that is present in a riverbed and is available for transport by streamflow. The variability in bed-material flux

throughout a river channel results in spatial patterns in sediment storage. These storage patterns influence the formation of the channel (e.g. point bars) and its functioning (e.g. depth of flow over an portion of a cross section). Accordingly, sediment storage can be thought of as a first-order determinant of habitat conditions in a river reach.

Long-term estimates of bed-material sediment flux and net storage in large rivers are required for various purposes ranging from applications in flood control (bed elevations) and river rehabilitation to research on sediment budgets and channel morphology. These estimates are generally reported as single values derived from sediment transport data with no assessment of the uncertainty in their calculation (e.g. [*Milliman and Meade*, 1983; *Milliman and Syvitski*, 1992]) or their inter-annual variation. *Dunne et al.* [1998] applied error propagation to sediment rating curve analyses of sediment fluxes and reach accumulations in the Amazon basin. But to my knowledge, there are limited methods available for representing inter-annual variability in load estimates due to a variable flow regime. Toward this end, I have calibrated a sediment transport formula with measurements from the Sacramento and other rivers, and connected it to HYDROCARLO, a stochastic model of streamflow [*Singer and Dunne*, Submitted]. I used the coupled models to estimate the probability distributions, including the extrema and central tendency, of bed-material discharge in various grain-size classes over a period of decades. I have applied this method at various cross sections along the mainstem Sacramento River and at the mouth of its

major tributaries, and thus developed a basinwide method for assessing the long-term influence of flood variability on bed-material transport.

Many studies have acknowledged the inaccuracies in sediment transport prediction arising from uncertainty in hydraulic variables [*McLean*, 1995], spatial distribution of bed shear stress [*Wilcock*, 1996], and assessment of critical shear stress [*Buffington and Montgomery*, 1997]. However, flow is an additional source of uncertainty introduced when one tries to obtain a decadal estimate of bedload flux. For even if one could properly constrain each of the aforementioned variables for a given set of flow conditions, it would still be necessary to properly characterize the stochastic frequency, magnitude, and duration of flow at a given cross-section, in order to obtain an appropriate estimate of long-term bed-material flux. Such a strategy is particularly important to determining the role of floods in sediment transport and channel formation, and for assessing riverine habitat condition.

Long-term sediment flux prediction that incorporates the real variability inherent in a fluvial system would be useful on the scale of a cross section where computations are made (e.g. to evaluate local adjustment to a rehabilitation strategy) and that of a basin as a whole (e.g. to assess a the influence of system-wide perturbations on the sediment budget). In order to design a gravel augmentation strategy on the local scale, for example, it would be useful to quantify the central tendency and extrema of spawning-sized gravel transport past a particular cross section. On the basin scale, it would be useful to assess the influence of land-use change (e.g. an increase in sand loading to the channel) on bed-material transport in

various grain sizes throughout the mainstem. This paper outlines a basinwide method for quantifying the variations in bed-material transport over a period of decades punctuated by flood events of variable frequency, magnitude, duration, drawdown rate, and interarrival time.

I built this method using data from the Sacramento River basin in California. I perform the following at mainstem and tributary cross sections along the Sacramento River: 1) stochastically simulate daily flow for 30 years [*Singer and Dunne*, Submitted]; 2) simplify cross-sectional geometry and calculate hydraulic variables for distinct portions of the cross section; 3) obtain the grain-size distribution from bulk material surveys; 4) determine dimensionless critical shear stress from bedload data; 5) modify a common sediment transport formula to incorporate local critical shear stress, fractional transport prediction, and prediction in distinct portions of a cross section; 6) calibrate the modified equation to various bedload data; 7) calibrate the modified equation to the grain-size distribution of the local bed-material; 8) simulate daily bedload flux for 30 years in various grain size classes; 9) combine long-term bedload estimates with my prior estimates of long-term suspended sediment discharge [*Singer and Dunne*, 2001] at mainstem locations to evaluate the contribution of bedload to total load; and 10) construct simple bed-material sediment budgets (annual total and one-day peak values) for reaches of the Sacramento fluvial system.

Study Basin

The Sacramento River basin is approximately 70,000 km^2 in drainage area and the river flows from its headwaters near Mount Shasta through the northern Central Valley to the San Francisco Bay-Delta in California. It is controlled at the northern end by Shasta Dam, which was built in 1943. The Sacramento spans a range of fluvial environments. From Shasta Dam, it winds southward through Sacramento Canyon, incises into Pleistocene deposits on the Redding plain, and bends through Iron Canyon to Bend Bridge (BB in Figure 3.1). This part of the river, called Reach 0 (Figure 3.1) in this study, is ~40 km in length, consists of a mixed bed (~28% sand in bed-material at BB), width of ~150 m, slope of ~8.9×10^{-4} and has point bar topography. South of Bend Bridge the Sacramento enters the Central Valley, where it meanders across a wide floodplain through Pleistocene river gravels to Hamilton City (HC). Reach 1 is ~60 km in length, consists of a gravel and sand bed (~40% sand at HC), width of ~200 m and slope of ~5.4×10^{-4}, with shallow cross sections characterized by ~2 m natural levees. Below Hamilton City the Sacramento continues meandering through the valley, but is partially constrained by flood control levees, which influence the river's course upstream of Butte City (BC). Reach 2 is ~30 km in length, consists of similar bed-material (~49% sand at BC), cross-sectional topography, and width as Reach 1, but with a lower slope (~2.5×10^{-4}). Below Butte City the Sacramento enters a reach where flood control levees are set back ~1 km from the channel until Colusa (CO). Reach 3 is ~25 km in length, consists of a sand bed (~75% sand at CO), width and cross sectional topography similar to the upstream reaches, and a slope of ~2.3×10^{-4}. It is controlled at the downstream end by an

eastward deflection around the Colusa Dome, which forces sequestration of water and deposition of sediment [*Singer and Dunne*, 2001]. Downstream of Colusa the Sacramento is incised into the Pleistocene deposits of the Cache Creek fan and is completely constrained by flood control levees built on channel banks to Knights Landing (KL). Reach 4 is ~55 km in length, consists of a sand bed (~73% sand at KL) with lenses of gravel, width of ~100 m, largely symmetrical cross sections, and slope of ~1.0×10^{-4}. The Sacramento River below Knights Landing continues south to Sacramento (SA), where the river is influenced by tides. Reach 5 is ~30 km in length, consists of a sand bed (99% sand at SA) ~0.8×10^{-4}.

I compute sediment discharge at cross sections that bound these river reaches and directly correspond with gauging stations for which I previously made long-term estimates of suspended sediment transport [*Singer and Dunne*, 2001]. Most cross sections used in this study have fixed widths over the range of moderate-to-high flows due to combinations of flood control levees, riprap, and revetment.

The tributaries of the Sacramento flow from four geologic provinces, each of which is assumed to deliver a uniform sediment yield per unit drainage area. I compute bed-material transport into the Sacramento from each tributary in a unit by computing the load for a signature tributary on the province and scaling it by the ratio of drainage areas for the remaining tributaries. The signature tributaries for this study are Cottonwood Creek, Cow Creek, Thomes Creek, and Feather River, draining the Trinity Mountains, Modoc Plateau, Coast Ranges, and Sierra Nevada, respectively.

Data

I employ channel cross sections extracted from high-resolution (0.7 m contours) digital terrain models of the mainstem Sacramento provided by the US Army Corps of Engineers (USACE) and the California Department of Water Resources (CDWR). These datasets were obtained by bathymetric surveys in 1997 and 2000, respectively. Together, they form a seamless set of contemporaneous (within 3 years) cross sections through which flow routing and sediment transport may be computed. Flow data from the Sacramento's major tributary gauges were obtained from the US Geological Survey (USGS) as described in [*Singer and Dunne*, Submitted]. To define grain-size distributions and calibrate sediment transport formulae, I use bedload and suspended load data from USGS gauging stations, and bed-material grain-size distributions from the USGS and CDWR bulk material surveys.

Stochastic Hydrology Model

In order to drive the sediment transport calculations, I developed a stochastic hydrology model that simulates inflow to the mainstem of a large river from its major tributaries by semi-random sampling of tributary flood events. The model, HYDROCARLO [*Singer and Dunne*, Submitted], produces synchronous inflow from tributaries by replicating empirical patterns in flood occurrence and correlation in flood peak magnitude between tributary gauges. In applying it to the Sacramento River basin, I demonstrated the overwhelming influence of basinwide storms that

induce synchronous flood conditions at all tributary gauges. I also showed that the model produces plausible patterns of tributary inflow which, when routed through the mainstem produce hydrographs with characteristics (e.g. peak, duration, interarrival time) similar to those of observed mainstem hydrographs.

In the sediment transport study, I used HYDROCARLO to simulate daily inflow to the mainstem Sacramento River for a 30-year period that represents the hydrology of the era since the construction of Shasta Dam. I routed this inflow through the mainstem to each of the selected cross sections (Figure 3.1) using the flow routing software, HEC-RAS, and extracted mean daily flow stage for the duration of each 30-year simulation. I conducted 50 such simulations to stochastically represent a large range of flood events in the basin and to converge on extrema and central tendency of bedload flux associated with them.

Cross-Sectional Geometry and Hydraulics

Bedload flux may differ in distinct portions of a river channel cross section due to differences in flow depth that lead to spatial variability in shear stress [*Wilcock*, 1996]. For example, shear stresses are higher in the thalweg than on a high bar surface (Figure 3.2), if the bed-material grain-size distribution is spatially uniform. Therefore, calculating rates of sediment transport for an entire cross-section based on mean flow depth could introduce inaccuracies into the results. I have simplified the geometry for each of my cross sections to represent the varying depths that could lead to differential transport rates in distinct portions of the section based

on a single cross-sectional stage. I divided cross-sections into portions, each with its own elevation datum and width (Figure 3.2).

I used daily flow elevation extracted from HEC-RAS to compute daily water surface slope, s, for the cross-section as a whole as

$$s_x = \frac{\left(\frac{z_{x+1} - z_x}{c_1} + \frac{z_x - z_{x-1}}{c_2} \right)}{2} \quad (1)$$

where z is water surface elevation, the subscripts *x, x+1, and x-1* denote the cross section average of the section in question, the next upstream section, and the next downstream section, respectively, c_1 is the centerline distance between sections $x+1$ and x, and c_2 is the centerline distance between sections x and $x-1$. Centerline distances between cross sections are ~800 m. Hereafter I refer to section average quantities with the subscript x and quantities for a portion of the cross section with the subscript p. Flow depth for a portion of the cross section, h_p, is calculated by subtracting the bed elevation of that portion, z_p, from the water surface elevation for the section as a whole, z_x. I used the resulting flow depths, h_p, and the section-average water surface slope, s_x, from (1) to compute mean daily velocity for each portion of the cross section using the Manning equation:

$$v_p = \frac{h_p^{2/3} s_x^{1/2}}{n_x} \tag{2}$$

where v is velocity, n is the Manning's roughness coefficient. I obtained constant Manning's roughness values for each cross section from prior hydraulic calibrations of bathymetric datasets by USACE and CDWR. Next I calculated bed shear stress for each portion of a section, τ_p:

$$\tau_p = \rho g h_p s_x \tag{3}$$

where ρ is the density of water (assumed to be 1000 kg/m^3) and g is gravitational acceleration. In other words, I am making the approximation that all flow is parallel to the banks and bed. I converted shear stress to its dimensionless form [*Shields*, 1936]:

$$\tau_p^* = \frac{\tau_p}{(\rho_s - \rho) g d_{50_x}} \tag{4}$$

where τ^* is dimensionless shear stress (i.e. Shields stress), ρ_s is density of sediment (assumed to be 2650 kg/m^3), and d_{50} is median grain size of the bed material, obtained for each section from bulk material sampling [*California Dept. of Water*

Resources, 1994]. Lateral characterization of dimensionless shear stress (i.e. across the channel) could be improved by higher resolution bulk surveys of bed material, which would provide median grain size for each portion of the cross section, d_{50p}. This may particularly important in cases where there is marked lateral sorting of bed sediments (e.g. sections with coarse bars and fine pools).

Bed-material Grain Size

Correct specification of sediment grain size is necessary in order to obtain realistic predictions of sediment flux because of the sensitivity of sediment transport equations to grain size distribution. For example, washload (i.e. that part of the sediment load which is not present on the riverbed) should not be computed with an equation designed to predict transport of bed material. The grain size range of a particular transport mode can be defined operationally as that which can be caught in a particular sampler (e.g. [*Edwards and Glysson*, 1999]). The Helley-Smith bedload sampler [*Helley and Smith*, 1971] has been shown to be 100% effective in trapping grain sizes between 0.5 and 16 mm for a 75 mm intake (or 32 mm with a 150 mm intake) [*Emmett*, 1980]. Although particles as fine as 0.2 mm can be physically caught by the Helley-Smith, the mode of their transport is uncertain [*Emmett*, 1980]. The DH-series, depth-integrated suspended sediment sampler is statistically effective at capturing sediment ranging from 0.001 to 0.5 mm in diameter [*Edwards and Glysson*, 1999], traveling within 75 mm of the bed.

I compared grain-size distributions for bed material, suspended load, and bedload (for stations that had such data) collected for mainstem Sacramento River stations between 1977 and 1980 (Figure 3.3). These data show that 0.5 mm is an approximate lower limit grain size for bed material at most stations in the basin. Grain sizes larger than 0.5 mm are present in less than 5% of suspended load samples and more than 5% of bed material samples in the gravelly reaches. These factors indicate that 0.5 mm is the natural separation between washload and bed-material transport (whether bedload or suspended load) for the Sacramento basin. The sand-bed reaches at Butte City, Knights Landing, and Sacramento, have 0.25 mm as their lower limit (Figure 3.3c, e, and f). Suspended sediment is almost entirely comprised of washload in the Sacramento (Figure 3.3) and its tributaries. The exceptions are the Sacramento station and the Feather River station (Figure 3.1), where fine-grained bed material mostly moves in suspension. However, for the remaining sections, there are two populations of sediment moving in distinct transport modes. Herein I model bed-material discharge with the assumption that there is no overlap between them. I compute sediment discharge for up to nine grain size classes, i, (d_{50i} (mm) = 0.38, 0.75, 1.5, 3, 6, 12, 24, 48, and 96). However, at the lower end of the distribution, I limit the computations to grain sizes that constitute less than 5% of the suspended load at a given cross section. This is particularly important because I employ a sediment transport equation designed only for bed material transport calculations (see below).

Critical Shear Stress

Recent research in gravel transport has emphasized the importance of characterizing the threshold of incipient motion to ensure that sediment transport is not predicted in cases where the threshold for movement is not met. More than a threefold range in this threshold arises from the condition of the bed (e.g. grain shape, size, and packing, pocket angle). Numerous methods have been developed over eight decades of research [*Buffington and Montgomery*, 1997] to compute dimensionless critical shear stress, τ^*_c, and it is common practice to employ a characteristic value (e.g. $\tau^*_c = 0.047$ for gravel) when local transport data are unavailable. However, in cases where bedload data are available, it is preferable to compute the local threshold value. This has been commonly done by a technique called similarity collapse originally developed in Japan [*Ashida and Michiue*, 1972; *Parker et al.*, 1982].

Parker, et al. [1982] plotted dimensionless transport rate against dimensionless shear stress in each grain size class. They fitted a curve to the data within each grain size class and extended this curve down to a reference transport rate of 0.002 to obtain a reference shear stress, or a surrogate of the dimensionless critical shear stress for that grain size. They plotted these dimensionless reference shear stresses against the ratio of the median grain size (of each bedload size class) to the median grain size of the bed subsurface. This yielded a power relationship with a coefficient that approximates the dimensionless critical shear stress, τ^*_c, for incipient motion of the entire mixture.

However, the current study is not concerned with incipient motion of sediments. It is instead concerned with defining a threshold for sediment transport that can be measured with a bedload sampler. Therefore, I compute τ^*_c as the lowest Shields stress, τ^*_x, that yields transport for the lowest observed bedload rate. In other words, I obtain τ^*_c by adjusting its value until excess shear stress (i.e. τ^*_x - τ^*_c) is positive for the hydraulic conditions of the lowest measured transport rate where both sand and gravel were in motion. This approach is especially useful to define a transport threshold in cases where a scarcity of bedload measurements leads to difficulties in defining the relationship between dimensionless transport and dimensionless shear stress. For one station where I had ample bedload data (Bend Bridge, Figure 3.1), the similarity collapse yielded $\tau^*_c = 0.040$ and my method yielded $\tau^*_c = 0.053$. Table 3.1 provides information for each station including τ^*_c, drainage area, and median bed-material grain size.

Sediment Transport Equation Modification and Calibration

Previous researchers have computed sediment transport with formulae calibrated to specific laboratory and/or field data. Many such formulae have been extensively reviewed (e.g. [*White et al.*, 1975; *Gomez and Church*, 1989]). The equations that *Gomez and Church* [1989] found to be most accurate (*Bagnold* and *Parker, et al.*) were extensively calibrated on the best available measurements of bedload in gravel-bed rivers. Most shear stress-based sediment transport equations are of a similar form [*Gomez and Church*, 1989], e.g. containing an excess shear

stress term, or a ratio or difference of computed shear stress and critical shear stress raised to some power. Therefore, I reason that it matters less, which equation is used, but how well a particular equation can be calibrated to predict sediment transport in a particular river system. This is especially important because sediment transport computed with commonly-used equations may predict rates a factor of 2-10 times observed bedload rates, particularly for the highest recorded values. Until the theory of sediment transport improves to represent the range of laboratory flume and field sediment transport conditions, there is little utility in applying specific empirical equations to a new place without recalibrating to local transport data, if they exist. Although such a practice has merit in studies investigating the applicability of particular equations (e.g. [*Andrews*, 1981; *Batalla*, 1997]), it has limited use in long-term prediction of sediment transport rates. Here I demonstrate that prediction of sediment transport rates in a particular place can be improved by calibrating one of a number of commonly-used sediment transport formulae to local bedload and bed material data and simulating over a range of hydraulic conditions.

For this study, I have chosen the Engelund-Hansen formula [*Engelund and Hansen*, 1967; *Vanoni*, 1975] for total load. The original equation was developed by relating sediment transport to excess shear stress and bed friction using data from flume experiments on a dune-covered sandy bed [*Guy et al.*, 1966]. It has had reasonable success in predicting sediment transport in a variety of sand and gravel environments (e.g. [*White et al.*, 1975; *Yang and Wan*, 1991; *Reid and Dunne*, 1996; *Batalla*, 1997]). In their calibration of the equation, Engelund and Hansen [1967]

eliminated an excess shear stress term by setting the critical shear stress equal to 0.06 (from the original Shields diagram) and adjusting the exponent of the τ^* accordingly:

$$i_{b_x} = 0.05\rho_s {v_x}^2 \sqrt{\frac{d_{50_x}}{g\left(\frac{\rho_s}{\rho}-1\right)}}(\tau_x^*)^{1.5} \tag{5}$$

where i_{bx} is the unit bedload transport rate in kg/s per m of width, ρ_s is density of sediment (assumed to be 2650 kg/m^3), and d_{50} is the median grain size (m) of a particular size class. (Equation (5) is a correction of Equation 2.234e, [*Vanoni*, 1975] for dimensional homogeneity). Again the subscript *x* denotes computations for the cross section as a whole.

It is undesirable to have τ^*_c hard-wired into the equation and I have thus used the original (uncalibrated) equation (not in [*Vanoni*, 1975]), which contains an excess shear stress term, for which I can specify the critical shear stress. I have thus revived the original equation and modified it to predict transport by grain size class and in distinct portions of the cross section:

$$i_{b_{ip}} = \alpha\left(\frac{\rho_s {v_p}^2 d_{50_i}(\tau_p^* - \tau_c^*)^{1.5}}{2\sqrt{gh_p s_x}}\right) \tag{6}$$

where i_{bip} is the unit bedload transport rate in kg/s per m of width of size class i in portion p of the cross section, τ^*_x is the Shields number computed for h_x and d_{50x}, τ^*_c is the dimensionless critical shear stress for the whole mixture, and α is a fitting parameter. Note there are other difference between (5) and (6) which result from differences in derivation. However, each is dimensionally homogenous. The modified equation ensures that transport will only be predicted if shear stress exceeds the threshold value. I calibrated (6) to bedload datasets collected in the Sacramento River and other fluvial environments.

I fitted the α parameter to bedload data in various grain size classes for each cross section with bedload data. The parameter was adjusted to achieve the best fit between computed and measured bedload for transport rates greater than 100 kg/s. Figure 3.4 shows the power of (5) and (6) to predict fractional sediment transport for bedload data from the Clearwater River in Idaho. The figure shows the original (unmodified) Engelund-Hansen equation (a) and my modified and calibrated version of the equation (b). Clearly there is an improvement in prediction with the modified, calibrated equation. The original equation fails to predict transport rates within a factor of two for most of the data. This is probably due to the fact that the original equation was not designed for fractional transport, but for total loads that include multiple grain sizes. My modifications allow for adjustment of transport in each grain size class, and a variable critical shear stress.

High flux rates of bedload are the main concern because of the general experience that the majority of a river's sediment is transported by a few high flows [*Lustig*, 1965; *Stewart and LaMarche*, 1967; *Pitlick*, 1988]. They represent a lower limit of transport events that overwhelm the capacity of a bedload sampling device. My stochastic flow model, HYDROCARLO, was designed to simulate flow above a flood threshold [*Singer and Dunne*, Submitted], in order to model the effect of large events on, among other things, bedload flux. Therefore I calibrated my modified equation only to total transport rates greater than 100 t/d. This will improve the prediction of sediment transport during the highest flood peaks and my overall estimation of long-term bedload flux.

In the calibrations of the modified Engelund-Hansen equation (6), I sought to develop a calibrated equation that could be applied to predict sediment transport of any grain size class and at any cross section within the Sacramento basin. However, ample mainstem bedload data (e.g. at least 10 measurements) for calibration were limited to two gauging stations (Bend Bridge and Hamilton City, Figure 3.1) and included only the finer grain sizes present in the bed material. Therefore, I calibrated my modified equation for each grain size class (i.e. including all fractions present in the bed material, but not significantly represented in suspended samples, Figure 3.3) using data from other fluvial environments. In addition to the aforementioned Sacramento data, I used Helley-Smith bedload data from Clearwater and Snake Rivers in Idaho and the Tanana River in Alaska, which were publicly available [*Emmett and Seitz*, 1973; *Emmett and Seitz*, 1974; *Jones and Seitz*, 1979; *Jones and*

Seitz, 1980; *Burrows et al.*, 1981; *Harrold and Burrows*, 1983]. Figure 3.5 shows my fitted α values plotted against grain size for five datasets, including the two from the Sacramento River.

It is apparent from this plot that fitted alpha values show a relationship with grain size. It also appears that the curves are superposed. I analyzed fitted alpha values for the various datasets and determined that superposition of the alpha curves can be explained as a function of both grain size and bed material sorting. Sorting is sedimentology parlance for the "spread" or standard deviation of a grain size distribution. The sorting coefficient of the bed material, first presented by [*Krumbein*, 1938], describes the sorting of the bed. High values of sorting coefficient signify a large standard deviation and vice versa. I computed sorting coefficient (phi scale) by the method of moments within GRADISTAT, a grain size analysis software [*Blott and Pye*, 2001].

I computed alpha in a multiple regression model as a function of grain size and bed-material sorting (adjusted $R^2 = 0.86$):

$$\log_{10} \alpha = 1.95 * \sigma_{\phi} - 0.420 * \log_2 d_{50_i} - 4.664 \qquad (7)$$

where σ_{ϕ} is sorting coefficient of the bed material (phi scale). I tested model assumptions by assessing the normality and randomness of the standardized residuals.

This relationship probably emerges because poorly sorted beds have lower pocket angles leading to lower critical shear stresses and higher sediment transport

rates [*Wilcock*, 1998]. I use (7) to determine alpha for cross sections with no bedload data (only bed-material grain size data) and to extend alpha for larger grain sizes because Sacramento bedload data are limited to sizes less than 16 mm.

Daily Bedload Flux Simulation and Total Load Evaluation

To summarize my method, I ran HEC-RAS driven by fifty, 30-year HYDROCARLO streamflow simulations and use the stage output with (1), (2), (3), (4), and (6) to obtain daily sediment transport estimates for each grain size class in each portion of a cross section. I compute bed-material flux for each grain size class multiplied by its percentage in the bed material (excluding surface armor).

For simplicity, I also assumed one-dimensional flow, no armoring of the bed surface, and no cross-sectional change, all of which could be relaxed in later iterations of the model. Beyond the percentages of each grain size class present in the bed material, I place no limits on sediment supply as transport rates increase (e.g. armoring, scour depth) in the current version of this method. Armoring of the river bed due to selective transport of small grain sizes increases the median grain size and increases sorting (decreases the sorting coefficient, or standard deviation of grain sizes), resulting in less sediment transport. Scour of bed sediments during flood events generally only occurs down to a depth limited by local geology and grain sizes at this depth. Therefore, sediment transport during a flood event can only occur until the scour depth is reached, at which point it would shut off. Although these effects are clearly important in order to obtain accurate estimates of bed-material transport,

there are currently no data for assessing their influence in the Sacramento. Consequently, I have not as yet incorporated armoring and scour depth into this version of the modeling method. However, this study is concerned with modeling spatial patterns in sediment storage, which may computed to first order with the current method. As such, the estimates of bed-material transport and storage presented here are meant to generate an understanding of spatial patterns of sediment transport through a large river system and should not be used for any design purpose. I have a plan to systematically assess Sacramento River bed-material and scour depths in future work. This will enable me to adapt the method to account for armoring and limits on scour.

I computed daily bed-material loads for the entire cross section in each size class for each simulation as:

$$i_{bD_{ix}} = \sum_{p} i_{b_{ip}} w_p \quad . \tag{8}$$

where i_{bDij} is daily (D) bed-material transport and w_p is the width of a particular portion of the cross section. Next, I computed long-term average sediment load for each simulation:

$$i_{bY_{ix}} = \frac{\sum_{D} i_{bD_{ix}}}{t} \tag{9}$$

where i_{bYix} is annual (Y) total bed-material load and t is the number of years in each simulation. And finally, I calculated the annual transport extrema (i.e. maximum and minimum) and median for all simulations. Thus, my method results in estimates of central tendency, as well as variability in transport prediction (based on stochastic hydrology).

It is important to distinguish my method from one that seeks to characterize measurement or modeling uncertainty (e.g. [*Wilcock*, 2001]). My method uses the variability in the flow regime to define the range and probability distribution of sediment flux as to be expected from the variable flow (and ultimately precipitation). I have minimized the uncertainty in hydrology by modeling it [*Singer and Dunne*, Submitted]. If one were trying to make a single estimate of long-term sediment flux, my method provides additional estimates of the range around that long-term value. I obtain these additional estimates by statistically analyzing the results of multiple long-term simulations of stochastic hydrology. The error bars around an estimate, therefore, are not estimates of uncertainty; they are estimates of variability due to flow.

Figure 3.6 shows annual total bed-material load in tons/year plotted against exceedence probability for gravel and sand at one mainstem station (Hamilton City,

Figure 3.1). This figure combines simulated bed-material loads for gravel and sand grain sizes into sand and gravel classes, respectively, for simplicity of illustration. Each simulation produces a set of dots, one for each exceedence probability. Each set of thirty dots can be thought of as a sediment load frequency curve, akin to a flood frequency curve. The solid line represents the median value of all simulations and the dashed lines represent the extrema. For example, my simulations show that in about 50% of years annual total gravel transport at Hamilton City exceeds a value that ranges from ~20-400 kt/y with a median of ~200 kt/y. For resolution of this calculation, a reach width of 200 m, an upstream recruitment distance of 800 m (average annual transport distance of gravel tracers in [*California Department of Water Resources*, 1992] is within a range suggested by [*Bunte and MacDonald*, 1999]), and a sediment bulk density of 1.8 t/m^3, the computed annual sediment load at Hamilton City would scour to a depth of ~0.7 m. Although this calculation does not reflect process of scour and fill that may prevail over a year, it does illustrate the need to account for scour depth and armoring in future iterations of this method.

In the following paragraphs I present transport results for each mainstem gauging station based on these simulations. In the subsequent section, I use these transport estimates and those from tributaries to evaluate net changes in storage in the reaches of river between each mainstem gauging station. I assume that net changes in storage are spread evenly throughout a river reach.

Figure 3.7 shows the results of gravel and sand bed-material transport for my simulations at all mainstem cross sections. I have also plotted suspended load

simulated in my previous analysis [*Singer and Dunne*, 2001] and total load obtained by summing sand, gravel, and suspended loads. The method predicts that gravel transport makes up anywhere from 0-33% of the total load depending on the station, which is an expectable range.

A few noteworthy general results about local transport emerge from the modeling. Most importantly, local hydraulics and bed-material grain size distributions conspire to control annual transport rates at a given cross section. The effect of hydraulics on transport rates at mainstem stations is apparent in that downstream changes in annual load correlate with changes in local water surface slope (Figure 3.7 and Table 1). Bed grain sizes influence transport patterns in two ways. First, at locations where bed sediments are well sorted (e.g. Sacramento (SA), Table 3.1), transport rates are low (Figure 3.7), and at locations where there is high variance in bed grain sizes (e.g. Knights Landing (KL), Table 3.1), transport rates are high (Figure 3.7). Second, the percentage of a particular grain size in the bed at a cross section controls its transport relative to other size classes. For example, gravel bed-material load is slightly higher than sand bed-material load at Bend Bridge (BB) due to a relative scarcity of sand in the bed (17% sand > 0.5 mm). Although both of these conclusions are consequences of modeling assumptions, they appear to reflect empiricism. In fact, the high value of R^2 (0.86) for the multiple regression model (7) used to estimate the alpha parameter in (6) indicates the large influence that bed-material grain sizes have on bedload transport rates for various datasets.

The presented method produces transport patterns similar to those obtained for suspended sediment transport modeling by empiricism, suggesting that the method is capable of reproducing empirical patterns in bed-material transport. For example, both transport studies predict an increase in transport between Hamilton City (HC) and Butte City (BC), which was explained for suspended load by the influence of flood control levees in Reach 2 [*Singer and Dunne*, 2001]. It appears that the predicted increase in bed-material transport is, at least in part, due to a decrease in coarse sediments and an increase of medium sand in the bed material at BC (Figure 3.3). This change in bed material probably arises because the Sacramento River downstream of HC has no contiguous contact with Pleistocene river gravels (Red Bluff formation in 1:250,000 Calif. Division of Mines and Geol. quadrangles). My method also predicts a decrease in bed-material load between Butte City (BC) and Colusa (CO), which is consistent with the dramatic reduction in suspended sediment load simulated in a previous study [*Singer and Dunne*, 2001]. Colusa signifies a transition in transport pattern, where a major deflection of the river eastward around the Colusa Dome, the result of a magmatic intrusion 1.4-2.4 Mya and localized movement on the Willows fault [*Harwood and Helley*, 1987], appears to force decanting of washload into upstream flood bypasses [*Singer and Dunne*, 2001] and systematic deposition of sediments in the wide upstream reach of valley.

In other locations, predicted bed-material transport patterns diverge from their suspended load counterparts. This method predicts a decrease in bed-material transport between BB and HC (Figure 3.7), which probably reflects the increase in

valley width associated with the Sacramento's transition from an entrenched river in Iron Canyon to an aggraded, lowland river in the Central Valley. The valley width increase allows for more in-channel accommodation space, where bed sediments can organize into defined bedforms, perhaps resulting in better sorting of the bed-material mixture (i.e. lower sorting coefficient). Bed-material calculations also show an increase in bed-material load between CO and KL (Figure 3.7), which is consistent with the observation of an abrupt increase in 8-32 mm gravels and medium sand in the bed material at Knights Landing (Figure 3.3). These factors suggest that there is a sediment source in Reach 4. Inspection of the Sacramento geologic quadrangle (1:250,000, Calif. Div. of Mines and Geol.) reveals that the Sacramento River is dissecting Pleistocene fanglomerates of Cache Creek, which extend across the floodplain in Reach 4. The local change in bed-material results in a relatively high sorting coefficient (Table 3.1) and thus, high bed-material transport. Finally, bed-material calculations predict huge declines in transport between KL and Sacramento (SA). This result stems from an extremely low sorting coefficient at SA (Table 3.1), minute quantities of gravel in the bed material (Figure 3.3f), and low (or occasionally negative) water surface slopes at this section, which is located in the tidal zone. These factors do not, however, appear to influence suspended load, which increases at Sacramento probably because of fine sediment delivery from Feather and American Rivers (tributaries shown in Figure 3.1).

The method presented here can also be used to simulate annual peaks in bed-material load to ascertain the role of individual flood events on sediment transport. I

computed annual peak bed-material load as the one-day maximum load for each year. As before median and extrema of this value, for a given exceedence probability, are determined for the 50 simulations. Figure 3.8 shows one-day peak bed-material load for sand and gravel. The highest one-day sand transport peak for all simulations is ~340 kt, or ~170% of the median annual total sand flux at Hamilton City. Annual totals and one-day peaks of bed-material transport will be used in the next section to evaluate net changes in reach-averaged sediment storage.

Bed-material Budgets

I evaluated simple mainstem sediment budgets from the estimates of total annual bed-material load and one-day maximum bed-material load into the Sacramento from tributaries and past each mainstem gauging station. These are crude mass balances in the sense that I compute how much sediment gets stored in or eroded from a given reach, but I provide no mechanistic explanation of how the mass balance is being struck within the reach (e.g. changes in morphology). For simplicity, I assume that simulated erosion for a reach is distributed uniformly over the bed surface, in order to compute reach-averaged erosion rates.

I computed bed-material influx to the Sacramento River from four signature tributaries, which represent the four geologic provinces used in *Singer and Dunne* [2001]. Tributary loads were also computed by driving (6) with discharge data simulated by HYDROCARLO [*Singer and Dunne*, 2001]. However, instead of routing this flow with HEC-RAS, I obtained mean flow depths, h_x, for each day from

stage-discharge rating curves. Since I had no calibrated values of Manning's n to compute velocity in (2), I used a velocity-stage rating curve from USGS field measurements. And I measured slopes from USGS 7.5-minute topographic quadrangles for use in (3). As in the suspended load study, I scaled the computed signature tributary loads (and their uncertainties) by the ratio of drainage areas to compute the load entering the mainstem from each Sacramento tributary. I combined these time varying loads with those computed for mainstem stations to evaluate simple, reach-averaged, bed-material budgets.

Annual Total Bed-material Load

I computed simple budgets for annual total bed-material load, which indicates long-term spatial patterns in mainstem sediment transport. Annual divergence, or net difference in bed-material load, was computed for each reach as:

$$\Delta i_{bYR} = i_{bYU} - i_{bYE} + i_{bYL} \qquad (10)$$

where Δi_{bYR} is reach-averaged (R) change in annual (Y) total bed-material load; i_{bYU} is annual total bed-material load entering the reach from upstream (U); i_{bYD} is annual total bed-material load leaving the reach at its downstream end (E for efflux); and i_{bYL} is the annual bed-material load entering the reach from tributaries (L for lateral input). I assume that no bed-material load leaves the reach through flood diversions, which decant mostly washload [*Singer and Dunne*, 2001], and that fining by attrition is

negligible. This type of budget may be computed for each grain size (because I compute fractional transport rates), but for simplicity I present results from budgets computed for total bed material load (a), gravel load (b), and sand load (c) (Figure 3.9). The computational spreadsheets for annual gravel and sand bed-material load are contained in Appendix C and D.

The bars in Figure 3.9 represent the median of the expected range (i.e. the 50% exceedence probability) of net erosion or deposition for a year and for a reach, and the T-bars represent the extrema of this range resulting from all simulations of stochastic hydrology (i.e. fifty 30-year runs). The T-bars increase in magnitude in the downstream direction because I propagated the variability. The upper T-bars, for example, represent the maximum of the expected range (i.e. the 50% exceedence probability) for all upstream mainstem stations and tributaries added together. The lower T-bars represent the same for the minimum of the range.

The budget for annual total bed-material load indicates significant net bed-material erosion in Reaches 0, 2, and 4, and deposition in Reaches 1, 3, and 5 (Figure 3.1). I compared this budget with one previously evaluated for suspended load (Figure 6 in [*Singer and Dunne*, 2001]), which identified erosion in Reaches 2, 4, and 5 and net deposition in Reaches 0, 1, and 3. Reaches 1, 2, 3, and 4 show a similar pattern in both budgets, indicating there are potentially similarities in storage patterns between the various modes of sediment transport. It should be noted that the suspended load budget was evaluated using historical flow, because the time series approach used in that study does not lend itself to simulation under a range of flow

conditions. An explanation of the differences between the bed-material load and suspended load budgets requires a better understanding of the sources of and the controls on washload in the Sacramento basin, so the following discussion will be limited to the simulated bed-material budgets.

Figures 3.9b and 3.9c show annual total budgets for gravel and sand, respectively. These budgets are subsets of Figure 3.9a that reveal which grain size fractions are responsible for the net divergence in a given reach. The majority of the simulated divergences result from imbalances in sand bed-material transport, as one would expect. However, significant gravel divergences can indicate the state of the riverbed in a given reach.

For example, gravel erosion is predicted in Reaches 0, 2, and 4. Annual gravel erosion in Reach 0 is predicted to be 7 cm/y when averaged over the area of the bed in that reach (assuming sediment density of 1.8 t/m^3 and transporting width of 150 m). With no additional upstream sources of gravel entering the reach (i.e. beyond the simulated tributary input), net erosion in this reach is predicted to prevail. Annual gravel erosion rates in Reaches 2 and 4 are predicted to be 5 cm/y and 15 cm/y, respectively. Perhaps most interesting is the high gravel erosion rate predicted in Reach 4. As previously discussed, this erosion likely results from the dissection of a Pleistocene fan composed of fine and medium size gravels. An increase in gravel transport seems reasonable in a locale where a local source of gravel can be transported over an increasingly sandy bed (Figure 3.3). It is not reasonable, however, to expect that predicted erosion in any river reach would be spatially

uniform. The method presented here can resolve transport rates for each portion of a cross section, but no such assessments can be made of river reaches. I have a plan to conduct high-resolution sediment routing through each reach to determine where topographic adjustments within a river reach might be expected.

Significant sand erosion is predicted in Reaches 2 and 4, but is highest in Reach 4. The erosion of sand predicted in this reach is in part, due to a shift in grain sizes in suspension. For reasons that are not clear, Figures 3.3d and e show the suspended load fines between CO and KL. For example, the 0.38 mm fraction decreases from 7% to 2.5% of the suspended load, with no apparent change in its presence in the bed material. Consequently, I included the 0.38 mm size fraction in my computations of bed-material load, and this, alone, may account for the high erosion of sand bed-material predicted in Reach 4.

The deposition in Reach 3 probably results from water sequestration above Colusa as previously discussed. Deposition in Reach 5 is the combined effect of large sand loads into this reach from the Feather River and significant fine gravel loads entering from upstream. It appears that Reach 5 is a sink for gravel. Based on recent floodplain cores we have extracted from Yolo Bypass (unpublished data), it is likely that a large percentage of the sand bed material (e.g. the fine fractions) being deposited in this reach actually passes over Fremont Weir into Yolo Bypass (Figure 3.1), which shunts flood flow from the Sacramento River.

One-day Peak Bed-material Load

I computed a simple budget for one-day annual peak bed-material load, which indicates the spatial effects of maximum flux into and through the mainstem Sacramento. I simulated peak sediment delivery to the Sacramento from tributaries and past mainstem gauging points. This calculation indicates the short-term consequences of scour and fill in large floods. The peak budget is computed as:

$$\Delta i_{bD_{\max}R} = i_{bD_{\max}U} - i_{bD_{\max}E} + i_{bD_{\max}L} \qquad (11)$$

where the symbols are the same as in (10), but the subscript D_{max} refers to one-day annual peak bed-material load. Figure 3.10 shows the results of this budget, where the symbols are the same as in Figure 3.9. The computational spreadsheets for peak gravel and sand bed-material load are contained in Appendix E and F. The spatial patterns for this budget are similar to those of the annual total budget. Erosion is predicted in Reaches 0, 2, and 4 and deposition prevails in Reaches 0, 3, and 5. In other words, the total annual budget is an integration of flood conditions that induce similar patterns in net bed-material load divergence.

Discussion

I have developed a method for simulating daily bed material flux, but it cannot yet be tested empirically, because such data do not exist. To reduce sources of uncertainty not associated with stochastic hydrology, I have tried to accurately parameterize each equation based on the best available datasets of channel

dimensions and hydraulic data, bed material texture, and bedload transport. The accuracy of transport predictions (and budgets) can be improved for a particular basin by collecting more field data. I have already discussed the need for assessing armoring and scour depth, but there are other data collection opportunities that would improve this method. For example, simulations on the Sacramento would benefit from bedload measurements and bed material surveys for each major tributary to simulate influx from each separately, instead of scaling loads from signature tributaries. Additional cross sections could also be surveyed in tributary basins so that explicit flood routing could be conducted to obtain water surface profiles for use in (2), and to calibrate Manning's n for use in (3). Bedload flux measurements for Knights Landing, Sacramento, Feather River, and other sandy environments would also be useful to determine τ^*_c for these stations and to improve transport calibrations for sand-bed rivers. More bed material samples are required to accurately characterize grain size distributions at all stations, especially Bend Bridge and Hamilton City where these data are limited.

The method introduced here simulates sediment flux associated with flood days above a threshold. This threshold was developed by a repeatable statistical procedure [*Singer and Dunne*, Submitted], without consideration of thresholds for sediment transport, for instance. This is because HYDROCARLO was designed to simulate flows at the upper, less frequent end of the flood frequency curve. I assume that these floods do most of the geomorphic 'work' (i.e. sediment transport) in sediment transport [*Lustig*, 1965; *Stewart and LaMarche*, 1967; *Pitlick*, 1988].

I tested the assumption that flood events transport the majority of sediment in the Sacramento basin. I computed bed material sediment load for non-floods by driving equations (1), (2), (3), (4), and (6) with the threshold flood condition for each station. I multiplied the geometric mean of baseline transport (i.e. square root of the computed bed-material transport at the flood threshold) by 365 days to assess annual transport rates during non-floods. Consistent with other findings on California rivers [*Lustig*, 1965; *Stewart and LaMarche*, 1967; *Pitlick*, 1988], sediment transport in the Sacramento River is dominated by floods. According to my analysis, flood days are anywhere from 17 to 64 times more effective than non-flood days at transporting bed-material in the Sacramento River. Floods dominate geomorphic work in the Sacramento basin, thought it is a subject of further research to determine which floods (e.g. large, infrequent or small, frequent) do the majority of the geomorphic work [*Wolman and Miller*, 1960; *Wolman and Gerson*, 1978].

I have demonstrated how my method of basinwide sediment flux simulation may be applied to sediment budgets, but it may also be useful in predicting channel geometry resulting from an integration of rare, large flows over a period of years or decades. It has further potential to aid in the design and implementation of river rehabilitation strategies (e.g. gravel augmentation), which generally require a prediction horizon of decades and a characterization of risk.

Conclusion

I have developed and demonstrated a method for simulating basinwide bed-material flux and storage change based on variability in flow. I applied the model to the Sacramento River basin to simulate daily influx to and through the mainstem Sacramento. The model may be used to estimate the central tendency and extrema of annual total and one-day peak flux. These estimates can then be used in work on sediment budgets, channel morphology, and river rehabilitation. Simulations in the Sacramento basin highlight imbalances in bed-material transport and storage that, in a general way, point to local hydraulics and downstream changes in grain sizes in the riverbed. They also confirm the assumption that floods transport the majority of bed-material in the Sacramento River.

References

Andrews, E.D., Measurement and computation of bed-material discharge in a shallow sand-bed stream, Muddy Creek, Wyoming, *Water Resources Research*, *17* (1), 131-141, 1981.

Ashida, K., and M. Michiue, Study on hydraulic resistance and bedload transport rate in alluvial streams, *Transactions, Japan Society of Civil Eng.*, *206*, 59-69, 1972.

Batalla, R.J., Evaluating bed-material transport equations using field measurements in a sandy gravel-bed stream, Arbucies River, NE Spain, *Earth Surface Processes and Landforms*, *22*, 121-130, 1997.

Blott, S.J., and K. Pye, Gradistat: A grain size distribution and statistics package for the analysis of unconsolidated grains, *Earth Surface Processes & Landforms*, *26*, 1237-1248, 2001.

Buffington, J.M., and D.R. Montgomery, A systematic analysis of eight decades of incipient motion studies with special reference to gravel-bedded rivers, *Water Resources Research*, *33* (8), 1993-2029, 1997.

Bunte, K., and L. MacDonald, Scale considerations and the detectability of sedimentary cumulative watershed effects, pp. 328, National Council for Air and Stream Improvement, Technical Bull. 776, Research Triangle Park, NC, 1999.

Burrows, R.L., W.W. Emmett, and B. Parks, Sediment transport in the Tanana River near Fairbanks, Alaska, 1977-79, pp. 56, US Geological Survey Water Resources Investigation Report 81-20, 1981.

California Department of Water Resources, Sacramento River spawning gravel restoration phase I progress resport, pp. 37, Red Bluff, 1992.

California Dept. of Water Resources, Sacramento River bank erosion investigation, Dept. Water Resources, Sacramento, CA, 1994.

Dunne, T., L. Mertes, R. Meade, and J. Richey, Exchanges of sediment between the flood plain and channel of the Amazon River in Brazil., *Geol. Soc. Amer. Bulletin*, *110* (4), 450-467, 1998.

Edwards, T.K., and G.D. Glysson, Field methods for measurement of fluvial sediment, U.S. Geological Survey., Reston, VA, 1999.

Emmett, W.W., A field calibration of the sediment-trapping characteristics of the Helley-Smith bedload sampler, US Geological Survey, Professional Paper 1139, Washington, D.C., 1980.

Emmett, W.W., and H.R. Seitz, Suspended- and bedload-sediment transport in the Snake and Clearwater rivers in the vicinity of Lewiston, Idaho, March, 1972 through June,1973, US Geological Survey Report, 1973.

Emmett, W.W., and H.R. Seitz, Suspended- and bedload-sediment transport in the Snake and Clearwater Rivers in the vicinity of Lewiston, Idaho : July, 1973 through July, 1974, US Geological Survey Report, 1974.

Engelund, F., and E. Hansen, A monograph on sediment transport in alluvial streams, in *Teknisk Vorlag*, pp. 63, Technical University of Denmark, Copenhagen, Denmark, 1967.

Gomez, B., and M. Church, An assessment of bed load sediment transport formulae for gravel bed rivers, *Water Resources Research*, *25* (6), 1161-1186, 1989.

Guy, H.P., D.B. Simons, and E.V. Richardson, Summary of alluvial channel data from flume experiments, 1956-61, US Geological Survey Professional Paper 462-I, Washington, D.C., 1966.

Harrold, P.E., and R.L. Burrows, Sediment transport in the Tanana River near Fairbanks, Alaska, 1982, US Geological Survey Water Resources Investigation Report 83-4213, 1983.

Harwood, D.S., and E.J. Helley, Late Cenozoic tectonism of the Sacramento Valley, California, US Geol. Survey Prof. Paper 1359, Wash., D.C., 1987.

Helley, E.J., and W. Smith, Development and calibration of a pressure-difference bedload sampler, pp. 18, US Geological Survey, Open-File Report, Menlo Park, CA, 1971.

Jones, M.L., and H.R. Seitz, Suspended- and bedload-sediment transport in the Snake and Clearwater rivers in the vicinity of Lewiston, Idaho, August 1976 through July 1978, pp. 87, US Geological Survey Open File Report 79-417, 1979.

Jones, M.L., and H.R. Seitz, Sediment transport in the Snake and Clearwater Rivers in the vicinity of Lewiston, Idaho, pp. 179, US Geological Survey Open File Report 80-690, 1980.

Krumbein, W.C., Size-frequency distributions of sediments and the normal phi curve, *J. Sedimentary Petrology*, *8*, 84-90, 1938.

Lustig, L.K., Sediment yield of the Castaic watershed, Western Los Angeles County California-A quantitative approach, pp. 23, US Geological Survey Professional Paper 422-F, Washington, DC, 1965.

McLean, D.G., Sensitivity analysis of bedload equations, in *Proceedings Canadian Society of Civil Engineering Annual Conference*, pp. 1-15, Saskatoon, 1995.

Milliman, J.D., and R.H. Meade, World-wide delivery of river sediment to the oceans, *J. Geology*, *91*, 1-21, 1983.

Milliman, J.D., and J.P.M. Syvitski, Geomorphic/tectonic control of sediment discharge to the ocean: The importance of small mountainous rivers, *J. Geology*, *100*, 525-544, 1992.

Parker, G., P.C. Klingeman, and D.G. McLean, Bedload and size distribution in paved gravel-bed streams, *ASCE, Proceedings, J. Hydraulics Div.*, *108*, 544-571, 1982.

Pitlick, J., The response of coarse-bed rivers to large floods in California and Colorado, Dissertation thesis, Colorado State University, Fort Collins, CO, 1988.

Reid, L.M., and T. Dunne, *Rapid Evaluation of Sediment Budgets*, 160 pp., Catena-Verlag, Cremlingen, Germany, 1996.

Shields, A., Anwendung der aenlichkeitsmechanik und der turbulenzforschung auf die geschiebebewegung, Mitteilungen der Preussischen Versuchsanstalt fur Wasserbau und Schiffbau,, Berlin, Germany (Translated to English by W.P. Ott and J.C. van Uchelen, CalTech, Pasadena, CA), 1936.

Singer, M.B., and T. Dunne, Identifying eroding and depositional reaches of valley by analysis of suspended-sediment transport in the Sacramento River, California, *Water Resources Research*, *37* (12), 3371-3381, 2001.

Singer, M.B., and T. Dunne, An empirical-stochastic, event-based model for simulating inflow from a tributary network: Theoretical framework and application to the Sacramento River basin, California, Submitted.

Stewart, J.H., and V.C. LaMarche, Erosion and deposition produced by the flood of December 1964 on Coffee Creek Trinity County, California, pp. 22, US Geological Survey Professional Paper 422-K, Washington, DC, 1967.

Vanoni, V., *Sedimentation Engineering*, 745 pp., American Soc. Civil Eng., New York, NY, 1975.

White, W.R., W.R. Milli, and A.D. Crabbe, Sediment transport theories: a review, *Proceedings of the Institution of Civil Eng.*, *59* (2), 265-292, 1975.

Wilcock, P.R., Estimating local bed shear stress from velocity observations, *Water Resources Research*, *32*, 3361-3366, 1996.

Wilcock, P.R., Two-fraction model of initial sediment motion in gravel-bed rivers, *Science*, *280*, 410-412, 1998.

Wilcock, P.R., Toward a practical method for estimating sediment-transport rates in gravel-bed rivers, *Earth Surface Processes & Landforms*, *26*, 1395-1408, 2001.

Wolman, M.G., and R. Gerson, Relative time scales of time and effectiveness of climate in watershed geomorphology, *Earth Surface Processes & Landforms*, *3*, 189-208, 1978.

Wolman, M.G., and J.P. Miller, Magnitude and frequency of forces in geomorphic processes, *J. Geology*, *68*, 54-74, 1960.

Yang, C.T., and S. Wan, Comparisons of selected bed-material load formulas, *J. Hydraulic Engineering*, *117* (8), 973-989, 1991.

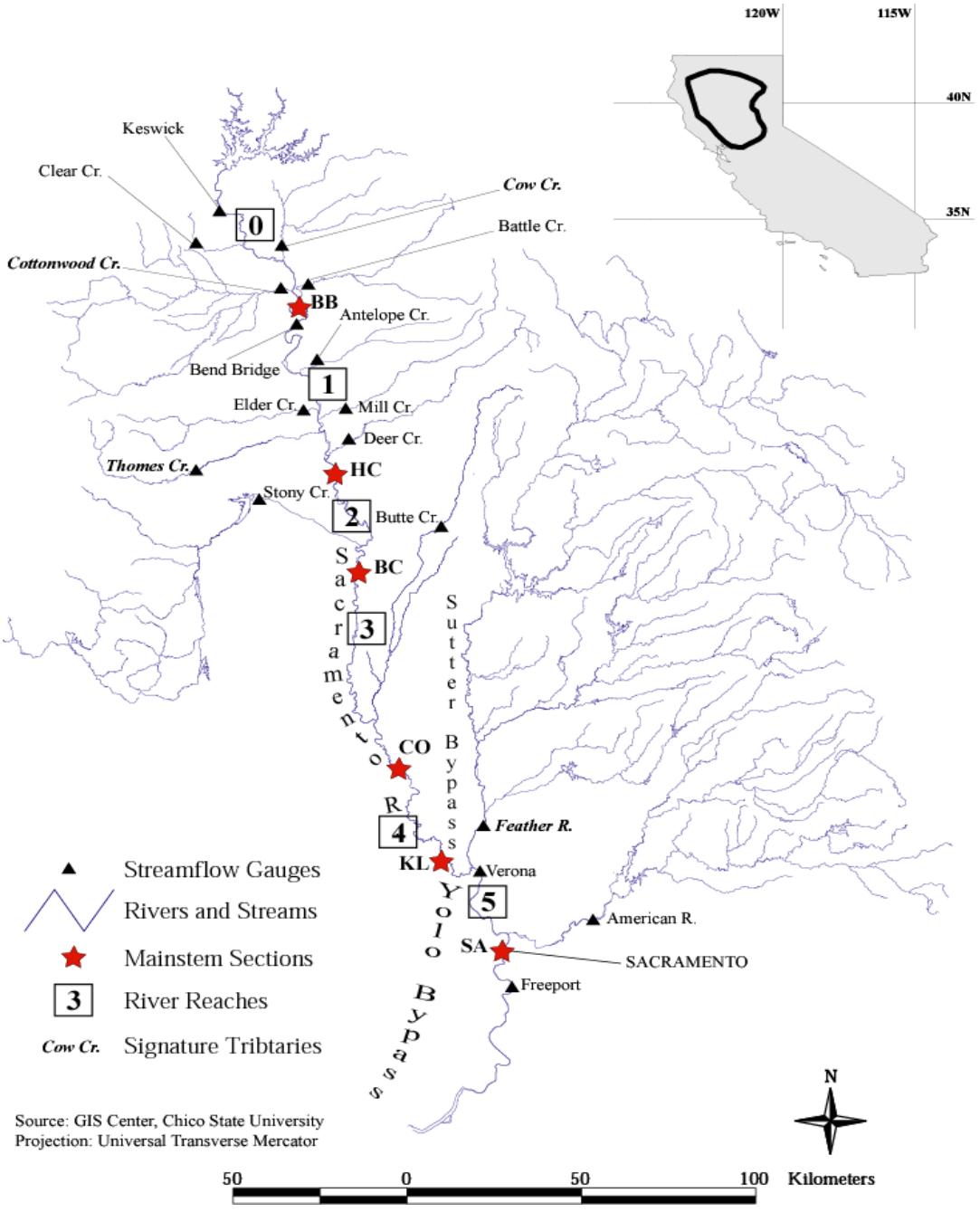

Figure 3.1 Map of study basin showing streamflow gauges used for stochastic flow simulation, stream network, mainstem sections through which bed-material transport was computed, river reaches for which simple sediment budgets were evaluated, and signature tributaries used to compute sediment entering the mainstem from common geologic provinces (scaled by drainage area).

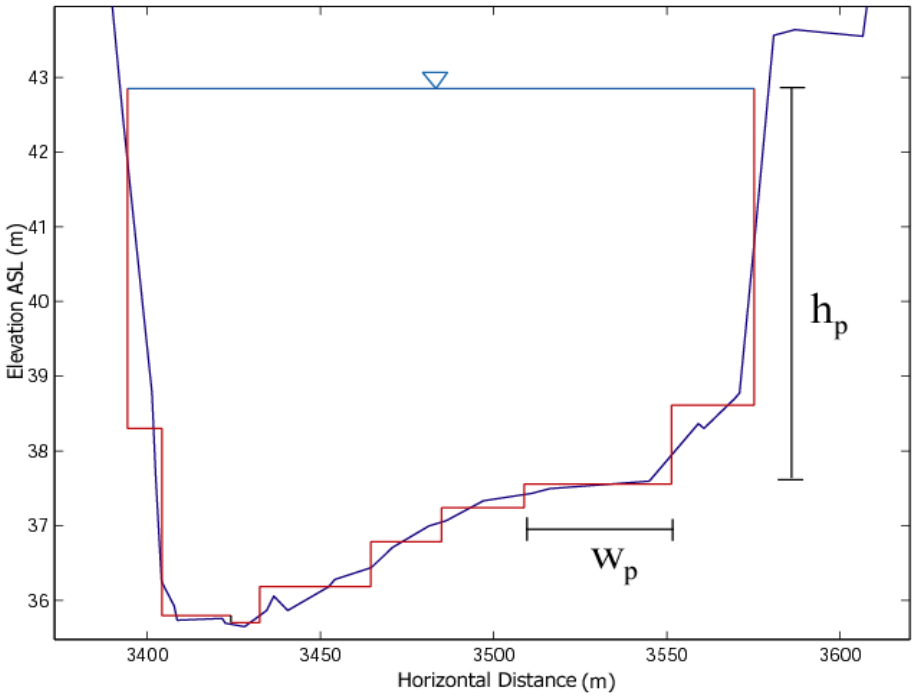

Figure 3.2 Plot of the cross section at Hamilton City illustrating the simplification of cross sections into seven distinct portions for which I computed sediment transport. Each portion, *p*, has a flow depth, *h*, and a width, *x*.

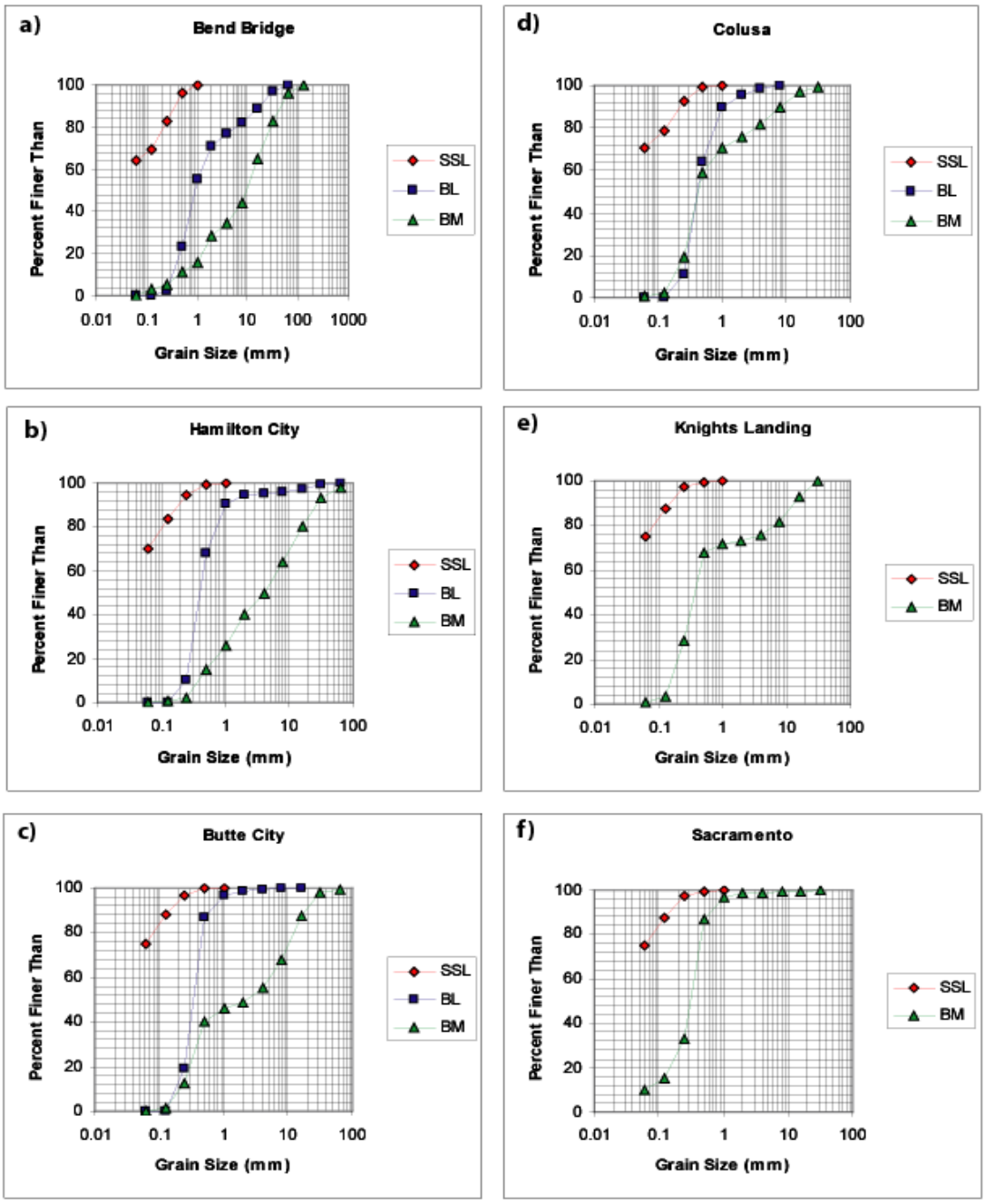

Figure 3.3 Grain-size distributions of suspended load (SSL), bedload (BL), and bed material (BM) for the six mainstem cross sections. Generally, 0.5 mm represents a lower limit grain size of the bed material. This grain size is present in < 5% of suspended load samples and > 5% of bed material samples. Suspended load curves are generated from > 10 samples. Bedload curves are generated from between 5 and 25 samples. Bed material curves are generated from between 1 and 20 samples.

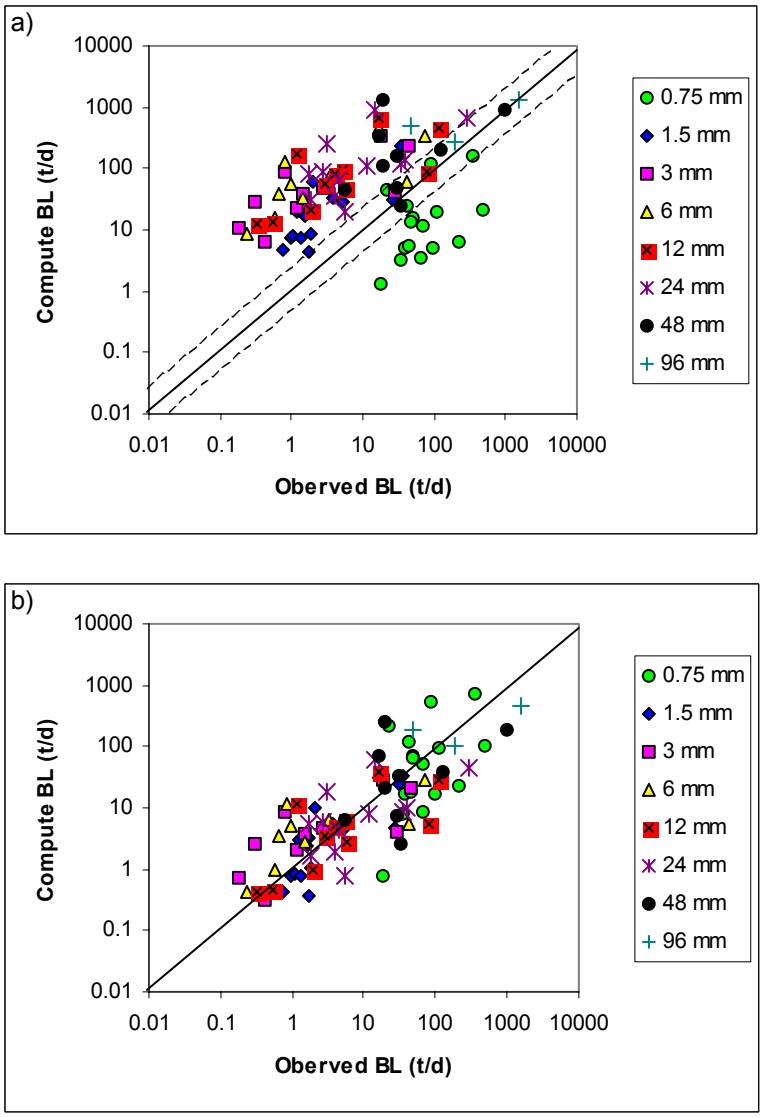

Figure 3.4 Plots of computed bedload v. observed bedload for Clearwater River, Idaho. The different panels are a) Engelund-Hansen formula (5) predictions; b) my modified version (6) calibrated to the majority of data in each grain size class. I restricted my calibration to total transport rates (sum of all transported grain sizes) greater than 100 t/d.

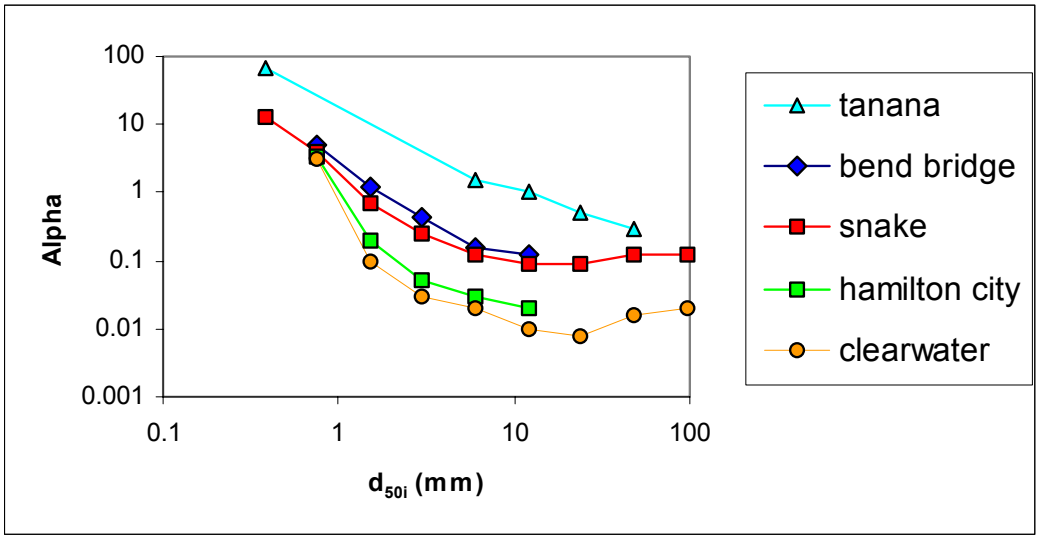

Figure 3.5 Fitted alpha (coefficient in (6)) values from calibrations to bedload data in each grain size class. Again I restrict calibration to total transport rates greather than 100 t/d. The plot shows data from the Tanana River in Alaska, Bend Bridge and Hamilton City in the Sacramento basin, and the Snake and Clearwater Rivers in Idaho.

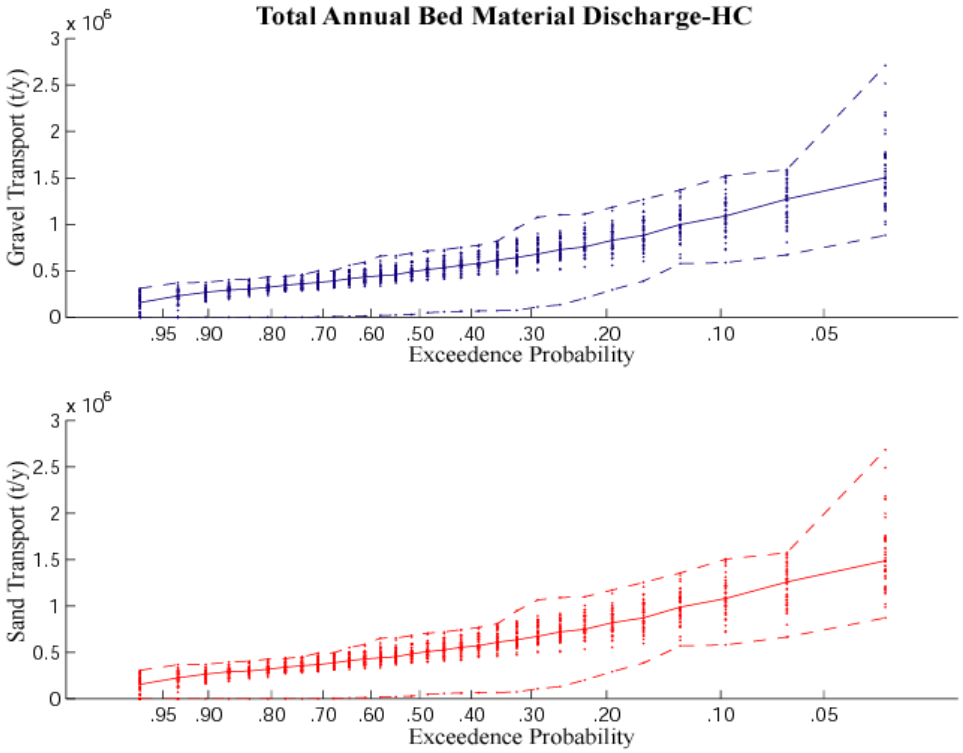

Figure 3.6 Total annual bed-material loads (t/y) for gravel (upper panel) and sand (lower panel) at Hamilton City plotted against exceedence probability. Each simulation produces 30 dots (one for each year). The median of all simulations is represented by the solid line and the extrema by dashed lines.

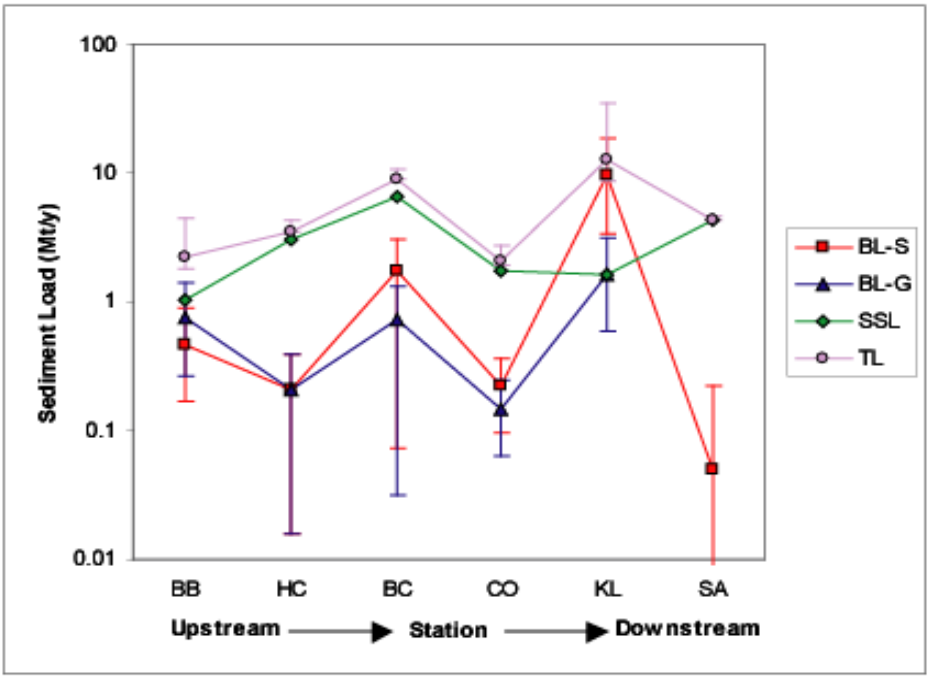

Figure 3.7 Mainstem sediment loads (Mt/y) including total load (TL), suspended load (SSL), sand bed-material load (BL-S), and gravel bed-material load (BL-G). Suspended loads were simulated in a previous study [Singer and Dunne, 2001]. The error bars on the bed-material estimates represent the uncertainty associated with stochastic hydrology.

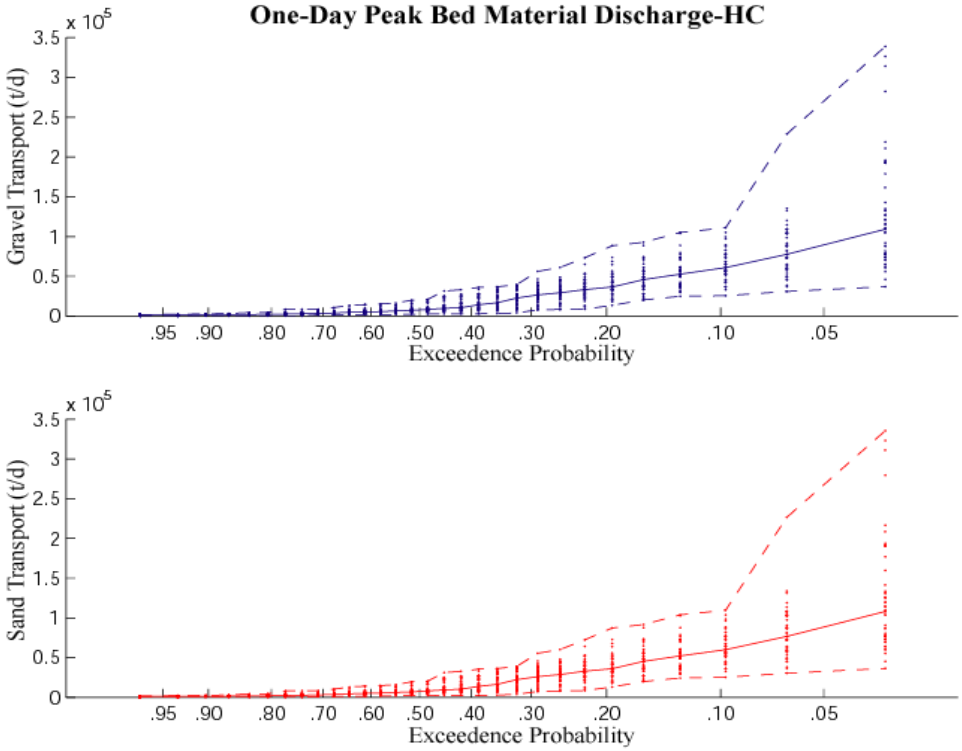

Figure 3.8 One-day peak bed-material loads (t/d) for gravel (upper panel) and sand (lower panel) at Hamilton City plotted against exceedence probability. Each simulation produces 30 dots (one for each year). The median of all simulations is represented by the solid line and the extrema by dashed lines.

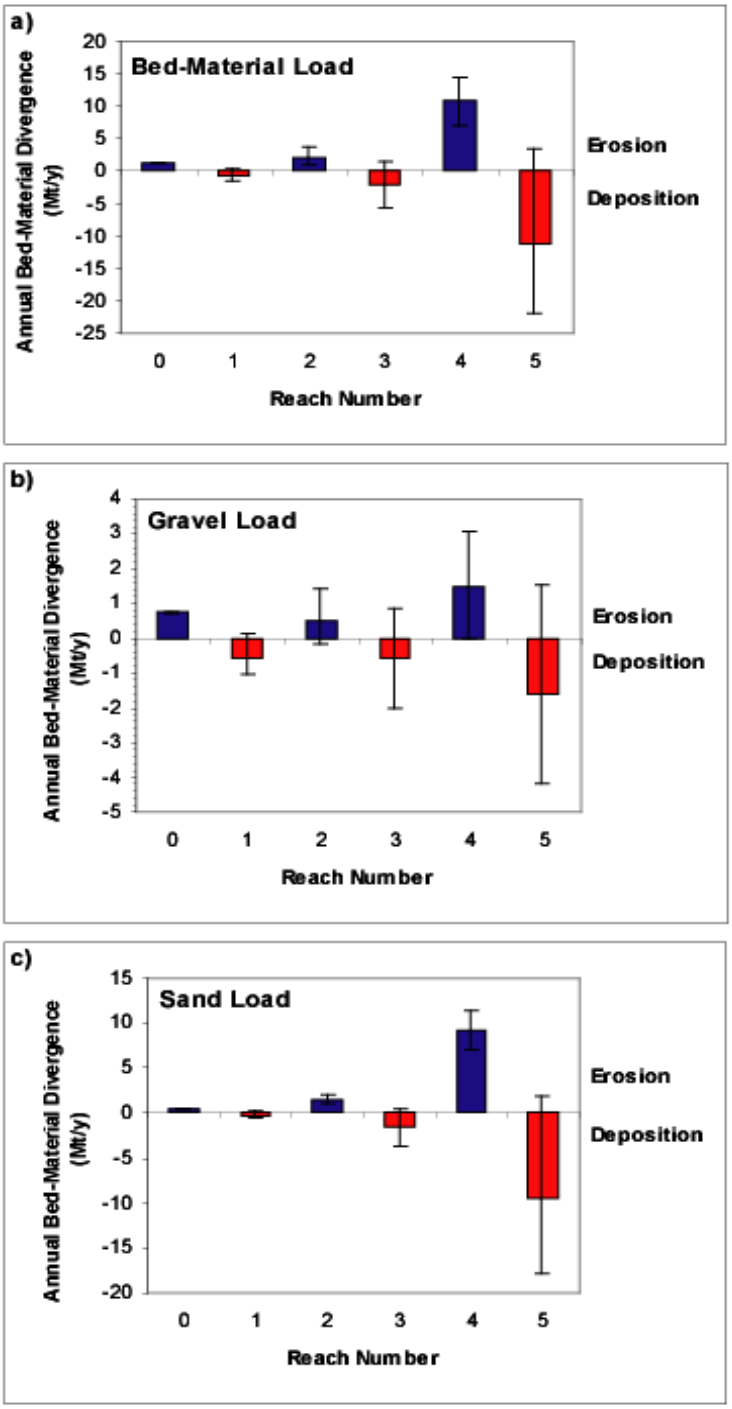

Figure 3.9 Simple total annual bed material budgets for all bed material (a), the gravel portion (b), and the sand portion (c). Divergences (Mt/y) are net differences in sediment transport for each reach. Negative divergence is deposition and positive is erosion. Error bars represent the variability in the annual total divergences associated with stochastic hydrology, which was propagated downstream.

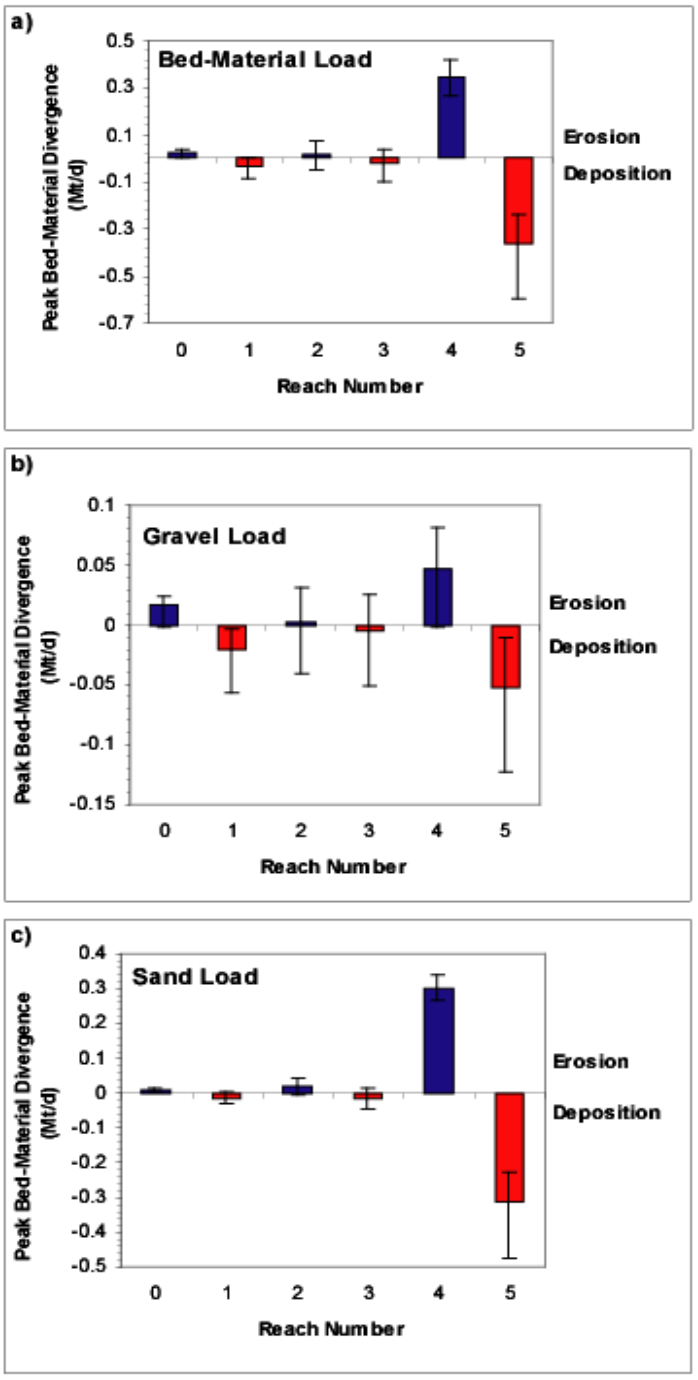

Figure 3.10 Simple one-day peak bed material budgets for all bed material (a), the gravel portion (b), and the sand portion (c). Divergences (Mt/d) are net differences in sediment transport for each reach. Negative divergence is deposition and positive is erosion. Error bars represent the variability in the one-day peak divergences associated with stochastic hydrology, which was propagated downstream.

Table 3.1 Station characteristics

Station	Drainage Area (km^2)	River km	Manning's n	WS Slope	$d50_j$(mm)	Tau^*_c	Sort
Bend Bridge	23051	418.9	0.035	0.00131	9.50	0.053	2.493
Hamilton Cty	28645	320.7	0.035	0.00026	4.00	0.136	2.300
Butte Cty	31274	271.2	0.035	0.00050	2.50	0.133	2.598
Colusa	31313	231.1	0.035	0.00009	0.42	0.429	2.055
Knights Lndg	37645	144.2	0.035	0.00011	0.35	**0.429**	2.436
Sacramento	60886	96.0	0.030	0.00003	0.03	**0.429**	0.985
Cottonwood	2401	-	-		2.50	0.013	1.790
Cow	1101	-	-		10.00	0.11	2.993
Thomes	736	-	-		4.50	0.012	1.807
Feather	2065	-	-		0.35	**0.429**	0.700

Table 3.1 Station, drainage area, river kilometer, Manning's n, water surface slope (for baseline conditions), d_{50j}, and τ^*_c. and sorting coefficient. The bold figures in the τ^*_c column represent stations for which no bedload data were available. I simply applied the τ^*_c from Colusa to compute bed-material load at these stations.

CHAPTER 4. MODELING THE DECADAL INFLUENCE OF RIVER REHABILITATION SCENARIOS ON BED-MATERIAL SEDIMENT TRANSPORT IN A LARGE RIVER BASIN

Abstract

To illustrate the utility of modeling tools described in the foregoing chapters, I simulated the impact of river rehabilitation strategies on decadal bed-material flux in the Sacramento River. I used a stochastic flood generator and calibrated sediment transport formulae to compute daily sediment flux past various mainstem cross sections and net accumulation between them. I modified constants in the model space to reflect the implementation of three major river rehabilitation strategies being considered in the Sacramento Valley: gravel augmentation, setback levees, and flow alteration [*CALFED*, 1997]. I compiled the results of 50 simulations, each of 30 years, to generalize about the long-term influence of these strategies on bed-material sediment transport and storage in the Sacramento. As such, the results describe changes in habitat distribution and condition before and decades after river rehabilitation. The results indicate that rehabilitation strategies modulate imbalances in total annual bed-material sediment budgets.

Introduction

Lowland aquatic riverine ecosystems have declined over the last century, primarily in response to deforestation and engineering intended to control floods, generate hydroelectricity, irrigate agricultural fields, and provide drinking water [*American Society of Civil Engineers*, 1992; *Power et al.*, 1995; *Vitousek et al.*, 1997; *Anderson*, 2000]. Dams have altered the timing, frequency, magnitude, and duration of floods and have cut off sediment supply from upstream [*Williams and Wolman*, 1984; *Richter et al.*, 1996; *Magilligan*, In Press]. Flood control levees have disconnected rivers from their floodplains, increased in-channel flow depths and shear stresses [*Laddish*, 1997; *Gergel et al.*, 2002], and prevented sediment recruitment from bank erosion sources. Gravel mining operations in riverbeds and floodplains have further limited sediment supply, especially coarse material required by salmonids. Due to reduced sediment supply, bed-material substrates have coarsened downstream of major dams, further limiting the ability of salmonids to find suitable spawning habitat [*Kondolf and Wolman*, 1993; *Kondolf*, 1995]. Sediment transport has also been affected by localized degradation due to channelization [*Biedenharn et al.*, 2000; *Singer and Dunne*, 2001], and deposition resulting from reduced flood peaks [*Kondolf and Wilcock*, 1996; *Pitlick and Van Steeter*, 1998]. These factors have altered the forcing conditions of processes that control rivers characteristics, the links between sediment and aquatic habitats [*American Society of Civil Engineers*, 1992], and thus the habitats themselves.

Much of the previous research on rehabilitation in fluvial systems has focused on descriptions of how flow regimes have been altered (e.g. [*Richter et al.*, 1996;

Richter et al., 1998; *Richter and Richter*, 2000; *Magilligan*, In Press]) and generally how these alterations affect aquatic and riparian ecosystems (e.g. [*Vannote*, 1980; *Junk et al.*, 1989; *Sparks*, 1992; *Stanford et al.*, 1996; *Poff et al.*, 1997]). Other work has focused on the frequency and timing of flood pulses that mobilize the bed, release fines, and clean fish roe of fine sediment and infuse them with oxygen [*Kondolf and Wilcock*, 1996; *Milhous*, 1998; *Pitlick and Van Steeter*, 1998; *Wu*, 2000], and 'ecologically acceptable' minimum flows required to maintain instream habitats [*Anderson*, 2000; *Gibbins and Acornley*, 2000]. *Pitlick and Van Steeter* [1998] linked flow frequency and bed-material transport to compute the effective discharge for channel maintenance in the Upper Colorado River. To my knowledge, there is only one unpublished study that has analyzed the effect of setback levees on shear stress in a river channel [*Laddish*, 1997]. This study used simplified channel geometry and hydraulics to compute the setback distance necessary to reduce channel shear stress to a value below the threshold for entrainment in a 10-mile reach of the upper Sacramento. The results were computed for the 2-year flood. Another unpublished study analyzed the effect of different setback distances on stage-discharge relationships in the lower Sacramento [*Bozkurt et al.*, 2000]. Still another quantitative study analyzed the effects of levee setbacks on riparian communities [*Gergel et al.*, 2002].

In response to decades of decline in the quality of aquatic and riparian habitats, river rehabilitation strategies are being proposed and implemented in major river basins such as the Sacramento in California, the Kissimmee in Florida, and

Danube in Romania. Rehabilitation in the form of flow alteration, sediment-supply manipulation, and removal of channel constraints has been proposed to improve the quality of riverine habitats over a period of decades. However, current modeling capability to assess the long-term influence of such strategies on sediment transport in river channels is limited.

The explicit links between channel sediment regime and aquatic riverine habitats have been reviewed elsewhere (e.g. [*American Society of Civil Engineers*, 1992]). In general, spatial and temporal patterns in sediment transport control long-term sediment budgets (e.g. net states of erosion or deposition), disturbance regimes (e.g. the frequency of gravel-bed mobilization), substrate conditions (e.g. the frequency of fine sediment flushing), and channel morphology (e.g. the habitat suitability of a particular river reach). Therefore, there is a need for modeling capability to analyze the response in sediment transport to rehabilitation scenarios within the context of streamflow variability. In this paper, I present an applied model that couples stochastic streamflow with bed-material flux calculations to simulate the adjustment in sediment flux to river rehabilitation scenarios. I demonstrate the model by simulating three river rehabilitation strategies in the Sacramento basin: gravel augmentation, flood control levee setbacks, and flow alteration.

However, to my knowledge, there is a paucity of literature on the long-term impact of proposed rehabilitation strategies on sediment transport, in general. It would be useful to know, for example, what effect rehabilitation strategies would have on sediment transport decades after their implementation. The lack of such a

predictive tool may have already contributed to timing errors in a flow experiment intended to create sand bars in the Colorado River [*Rubin et al.*, 2002]. I have developed the modeling capability to assess such long-term trends, including sediment supplies from tributaries, within the context of streamflow variability. This type of prediction would allow agencies responsible for river management to anticipate the central tendency, extrema, and probabilities of outcomes of these strategies, in particular river cross sections, in river reaches, or along entire river valleys.

Study Basin

The Sacramento River basin is ~70,000 km^2 in area and drains four geologic provinces. This study focuses on rehabilitation implementation in the mainstem Sacramento, which spans ~400 river kilometers and consists of an entrenched gravel-bed in the upper reaches and a mixed sand and gravel bed with a broad, flat floodplain in the lower reaches. It is a generally low gradient river (mean slope ~2.0 x 10^{-4}) that is affected by its tectonic and geologic legacy. Channel width varies from ~100 m in the upper reaches to ~250 m in the lower reaches. Much of the floodplain has been deforested and leveled, leaving few patches of riparian forest and scroll bar topography.

The bed of the upper Sacramento between Keswick and Bend Bridge (Figure 4.1) is poorly sorted [*Blott and Pye*, 2001] coarse gravel (subsurface d_{50} ~40 mm, surface d_{50} ~85 mm, unpublished data from Calif. Dept. of Water Resources), which

is armored in locations due to selective entrainment of finer gravels particles without their replacement from upstream sources. Between Bend Bridge and Knights Landing, the Sacramento flows over a very poorly sorted [*Blott and Pye*, 2001] bed of gravel and sand with localized sources of dissected coarse Pleistocene gravels. Between Knights Landing and Sacramento the river flows over a moderately sorted [*Blott and Pye*, 2001] sandy bed. Flood control levees have been built upon channel banks (especially in the lower Sacramento) to concentrate flow in the mainstem and shunt flood flow into bypasses via flood diversions. In this paper, I model river rehabilitation strategies in the mainstem Sacramento from below Shasta Dam (Keswick) down to the city of Sacramento (Figure 4.1). I compute transport at the following gauging stations: Bend Bridge (BB), Hamilton City (HC), Butte City (BC), Colusa (CO), Knights Landing (KL), Sacramento (SA). I also compute net accumulation of sediment in the river reaches between these stations.

Setting for Rehabilitation

Settlement of the Sacramento Valley began in earnest at the time of the California Gold Rush. Settlers farmed the floodplain contiguous to the Sacramento River to take advantage of the fertile soils. These settlers soon became frustrated by the frequency of flooding, which inundated large portions of the valley on an annual basis. Soon the combined influence of their political will and shoaling of the lower Sacramento due to hydraulic mining led to the implementation of a major flood control project funded by the United States government [*Kelley*, 1998]. The Army

Corps of Engineers constructed a system of levees and flood bypasses to convey flows below a threshold through the mainstem and shunt flows above the threshold through bypasses. The project was augmented between 1943 and 1967 with the construction of dams on the mainstem and its tributaries. Shasta Dam, constructed in 1943, has had the largest effect on streamflow in the Sacramento River [*US Army Corps of Engineers*, 1998].

Settlement of the Sacramento Valley over the last 150 years and the operation of the flood control system over the past 80 years have had negative effects on the riparian and aquatic habitats along the mainstem Sacramento, e.g. [*Thompson*, 1961; *Nielsen*, 1989; *Babcock*, 1995; *Taylor*, 1996; *Hunter*, 1999]. Terrestrial floodplain habitats have been degraded by human settlement, deforestation and severing of the connection between the Sacramento and its floodplain by high artificial levees. Aquatic habitats have declined due to alteration of natural streamflow below dams, increased flow velocity and stream temperature, decreased sediment supply because of bank protection and dams, and instream gravel mining [*California Department of Water Resources*, 1980; *Reeves and Roelofs*, 1982; 1985; *Kondolf*, 1995]. Fall run chinook, for example, had declined to ~50% of historic numbers by 1989 [*Nielsen*, 1989]. Spawning habitat in the basin is estimated to have been reduced to 4% of its historical total [*Peterson et al.*, 1982]. Additionally impoundments dampen flood peaks preventing flushing flows necessary for removing fine accumulations of sediment from spawning gravels [*Kondolf and Wilcock*, 1996; *Milhous*, 1998]. Channelization has also resulted in the loss of side channel habitat required by more

sedentary species and wintering salmon (as well as a loss of terrestrial riparian vegetation and the species it supports) because it prevents overbank flooding.

The degradation of these habitats has been the impetus for a major rehabilitation effort funded by the governments of the United States and the State of California. Among other things, federal and state agencies under the auspices of the CALFED Bay-Delta Program intend to improve the state of riparian and aquatic habitats while securing water supply and flood control [*CALFED*, 1997]. Proposed rehabilitation strategies include: 1) augmenting sediment supply to benefit anadramous fish; 2) setting back levees to create conservation areas; and 3) altering flows out of Shasta Dam to approximate the ecological benefits of pre-dam natural Central Valley streamflows [*CALFED*, 1997]. I analyzed the long-term, first-order impacts of these proposed strategies on bed-material sediment flux throughout the Sacramento basin.

Model Outline

I conducted this study using the wealth of data available for the Sacramento basin including bathymetry of the river channel, decades of historical daily streamflow, bed material surveys, and bedload measurements. I made assessments of the impact of rehabilitation strategies on total annual and one-day peak sediment budgets in river reaches of the Sacramento River from Shasta Dam to the city of Sacramento (Figure 4.1).

My method employs a stochastic hydrology model, flow routing software, and a bed-material flux simulation model. The development of the hydrology model and the bed-material flux model is discussed in detail in two previous papers [*Singer and Dunne*, Submitted-a; *Singer and Dunne*, Submitted-b], so I only outline them here. In this paper, I focus the discussion on how I alter the model space to reflect each rehabilitation strategy, the results of my modeling, and their implications for future work in river rehabilitation.

I developed a stochastic streamflow simulation model, HYDROCARLO, which semi-randomly samples from a collection of historical flood events at major tributary gauging stations [*Singer and Dunne*, Submitted-a]. HYDROCARLO was designed to simulate inflow into the mainstem of a large river from each of its major tributaries based on correlations in the flow records between them. I routed the simulated inflow through ~1000 cross sections (spaced ~800 m apart) along the mainstem Sacramento (extracted from bathymetry) using unsteady flow routing within HEC-RAS (HEC-RAS employs an implicit finite difference solution to the 1-D flow equations [*Barkau*, 1997]). Thus I simulated flow stage on a daily basis for many locations on the mainstem for a period of decades. Each simulation results in a stage and flow frequency curve for each location, which can be statistically analyzed to yield maxima, minima, and median values for each exceedence probability.

My bed-material flux model uses the stage output from HEC-RAS at selected mainstem locations to compute hydraulic variables. I modified and calibrated the Engelund-Hansen sediment transport formula [*Engelund and Hansen*, 1967] to

simulate daily bed-material transport in various grain size classes [*Singer and Dunne*, Submitted-b]. The model constants are cross-sectional geometry (extracted from bathymetry), bed-material grain size distribution (from bulk surveys), the alpha parameter for the transport equation (calibrated via multiple regression on grain size and local bed-material sorting coefficient), and dimensionless critical shear stress (computed from bedload data). I computed water surface slope at each cross section as a whole, and stage, velocity, shear stress, Shields stress, and excess shear stress for each portion of the cross section. I used these variables to compute daily bed-material flux at each station. These fluxes can be generalized to compute long-term estimates of total annual or one-day peak sediment flux. In conjunction with stochastic hydrology these estimates can be presented in a probabilistic framework to assess the risk of a particular outcome.

In my model development, I assumed one-dimensional flow, no bed armoring, sediment supply is limited by the proportions of each grain size present in the bed material, even distribution of bed material grain sizes across my sections, and no cross-sectional change. Furthermore, I compute mass balance for ~60 km river reaches, but make no mechanistic assessments of the resulting morphological change. As such, my assessments of transport and net divergence are first-order approximations made using the best available data. However, the values reported here provide a systematic view of the long-term spatial patterns in sediment transport resulting from major river rehabilitation strategies.

Rehabilitation Strategies

Gravel Augmentation

Gravel of suitable size for salmonid spawning habitat [*Kondolf and Wolman*, 1993] is limited in the Sacramento River due to major impoundments (e.g. Shasta Dam), bank protection [*California Dept. of Water Resources*, 1994], and in-channel gravel mining [*California Department of Water Resources*, 1980, 1985; *Kondolf*, 1995]. Work on sediment budgets has estimated that in-channel gravel mining can exceed rates of bedload transport by an order of magnitude [*Collins and Dunne*, 1989, 1990; *Kondolf and Swanson*, 1993]. There are additional unknown annual losses due to trapping behind Shasta Dam, itself (shown in Figure 4.1), though it is not clear how far downstream the consequential armor layer extends.

Gravel augmentation has been proposed and implemented periodically to replenish spawning gravels at strategic points along the Sacramento [*California Department of Water Resources*, 1980; 1985]. Various sites in Reach 0 were identified as active spawning sites and the added gravels were supposed to improve the existent spawning sites and create new ones [*California Department of Water Resources*, 1980]. Under the mandate of California Senate Bill (SB) 1086 (1986) and the federal Central Valley Project Improvement Act (CVPIA) (1992), ~1.5 Mt of gravel have been added to the upper Sacramento River below Shasta Dam between 1978 and 2000 at a cost of ~$26M (unpublished data from US Bureau of Reclamation). However, there has been little to no monitoring of augmented gravels to compute transport rates, nor to determine the efficacy of gravel augmentation in

improving in-stream habitat for fish (J. DeStaso, US Bureau of Reclamation, pers. comm.).

In a previous bed material study [*Singer and Dunne*, Submitted-b], I estimated long-term annual erosion of ~1.2 Mt/y in Reach 0, about ~0.7 Mt/y of which was eroded gravel size fractions (Tables 4.1 and 4.2). This erosion trend exacerbates the effect of up-basin gravel mining and dam trapping, depleting Reach 0 of gravel. One-day peak sediment budgets showed the same erosional trend with ~26 kt/d, about 17 kt/d of which was gravel (Tables 4.3 and 4.4).

I modeled gravel augmentation at the Bend Bridge (BB) cross section (at the lower end of Reach 0, Figure 4.1) to assess its effect on one-day peak and total annual sediment loads at this station and net accumulation for the upstream and downstream reaches. I represented augmentation by adjusting the grain size distribution of the bed material to reflect a mixture recommended to improve spawning habitat [*California Department of Water Resources*, 1980]. This mixture is reflected in the following percentages of each grain size class: 96 mm (10%), 48 mm (30%), 24 mm (20%), 12 mm (10%), 6 mm (5%), 3 mm (5%), 1.5 mm (5%), and 0.75 mm (5%). I assume that the added gravels completely cover the bed to the scour depth and define the bed material grain size distribution. Accordingly, the new, coarser distribution (Figure 4.2) increases the d_{50} (from 9.5 mm to 23 mm) and decreases the critical shear stress (from 0.053 to 0.020). The added mixture also decreases the sorting coefficient of the whole distribution (from 2.49 to 2.09), indicating a narrower distribution of grain

sizes and higher pocket angles. I re-calibrated my sediment transport equation based on these changes.

Setback Levees

Flood control levees are an integral part of the Sacramento flood control system. To convey high flows, the Army Corps of Engineers constructed ~3 m high levees to convey high flows in Reaches 2-5. Levees in Reaches 4 and 5 were built upon the original channel banks (in most locations). Levee setbacks were proposed in SB 1086 and CVPIA to increase flood capacity and to re-establish riparian vegetation communities [*Nielsen*, 1989]. These communities would provide shade and cover from predators for fish. The allowance for overbank flow would reduce flow depths in the river channel (Figure 4.3), thus reducing the risk of systematic bed degradation. Additionally, levee setbacks could lead to channel migration and the construction of point bars. The addition of this more complex channel morphology diversifies the lateral distribution of the substrate, the velocity field, sediment transport rate, and thus the aquatic habitat structure.

I modeled the effects of levee setbacks on bed-material transport in a constrained reach of the lower Sacramento River. My previous work on long-term sediment budgets identified Reach 4, between Colusa (CO) and Knights Landing (KL) (Figure 4.1), as one undergoing significant net erosion [*Singer and Dunne*, 2001; *Singer and Dunne*, Submitted-b]. I modeled levee setbacks by increasing (artificial) levee-to-levee width to ~3 km in a 16 km stretch of river (extending 8 km

upstream and 8 km downstream of Knights Landing) within my HEC-RAS geometry file. It should be noted that flood control levees are built to convey the highest floods of record. Under normal operation of the flood control system, the floodplain outside the levees is not inundated under the current flow regime. By setting back levees and maintaining their height, I am increasing the area of channel/floodplain that can be accessed by a given flood, thus reducing flow depth in the channel (Figure 4.3). I extracted daily stage at Knights Landing from HEC-RAS for 50 simulations of 30-year time series to determine the long-term effect of the setbacks on sediment transport at this section.

Flow Alteration

Streamflow in the Sacramento River has been dramatically altered by major dams operated for flood control, irrigation, and hydroelectricity. Figure 4.4 shows flood frequency curves for pre- (1891-1928) and post- (1964-2001) Shasta Dam discharge at Bend Bridge (Figure 4.4). These curves show a reduction in maximum peak flows at most exceedence probabilities. There is reason to believe that dam operation has had a large effect on sediment transport in the Sacramento River. For example, a flow of 1800 cms (approximately ¾ bankfull) was exceeded ~80% of the time in the pre-dam era and only ~55% of the time in the post-dam. I expect that such altered hydrology would have systematic impacts on the sediment budget throughout the Sacramento River.

Flow alteration has been proposed on the Sacramento River to increase maximum flood peaks in order to reintroduce disturbance (e.g. bank erosion, bar development) to the fluvial system. The proposal also calls for an increase in the frequency of flushing flows and a decrease in summer flows, which have been elevated for irrigation diversions. Studies on flow requirements for various aquatic and riparian species and their life stages are generally descriptive in nature. Therefore, optimizing a flow alteration rehabilitation strategy for entire ecosystems is problematic at this time, though it is a subject that requires further study. For example, *Kondolf and Wilcock* [1996] specify various types of flushing flows that could be prescribed to meet various aquatic and riparian habitat requirements. These authors discuss the conflicts inherent in meeting flow objectives for entire ecosystems.

For simplicity, I have modeled the influence of pre-dam hydrology on sediment transport in the recent Sacramento River channel. Although I recognize that such a rehabilitation strategy is unrealistic, I model it to understand the first-order impact of flow alteration on sediment transport. As research on the subject of flow alteration advances, my procedure could be amended to reflect a more refined flow alteration strategy.

Pre-dam hydrology represents flow simulated from all major tributaries prior to dam construction. As in my previous flow simulation study [*Singer and Dunne*, Submitted-a], I used simulated flow at Bend Bridge as my upstream boundary condition. As before, I routed this flow through the mainstem Sacramento using

unsteady flow routing in HEC-RAS. I extracted stage from 50 simulations of 30-year time series at each mainstem cross section used to compute hydraulic variables and sediment transport in my previous post-dam study [*Singer and Dunne*, Submitted-b]. I was interested to know if spatial patterns in sediment transport would persist under very different flow conditions (e.g. Figure 4.4).

Results and Discussion

I present median values of total annual and one-day peak bed-material load past mainstem stations and divergence in the river reaches shown in Figure 4.1. The results of all simulations are presented in Tables 4.1-4.4. The tables also contain the percent change in transport or divergence resulting from each rehabilitation strategy. Median values represent the middle of the range of all my simulations at the 0.5 exceedence probability and therefore represent expectable patterns. However, for the purpose of risk assessment, it may be of more interest to analyze less frequent outcomes arising from rehabilitation strategies. I discuss this briefly below.

Gravel Augmentation

The modeled gravel augmentation strategy at Bend Bridge had a large effect on both total annual and one-day peak sand and gravel transport. There were large declines (~96%) in annual gravel and sand flux at Bend Bridge and consequently, in annual gravel and sand erosion in Reach 0 (Tables 4.1 and 4.2). The decrease in transport at Bend Bridge largely results from coarsened bed material and narrowing

of the grain size distribution following augmentation (the added mixture is composed of only 10% sand, less than half the sand content of the pre-augmentation bed material). Because less sand and gravel are moving past Bend Bridge into the downstream reach under gravel augmentation, Reach 1 shifted from one of net bed-material deposition to net bed-material erosion (Table 4.2). Peak gravel and sand flux past Bend Bridge and peak divergences in Reaches 0 and 1 also declined (Tables 4.3 and 4.4).

The gravel augmentation strategy modeled here appears to provide local benefits to Reach 0, but may be harmful to existing spawning habitat in Reach 1. My modeling suggests that prior to gravel augmentation, Reach 1 was in a state of net gravel deposition. In other words, Reach 1 formerly benefited from high annual rates of gravel erosion in Reach 0. Eroded gravels from Reach 0 would likely form a substrate for high quality spawning habitat in this relatively wide and low-gradient reach [*Singer and Dunne*, Submitted-b]. However, following gravel augmentation, the coarse added mixture could dramatically slow the rate of gravel erosion in Reach 0 and shift Reach 1 to one of net gravel erosion, potentially degrading high quality spawning habitat. However, the results from gravel augmentation modeling are encouraging. They indicate that augmentation of gravels of an appropriate mixture could significantly impact transport rates and sediment storage patterns. Thus, if gravel were added to Reach 0 in volumes sufficient to alter the bed material grain size distribution and a mixture appropriate for maintaining a storage balance between Reach 0 and 1, three benefits would arise. First, there would be a local increase in

habitat area (i.e. increased spawning habitat in areas covered by the added gravel). Second, the added gravels would alter the bed-material grain-size distribution in the reach such that transport decreases at its downstream end (minimizing the volumes that would have to be added). Third, although bed-material transport would decrease at Bend Bridge, gravel in volumes sufficient to benefit spawning habitat would still move into Reach 1.

In summary of this modeling exercise, there are a few important issues to consider when designing a sustainable gravel augmentation strategy (in addition to where and how much gravel to add within a reach). First, the median grain size of the mixture added to a river reach affects transport rates (e.g. higher median grain size leads to lower transport rates, although this would be partially offset by a concomitant reduction in dimensionless critical shear stress). It is not surprising that grains in coarse riverbeds (armored beds are an extreme example) would move less frequently than those in fine riverbeds. Second, the sorting of grain sizes in the added mixture affects transport rates (e.g. a well-sorted mixture of sediments would decrease the sorting coefficient and thus lower transport rates for each grain size) [*Singer and Dunne*, Submitted-b]. Careful should be exercised in designing a sediment mixture that meets local (i.e. where the mixture is added) habitat goals and can be transported in sufficient quantities to provide benefits to downstream aquatic habitat. Third, the location of the added mixture affects cross sectional averaged transport rates. For example, the majority of bed-material transport happens in the thalweg (e.g. average annual transport of 48 mm gravel on the bar surface at Bend Bridge is <28% of the

that in the thalweg). Sediment could be added strategically within a cross section in order to maximize its benefit to habitat, while minimizing its transport. For example, instead of even application of gravel throughout a section (assumed in my model due to lack of information on bed-material patchiness within cross sections), gravel of an appropriate mixture could be preferentially added on bar surfaces that become inundated (to appropriate flow depths) during spawning seasons. Fourth, gravel augmentation may affect spatial patterns in net sediment storage, which in turn, may influence the condition of riverine habitats. For example, a shift from net deposition to net erosion in a reach could degrade spawning habitat in a reach downstream of the gravel augmentation.

The cost of gravel augmentation would include the purchase and transport of the gravel mixture from an off-channel gravel mine, placement of gravel in selected locations within reaches and cross sections, monitoring of placed gravels to track their transport, and monitoring of spawning habitat and fish use.

Setback Levees

Modeled levee setbacks had major influence on the transport of gravel and sand at Knights Landing (a decline of 54%, Tables 4.1 and 4.2). Total annual gravel divergences in Reaches 4 and 5 declined similarly. Under the modeled setback strategy, the changes in net accumulation in these reaches have a huge impact on the absolute values of the largest modeled imbalances in total annual sediment budgets in the Sacramento River [*Singer and Dunne*, Submitted-b](Tables 4.1 and 4.2). One-

day peak gravel and sand transport increased by 15% and 8%, respectively (Tables 4.3 and 4.4). These factors indicate that the increased resistance of the floodplain (now exposed to down-valley flow) may increase peak flood stage, and thus slightly increase one-day peak transport rates at Knights Landing. However, this effect appears to be short-lived under a strategy of levee setbacks, because the floodplain serves to modulate the effects of a prolonged flood event by providing out-of-channel flood accommodation space for flooding. Consequently, flow stage in the channel, while temporarily elevated, declines rapidly during floods, leading to lower bed-material transport volumes per flood. Thus, total annual transport of sand and gravel at Knights Landing is reduced.

The modeling suggests that setback levees are viable for reducing large reach divergences in bed-material transport. Implementation of a successful levee setback strategy, however, requires careful consideration of the changes in hydraulics during flood events. A two-dimensional flow model is necessary to assess the coupled effects of increased flow resistance and flood accommodation space on in-channel flow stage. The cost of setback levees would include the price of contiguous floodplain lands required to create a river corridor, earth-moving and construction costs, and monitoring of benefits to aquatic and riparian habitats. However, the cost of setback levees could be partially offset by obtaining easements or leasing the corridor for seasonal agricultural use (as is done in Sutter and Yolo Bypasses). Incidentally, my modeling of levee setbacks in the area around Knights Landing

resulted in no change in flow stage or bed-material transport at the Colusa and Sacramento cross sections (Figure 4.1 and Tables 4.1 and 4.2).

Flow Alteration

The results of flow alteration are presented in Tables 4.1-4.4 and illustrated in Figures 4.5 and 4.6. The bars in these figures represent divergences in sand (S) and gravel load (G) under the current (Current) and the altered (Flow Alt) flow regimes. The T-bars represent the variability in median estimates associated with stochastic hydrology [*Singer and Dunne*, Submitted-b]. Figure 4.6 shows total annual divergences and Figure 4.6 shows one-day peak divergences. Erosion is positive and deposition is negative.

The influence of modeled flow alteration on total annual bed-material transport and reach divergence is systemic. Flow alteration reduces sand and gravel transport divergences for all stations (except for Sacramento, where no changes occur) and reaches, respectively. Flow alteration increases one-day peak sand and gravel transport for most stations and peak reach divergences. The interpretation is that although the pre-dam flow regime (i.e. modeled flow alteration) is more variable and peaked, it has a lower median value of reach-scale scour and accumulation. This generally results in higher transport during flood peaks (i.e. due to higher flow peaks), but shorter peaks. Reservoir operation for flood control tends to prolong the release during floods, delivering the same amount of water over a longer duration. Because much of this water is released at flows above the critical transporting flow, higher

total transport results merely because of the duration of the release compared with the short, sharp peaks in the pre-dam era.

This suggests that flow alteration is a feasible strategy to benefit habitat without aggravating imbalances in total annual sediment budgets. My modeling indicates that periodic scour in a particular reach during a larger flood peak would eventually fill in on the steep falling limb of a natural Sacramento River hydrograph. It is beyond the scope of this paper to outline a strategy for flow alteration that would benefit an array of habitats and remain economically (and politically) feasible. However, my modeling suggests that any strategy that simulates aspects of the natural flow regime would not cause aggravated erosion or deposition in the Sacramento River. The cost of a flow alteration strategy would include design of a flow regime that balances the requirements for flood control, habitat, irrigation, and water supply, payment to companies and/or agencies for losses in hydroelectricity generation, and monitoring of benefits to habitat.

Risk Assessment

This paper reports median values of transport and net divergence in transport. My method is driven by a stochastic flow generator so multiple outcomes are produced. Each simulation produces a unique combination of flood frequency, duration, and magnitude along the mainstem based on variability in tributary inflow. In this application of the model, a sediment transport frequency curve is produced for each simulation. Multiple curves define a band of potential risk of outcomes from a

rehabilitation strategy (Figure 4.7). The median values reported in this paper represent the central tendency of the whole distribution of outcomes. The band of risk illustrated in Figure 4.7 can be also be used to define the highest and lowest values, or expected range, of sediment transport resulting from all simulations. This type of risk characterization could be useful in anticipating extremes within the distribution. In cases where large sums are being spent on major river rehabilitation, it may be necessary to more fully investigate the extremes within my modeled outcomes. However, such an analysis is beyond the scope of this paper.

Conclusion

I assessed the effect of three river rehabilitation strategies on long-term trends in sediment transport. Gravel augmentation was found to reduce sand and gravel transport, thus affecting reach divergences. A successful strategy of augmentation requires careful thought about the grain size distribution of the added gravels, location of their placement within a cross section, and spatial patterns in sediment storage, in addition to the volumes and locations within a reach. Setting back flood control levees was found to be a viable strategy for reducing sediment transport and modulating large net imbalances in the sediment budget. Flow alteration was found to decrease total annual transport and divergence throughout the river system, though it generally increases the effect of individual flood peaks. This paper is an early attempt to assess the decadal impact of habitat rehabilitation by general assessments habitat condition (e.g. sediment transport and storage) over large river reaches.

Future work in this area should be directed toward increasing the spatial resolution of transport and storage calculations and establishing direct links between physical habitat condition and species success.

References

American Society of Civil Engineers, Sediment and aquatic habitat in river systems, *J. Hyd. Eng.*, *118* (5), 669-687, 1992.

Anderson, J.D., Modeling impacts of multiple stresses on aquatic ecosystems: case study of juvenile chinook salmon in the Sacramento River system, Dissertation thesis, UC Davis, Davis, CA, 2000.

Babcock, K.W., Home range and habitat use of breeding Swainson's hawks in the Sacramento Valley of California, *J. Raptor Res.*, *29* (3), 193-197, 1995.

Barkau, R., One-dimensional unsteady flow through a full network of open channels, US Army Corps of Eng., Davis, CA, 1997.

Biedenharn, D.S., C.R. Thorne, and C.C. Watson, Recent morphological evolution of the Lower Mississippi River, *Geomorphology*, *34*, 227-249, 2000.

Blott, S.J., and K. Pye, Gradistat: A grain size distribution and statistics package for the analysis of unconsolidated grains, *Earth Surface Processes & Landforms*, *26*, 1237-1248, 2001.

Bozkurt, S., P. Dekens, R. Gartland, J. Gragg, J. Lawyer, and M. McGoogan, Evaluation of setback levees on the Sacramento River, pp. 118, UC Santa Barbara, Santa Barbara, CA, 2000.

CALFED, Ecosystem Restoration Program Plan, CALFED Bay Delta Program, Sacramento, 1997.

California Department of Water Resources, Upper Sacramento River spawning gravel study, CDWR, Red Bluff, CA, 1980.

California Department of Water Resources, Middle Sacramento River spawning gravel study, CDWR, Red Bluff, CA, 1985.

California Dept. of Water Resources, Sacramento River bank erosion investigation, Dept. Water Resources, Sacramento, CA, 1994.

Collins, B., and T. Dunne, Fluvial geomorphology and river-gravel mining : a guide for planners, case studies included, Cal. Div. Mines and Geol., Sacramento, 1990.

Collins, B.D., and T. Dunne, Gravel transport, gravel harvesting, and channel-bed degradation in rivers draining the southern Olympic Mountains, Washington, U.S.A., *Environmental Geology and Water Sciences*, *13* (3), 213-224, 1989.

Engelund, F., and E. Hansen, A monograph on sediment transport in alluvial streams, in *Teknisk Vorlag*, pp. 63, Technical University of Denmark, Copenhagen, Denmark, 1967.

Gergel, S.E., M.D. Dixon, and M.G. Turner, Consequences of human-altered floods: Levees, floods, and floodplain forests along the Wisconsin River, *Ecological Applications*, *12* (6), 1755-1770, 2002.

Gibbins, C.N., and R.M. Acornley, Salmonid habitat modelling studies and their contribution to the development of an ecologically acceptable release policy for Kielder Reservoir, North-east England, *Regulated Rivers: Research and Management*, *16*, 203-224, 2000.

Hunter, J.C., Prospect for preservation and restoration of riparian forests in the Sacramento Valley, California, USA, *Env. Mngmt.*, *24* (1), 65-75, 1999.

Junk, W.J., P.B. Bayley, and R.E. Sparks, The flood pulse concept, in *International Large River Symposium*, edited by D.P. Doge, pp. 110-127, Can. Fish. Aquatic Science Special Publ., 1989.

Kelley, R., *Battling the Inland Sea*, 395 pp., University of California Press, Berkeley, CA, 1998.

Kondolf, G.M., Managing bedload sediment in regulated rivers: Examples from California, USA, in *Natural and Anthropogenic Influences in Fluvial Geomorphology*, edited by J.E. Costa, A.J. Miller, K.W. Potter, and P.R. Wilcock, pp. 239, Amer. Geophysical Union, Wash. D.C., 1995.

Kondolf, G.M., and M.L. Swanson, Channel adjustments to reservoir construction and gravel extraction along Stony Creek, California, *Environ. Geol. Wat. Sci.*, *21*, 256-269, 1993.

Kondolf, G.M., and P.R. Wilcock, The flushing flow problem: Defining and evaluating objectives, *Water Resources Research*, *32*, 2589-2599, 1996.

Kondolf, G.M., and M.G. Wolman, The sizes of salmonid spawning gravels, *Water Res. Research*, *29* (7), 2275-2285, 1993.

Laddish, K.M., Mathematical modeling of levee setbacks for a hypothetical river: A comparison of shear stress and critical shear stress, Term Paper thesis, UC Berkeley, Berkeley, CA, 1997.

Magilligan, F.J., Dis-connectivity and changes in hydrologic regime by dams, *Geology*, In Press.

Milhous, R.T., Modelling of instream flow needs: the link between sediment and aquatic habitat, *Regulated Rivers: Res & Mngmt*, *14*, 79-94, 1998.

Nielsen, J., Upper Sacramento River:Fisheries and riparian habitat management plan, pp. 158, California Senate Bill 1086 Advisory Council, Sacramento, CA, 1989.

Peterson, D.F., D.F. Jacobs, B.J. Talley, R.N. Hinton, C.W. Pike, and A.F. Goodwin, Califronia's stream resources, Volume 1: Overview and assessment, California Department of Water Resources Bulletin 215, Sacramento, CA, 1982.

Pitlick, J., and M.M. Van Steeter, Geomorphology and endangered fish habitats in the upper Colorado River. 2. Linking sediment transport to habitat maintenance, *Water Resources Research*, *34* (2), 303-316, 1998.

Poff, N.L., J.D. Allan, M.B. Bain, J.R. Karr, K.L. Prestegaard, B.D. Richter, R.E. Sparks, and J.C. Stromberg, The natural flow regime, *Biosci.*, *47* (11), 769-784, 1997.

Power, M.E., A. Sun, G. Parker, W.E. Dietrich, and J.T. Wootton, Hydraulic food-chain models, *Biosci.*, *45* (3), 159-167, 1995.

Reeves, G.H., and T.D. Roelofs, Rehabilitating and enhancing stream habitat: 2. Field applications, US Forest Service, Arcata, CA, 1982.

Richter, B.D., J.V. Baumgartner, D.P. Braun, and J. Powell, A spatial assessment of hydrologic alteration within a river network, *Regulated Rivers: Research & Mngmt.*, *14*, 329-340, 1998.

Richter, B.D., J.V. Baumgartner, J. Powell, and D.P. Braun, A method for assessing hydrologic alteration within ecosystems, *Conserv. Bio.*, *10* (4), 1163-1174, 1996.

Richter, B.D., and H.E. Richter, Prescribing flood regimes to sustain riparian ecosystems along meandering rivers, *Conserv. Bio.*, *14* (5), 1467-1478, 2000.

Rubin, D.M., D.J. Topping, J.C. Schmidt, J. Hazel, M. Kaplinski, and T.S. Melis, Recent sediment studies refute Glen Canyon Dam hypothesis, *EOS Transactions, American Geophysical Union*, *83* (25), 273-278, 2002.

Singer, M.B., and T. Dunne, Identifying eroding and depositional reaches of valley by analysis of suspended-sediment transport in the Sacramento River, California, *Water Resources Research*, *37* (12), 3371-3381, 2001.

Singer, M.B., and T. Dunne, An empirical-stochastic, event-based model for simulating inflow from a tributary network: Theoretical framework and application to the Sacramento River basin, California, Submitted-a.

Singer, M.B., and T. Dunne, Modeling decadal bed-material flux based on stochastic hydrology, Submitted-b.

Sparks, R.E., Risks of altering the hydrologic regime of large rivers, in *Predicting Ecosystem Risk*, edited by J. Cairns, B.R. Niederlehner, and D.R. Orvos, pp. 119-152, Princeton Sci. Pub. Co., Princeton, NJ, 1992.

Stanford, J.A., J.V. Ward, W.J. Liss, C.A. Frissell, R.N. Williams, J.A. Lichatowich, and C.C. Coutant, A general protocol for restoration of regulated rivers, *Regulated Rivers: Research & Mngmt*, *12*, 391-413, 1996.

Taylor, G.E., Microbial ecology, toxicology and chemical fate of methyl isothiocyanate in riparian soils from the upper Sacramento River, *Env. Toxicol. & Chem.*, *15* (10), 1694-1701, 1996.

Thompson, K., Riparian forests of the Sacramento Valley, California, *Annals of the Assoc. of Amer. Geographers*, *51*, 294-315, 1961.

US Army Corps of Engineers, Post-Flood Assessment for 1983, 1986, 1995, and 1997, Central Valley, California, Sacramento District, Sacramento, CA, 1998.

Vannote, R.L., The river continuum concept, *Can. J. Fish. Aquat. Sci.*, *37*, 130-137, 1980.

Vitousek, P.M., H.A. Mooney, J. Lubchenco, and J.M. Melillo, Human domination of earth's ecosystems, *Science*, *277*, 494-499, 1997.

Williams, G.P., and M.G. Wolman, Downstream effects of dams on alluvial rivers, Geological Survey, Washington, D.C., 1984.

Wu, F.C., Modeling embryo survival affected by sediment deposition into salmonid spawning gravels: Application to flushing flow prescriptions, *Water Resources Research*, *36* (6), 1595-1603, 2000.

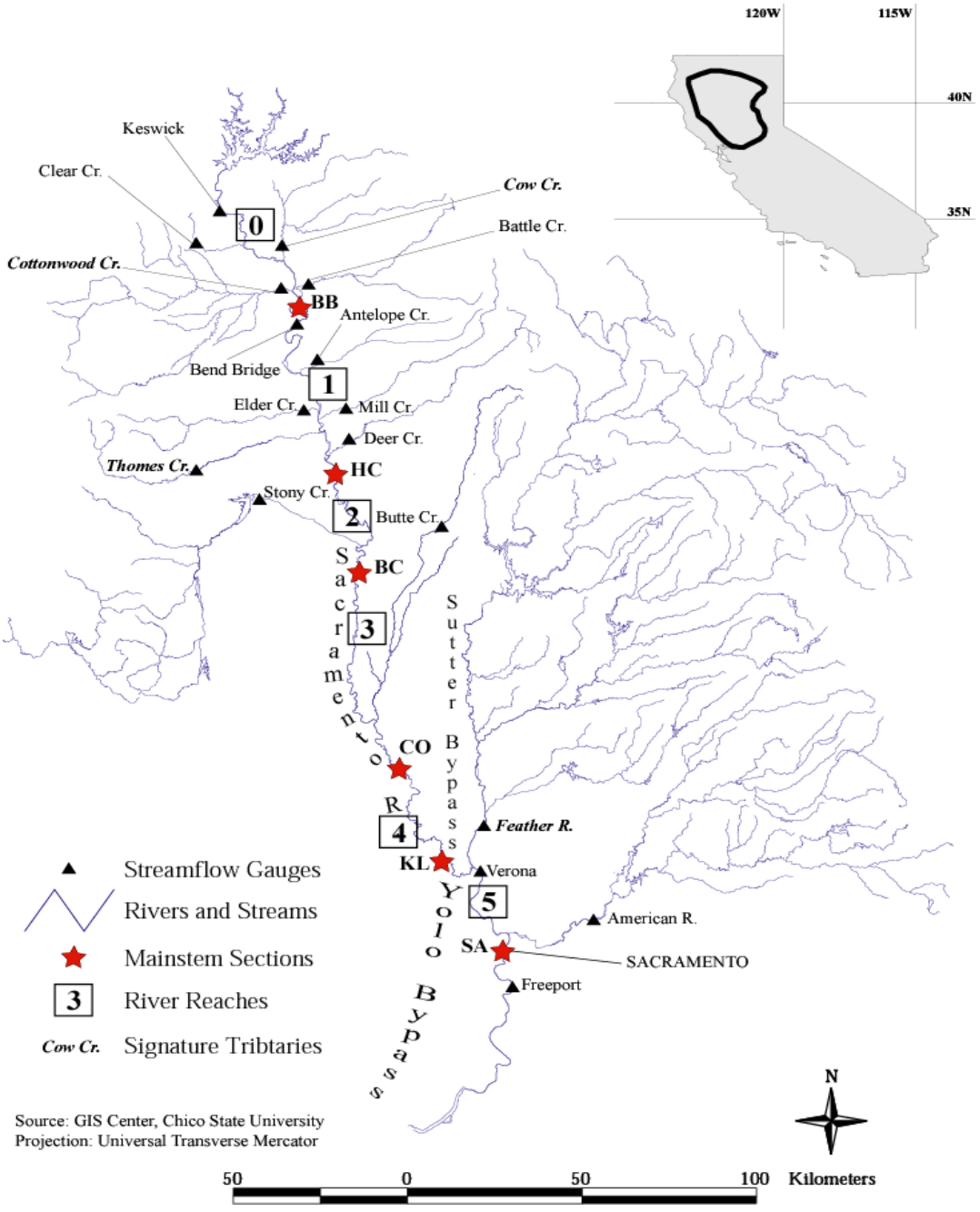

Figure 4.1 Map of study basin showing streamflow gauges used for stochastic flow simulation, stream network, mainstem sections through which bed-material transport was computed, river reaches for which simple sediment budgets were evaluated, and signature tributaries used to compute sediment entering the mainstem from common geologic provinces (scaled by drainage area).

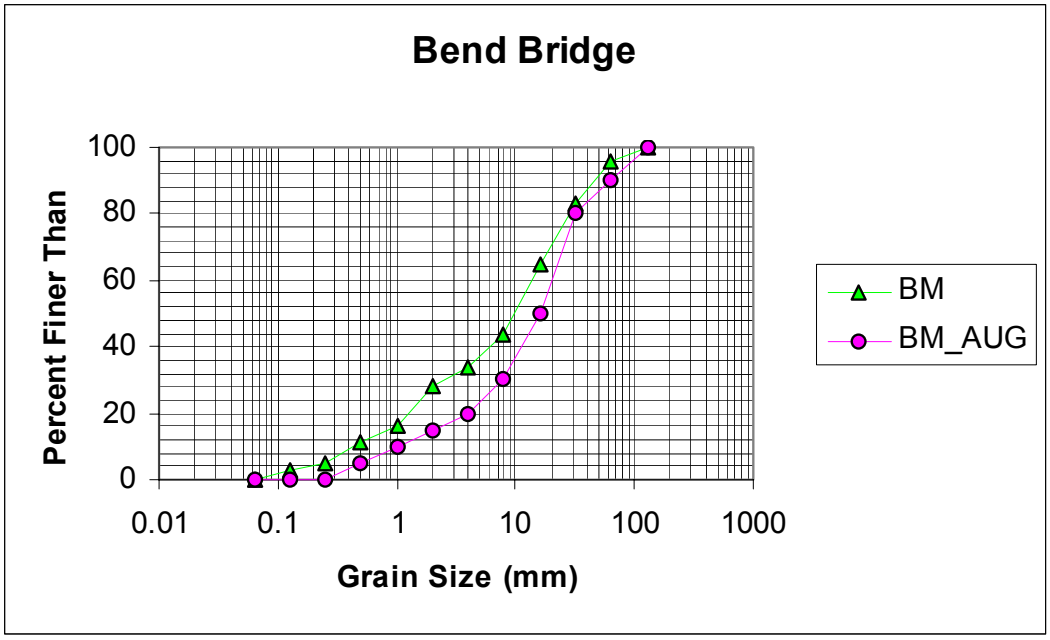

Figure 4.2 Comparison of original bed-material grain size distribution at Bend Bridge (BM) with that of the augmented gravel (BM AUG). Median grain size increased from 9.5 mm to 23 mm, sorting coefficient decreased from 2.49 to 2.09, and dimensionless critical shear stress decreased from 0.053 to 0.020.

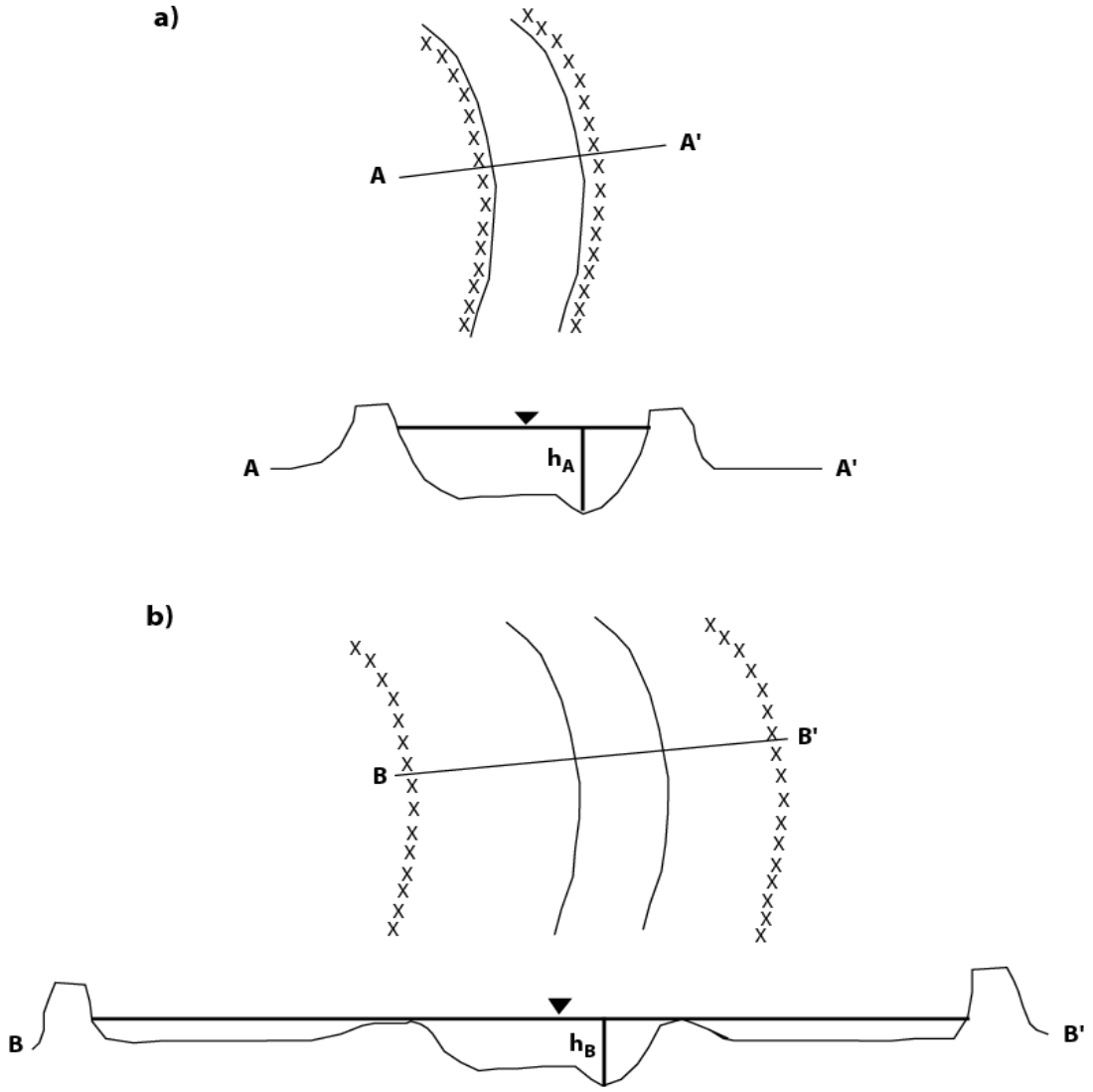

Figure 4.3 Schematic depicting the effect of levee setbacks on flow stage and thus shear stress in the channel. The figure shows (a) the original channel with levees built upon channel banks and (b) the channel under a levee setback rehabilitation strategy. The levee setbacks reduce high flow stage in the channel. Flow depth in the channel, h, would decrease for the same discharge after levees are set back (h_B).

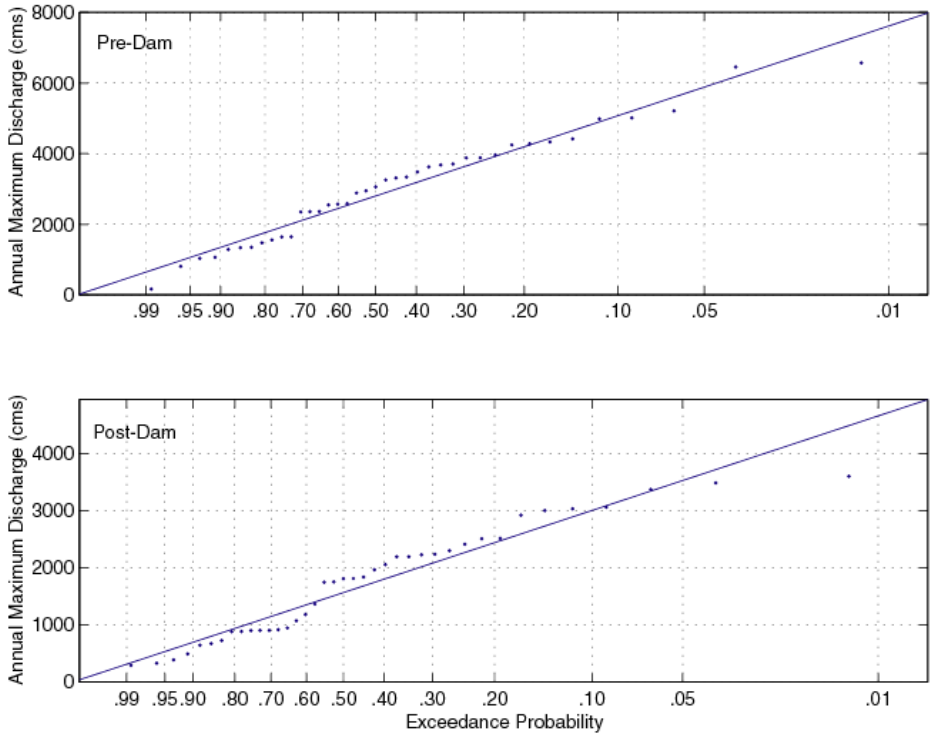

Figure 4.4 Plots show the effect of Shasta Dam (constructed in 1943) on flow frequency at Bend Bridge. The plot shows annual maxima for the pre-dam (a) and the post-dam (b) eras.

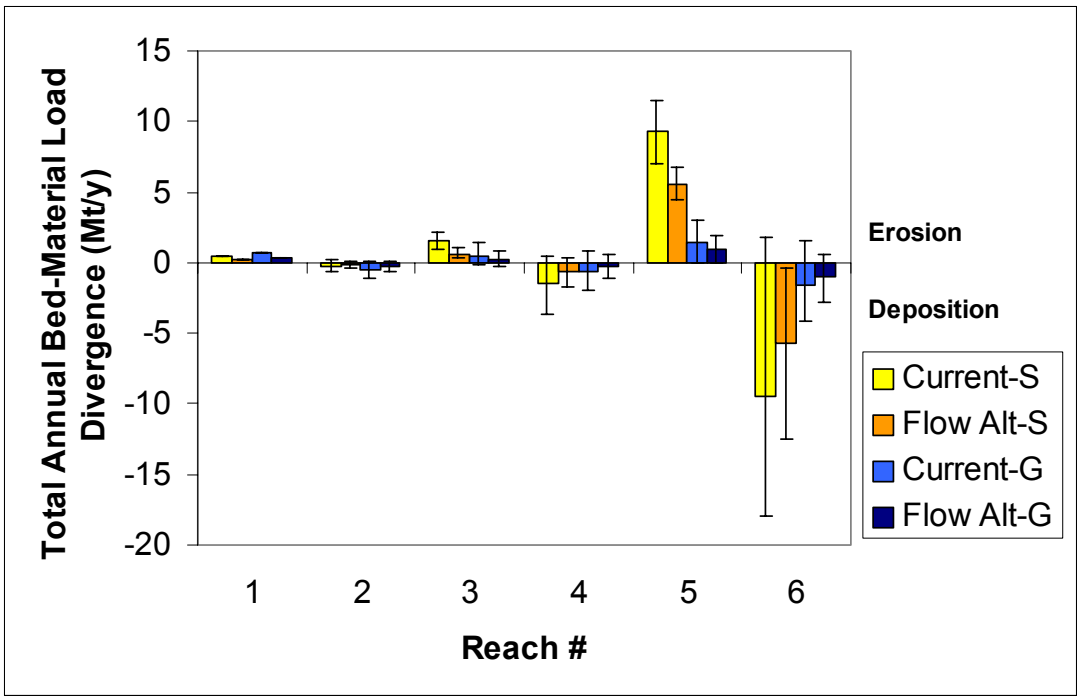

Figure 4.5 Total annual bed-material load divergence (Mt/y) for sand and gravel under current conditions (Current-S and Current-G, respectively) and for sand and gravel under a strategy of flow alteration (Flow Alt-S and Flow Alt-G, respectively). The plot shows that flow alteration modulates the long-term imbalances (i.e. erosion or deposition) in the sediment budget.

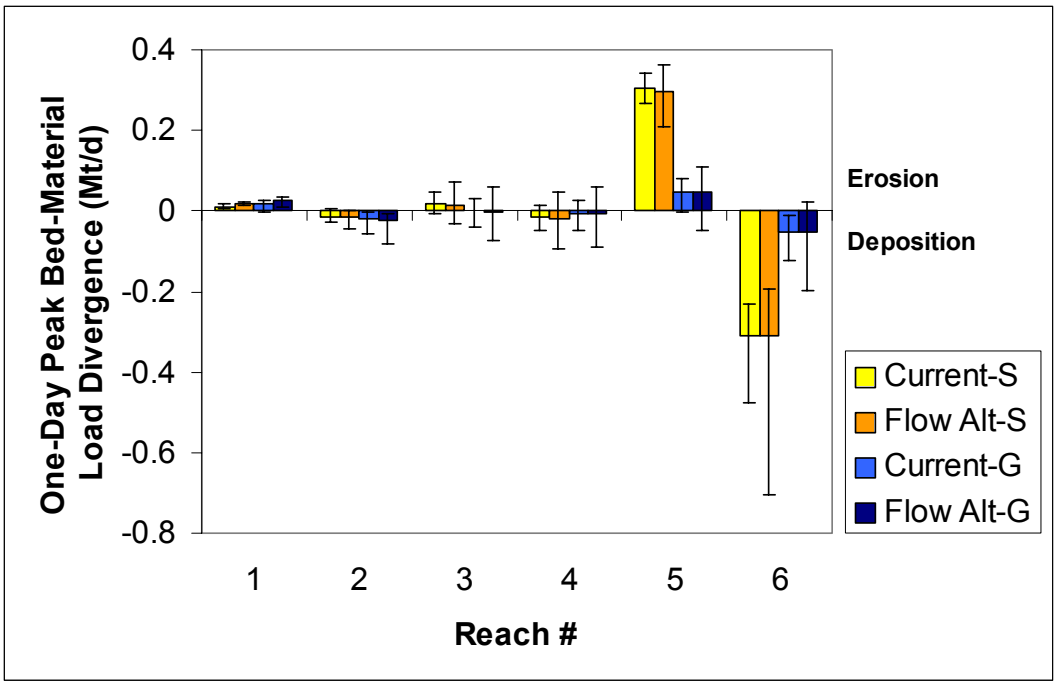

Figure 4.6 One-day peak bed-material load divergence (Mt/d) for sand and gravel under current conditions (Current-S and Current-G, respectively) and for sand and gravel under a strategy of flow alteration (Flow Alt-S and Flow Alt-G, respectively). The plot shows that flow alteration largely increases the peak imbalances (i.e. erosion or deposition) in the sediment budget.

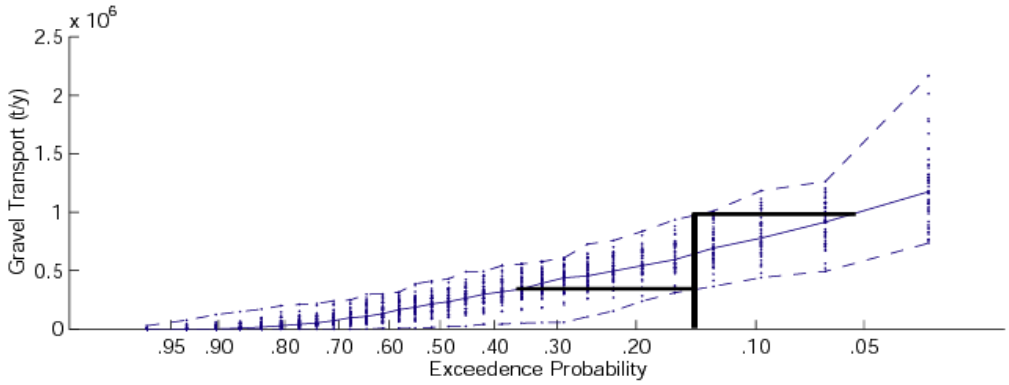

Figure 4.7 Total annual gravel load resulting from 50 simulations, each of 30 years. Gravel load (t/y) is plotted against exceedence probability. The range in transport for each exceedence probability is a result of the variability in stochastic hydrology. These ranges form of band of risk instead of a single frequency curve. This paper reports median values (i.e. solid line at 0.50 exceedence probability). However, for risk assessment, it may be more useful to analyze transport at low exceedence probabilities. For example, the figure shows that the maximum and minimum values at 0.15 approximately correspond to the median values at 0.05 and 0.45, respectively.

Table 4.1 Rehabilitation Strategy Modeling Results-Gravel							
Total Annual Qs (kt/y)							
Station	Current	Gravel Augment	Change	Levee Setback	Change	Flow Alteration	Change
BB	749	31	-96%			368	-51%
HC	208					109	-48%
BC	740					321	-57%
CO	149					56	-62%
KL	1627			746	-54%	969	-40%
SA	0					0	0%
Total Annual divQs (kt/y)							
Reach #	Current	Gravel Augment	Change	Levee Setback	Change	Flow Alteration	Change
0	738	20	-97%			357	-52%
1	-552	166	130%			-270	51%
2	528					208	-61%
3	-591					-265	55%
4	1478			597	-60%	913	-38%
5	-1627			-746	54%	-969	40%

Table 4.1 Results from modeling the influence of rehabilitation strategies on total annual gravel load at mainstem stations (Qs in upper) and total annual gravel divergence for river reaches (divQs in lower). The tables contain gravel load or divergence (both in Mt/y) currently (Current), following gravel augmentation (Gravel Augment), following levee setbacks (Levee Setback), and following flow alteration (Flow Alteration). The table also contains the percent change in each. Negative divergences indicate net deposition and positive values indicate net erosion.

Table 4.2 Rehabilitation Strategy Modeling Results-Sand							
Total Annual Qs (kt/y)							
Station	Current	Gravel Augment	Change	Levee Setback	Change	Flow Alteration	Change
BB	469	13	-97%			231	-51%
HC	206					108	-48%
BC	1724					747	-57%
CO	222					83	-63%
KL	9515			4360	-54%	5666	-40%
SA	5					5	0%
Total Annual divQs (kt/y)							
Reach #	Current	Gravel Augment	Change	Levee Setback	Change	Flow Alteration	Change
0	460	4	-99%			222	-52%
1	-272	184	168%			-132	51%
2	1512					633	-58%
3	-1502					-664	56%
4	9293			4138	-55%	5583	-40%
5	-9523			-4368	54%	-5624	41%

Table 4.2 Results from modeling the influence of rehabilitation strategies on total annual sand load at mainstem stations (Qs in upper) and total annual sand divergence for river reaches (divQs in lower). The tables contain sand load or divergence (both in Mt/y) currently (Current), following gravel augmentation (Gravel Augment), following levee setbacks (Levee Setback), and following flow alteration (Flow Alteration). The table also contains the percent change in each. Negative divergences indicate net deposition and positive values indicate net erosion.

Table 4.3 Rehabilitation Strategy Modeling Results-Gravel							
Peak Qs (kt/d)							
Station	Current	Gravel Augment	Change	Levee Setback	Change	Flow Alteration	Change
BB	21	1	-95%			31	48%
HC	6					12	100%
BC	11					13	18%
CO	6					8	33%
KL	53			61	15%	53	0%
SA	0					0	0%
Peak divQs (kt/d)							
Reach #	Current	Gravel Augment	Change	Levee Setback	Change	Flow Alteration	Change
0	17	-3	-118%			27	59%
1	-21	-1	95%			-25	-19%
2	2					-2	-200%
3	-5					-5	0%
4	47			28	-40%	45	-4%
5	-53			-34	36%	-53	0%

Table 4.3 Results from modeling the influence of rehabilitation strategies on one-day peak gravel load at mainstem stations (Qs in upper) and one-day peak gravel divergence for river reaches (divQs in lower). The tables contain gravel load or divergence (both in Mt/d) currently (Current), following gravel augmentation (Gravel Augment), following levee setbacks (Levee Setback), and following flow alteration (Flow Alteration). The table also contains the percent change in each. Negative divergences indicate net deposition and positive values indicate net erosion.

Table 4.4 Rehabilitation Strategy Modeling Results-Sand							
Peak Qs (kt/d)							
Station	Current	Gravel Augment	Change	Levee Setback	Change	Flow Alteration	Change
BB	13	1	-92%			20	54%
HC	6					12	100%
BC	26					30	15%
CO	9					12	33%
KL	312			336	8%	309	-1%
SA	1					1	0%
Peak divQs (kt/d)							
Reach #	Current	Gravel Augment	Change	Levee Setback	Change	Flow Alteration	Change
0	9	-3	-133%			16	78%
1	-13	-1	92%			-14	-8%
2	17					14	-18%
3	-17					-18	-6%
4	303			199	-34%	297	-2%
5	-312			-399	-28%	-309	1%

Table 4.4 Results from modeling the influence of rehabilitation strategies on one-day peak sand load at mainstem stations (Qs in upper) and one-day peak sand divergence for river reaches (divQs in lower). The tables contain sand load or divergence (both in Mt/d) currently (Current), following gravel augmentation (Gravel Augment), following levee setbacks (Levee Setback), and following flow alteration (Flow Alteration). The table also contains the percent change in each. Negative divergences indicate net deposition and positive values indicate net erosion.

APPENDIX A. Table of Time Series Models

This is a table showing the Box-Jenkins models used in to extend sediment concentration records. The table shows the following for each of six mainstem and four signature tributary gauging stations:

Column 1: "Station Name", name of gauging station.
Column 2: "D.A. (km^2), upstream drainage area.
Column 3: "Estimated BJ Model Equation", equation used for modeling.
Column 4: "U", number of parameters in fitted univariate model, first number is AR, second is MA.
Column 5: "AIC", Akaike's Information Coefficient (AIC), a measure of model fit from the bivariate model.
Column 6: "Qstat (d.f.)", lack-of-fit statistic with degrees of freedom in parentheses.
Column 7: "R^2", R-squared model efficiency statistic.

APPENDIX A. (continued)

Station	D.A. (km^2)	Estimated BJ Model Equation	U	AIC	Qstat (d.f.)	R^2
Mainstem						
Bend Bridge	23051	$\log_e Cs_t^* = 1.496(\log_e Q_t^*)$	2-2	0.169	25.5 (29)	0.75
Hamilton City	28063	$\log_e Cs_t^* = 0.761(\log_e Q_t^*) + 0.345(\log_e Cs_{t-1}^*)$	0-1	0.074	46.1 (28)	0.86
Butte City	31274	$\log_e Cs_t^* = 1.750(\log_e Q_t^*) - 0.256(\log_e Q_{t-1}^*)$	0-4	0.069	2.6 (28)	0.58
Colusa	31313	$\log_e Cs_t^* = 1.562(\log_e Q_t^*) - 0.296(\log_e Q_{t-1}^*)$	0-1	0.042	11.0 (28)	0.68
Knights Ldg.	37646	$\log_e Cs_t^* = 1.057(\log_e Q_t^*)$	0-1	0.042	42.0 (29)	0.99
Sacramento	60869	$\log_e Cs_t^* = 1.502(\log_e Q_t^* + 0.242(\log_e Q_{t-1}^*)$	1-1	0.034	23.4 (28)	0.72
Tributaries						
Cottonwood	2400	$\log_e Cs_t^* = 1.242(\log_e Q_t^*) - 1.180(\log_e Q_{t-1}^*) + 1.125(\log_e Cs_{t-1}^*) - 0.298(\log_e Cs_{t-2}^*)$	0-5	0.174	28.3 (26)	0.79
Cow	1100	$\log_e Cs_t^* = 1.289(\log_e Q_t^*)$	0-2	0.286	8.19 (29)	0.92
Elder	352	$\log_e Cs_t^* = 1.243(\log_e Q_t^*)$	2-0	0.239	16.9 (29)	0.94
Feather	5949	$\log_e Cs_t^* = 1.089(\log_e Q_t^*)$	1-1	0.01	20.0 (29)	0.99

APPENDIX B. SUSPENDED SEDIMENT BUDGET SPREADSHEET

Suspended sediment budget spreadsheet used for assessing reaches of valley in net states of erosion and deposition. The spreadsheet shows the following for each tributary and mainstem station:

Column 1: "Station Name", name of gauging station.
Column 2: "E/W", direction from which tributary enters the Sacramento (east or west).
Column 3: "RK", river kilometer counted upstream from the San Francisco Bay.
Column 4: "D.A. (km^2)", station's upstream drainage area below impoundments.
Column 5: "Geo Unit", geologic unit from which tributary rises; used to model sediment load.
Column 6: "Sig Load (t/y)", annual load of the signature station for that geologic unit.
Column 7: "D.A. Ratio", ratio of tributary drainage area to signature tributary drainage area.
Column 8: "Mod Load (t/y)", modeled sediment load.
Column 9: "Upstream", sediment load (t/y) into a reach from upstream sources (at each mainstem gauge).
Column 10: "Divergence", net sediment divergence (t/y) (at each mainstem gauge).

APPENDIX B. (continued)

Station Name	E/W	RK	D.A. (km^2)	Geo Unit	Sig Load (t/y)	D.A. Ratio	Mod Load (t/y	Upstream	Divergence
Rock Cr	W	485.9	16	Trinity	566000	0.0065	3663		
Middle Cr	W	484.4	10	Trinity	566000	0.0043	2442		
Salt Cr	W	484.1	8	Trinity	566000	0.0032	1832		
Local Area	W	483.6	8	Trinity	566000	0.0032	1832		
Local Area	E	483.4	3	Trinity	566000	0.0011	611		
Jenny Cr	W	482.0	5	Trinity	566000	0.0022	1221		
Anderson-Cottonwood I.D.	W	479.6			566000		0		
Sulphur Cr	E	478.9	13	Trinity	566000	0.0054	3053		
Local Area	E	478.0	13	Modoc	194000	0.0118	2282		
Local Area	W	474.0	10	Trinity	566000	0.0043	2442		
Canyon Hollow	W	472.5	8	Trinity	566000	0.0032	1832		
Oregon Gulch	W	471.7	16	Trinity	566000	0.0065	3663		
Local Area	E	468.3	5	Modoc	194000	0.0022	419		
Local Area	W	466.7	10	Trinity	566000	0.0043	2442		
Olney Cr	W	465.9	36	Trinity	566000	0.0151	8548		
Clear Cr. nr Igo	W	465.6	591	Trinity	566000	0.2460	139210		
Local Area	E	462.7	16	Modoc	194000	0.0141	2739		
Local Area	W	461.9	3	Trinity	566000	0.0011	611		
Spanish Canyon	W	459.5	28	Trinity	566000	0.0119	6716		
Churn Cr	E	458.0	31	Modoc	194000	0.0282	5478		
Clover Cr	E	454.8	21	Modoc	194000	0.0188	3652		
Stillwater Cr	E	452.2	174	Modoc	194000	0.1576	30584		
Local Area	E	450.9	26	Modoc	194000	0.0235	4565		
Cow Cr	E	450.8	1101	Modoc	194000	1.0000	194000		
Local Area	W	449.0	3	Trinity	566000	0.0011	611		
Bear Cr	E	446.6	197	Modoc	194000	0.1788	34692		
Ash Cr	E	445.9	83	Modoc	194000	0.0753	14607		
Local Area	W	442.7	13	Trinity	566000	0.0054	3053		
Buenaventura Cr	W	442.6	5	Trinity	566000	0.0022	1221		
Anderson Cr	W	440.6	54	Trinity	566000	0.0227	12822		
Local Area	E	440.2	5	Modoc	194000	0.0047	913		
Cottonwood Cr	W	440.0	2401	Trinity	566000	1.0000	566000		
Battle Cr	E	436.6	925	Modoc	194000	0.8400	162960		
Local Area	E	434.5	10	Modoc	194000	0.0094	1826		
Frazier Cr	W	431.0	5	Trinity	566000	0.0022	1221		

APPENDIX B. (continued)

Station Name	E/W	RK	D.A. (km^2)	Geo Unit	Sig Load (t/y)	D.A. Ratio	Mod Load (t/y)	Upstream	Divergence
Local Area	W	430.5	13	Trinity	566000	0.0054	3053		
Local Area	E	429.4	3	Modoc	194000	0.0024	456		
Table Mtn. Trib	W	428.2	8	Trinity	566000	0.0032	1832		
Onks Cr	E	425.8	70	Modoc	194000	0.0635	12325		
Local Area	W	425.0	3	Trinity	566000	0.0011	611		
E Trib No 1	E	424.1	10	Modoc	194000	0.0094	1826		
Local Area	E	422.5	5	Modoc	194000	0.0047	913		
Sacramento @ Bend Br.		418.9	23051				**1040000**	**1244777**	**-204777**
Local Area	W	416.8	16	Trinity	566000	0.0065	3663		
Lookout Mtn Trib	W	416.7	10	Trinity	566000	0.0043	2442		
Local Area	E	415.2	5	Modoc	194000	0.0047	913		
Spring Cr	W	414.6	10	Trinity	566000	0.0043	2442		
Paynes Cr	E	407.2	241	Modoc	194000	0.2188	42452		
Local Area	E	406.8	16	Modoc	194000	0.0141	2739		
Local Area	W	406.5	3	Trinity	566000	0.0011	611		
East Trib No. 2	E	406.0	8	Modoc	194000	0.0071	1369		
Local Area	W	404.8	3	Trinity	566000	0.0011	611		
Seven Mile Cr	E	403.6	18	Modoc	194000	0.0165	3195		
Blue Tent Cr	W	398.6	44	Trinity	566000	0.0183	10380		
Dibble Cr	W	396.9	83	Trinity	566000	0.0345	19538		
Local Area	W	395.3	21	Trinity	566000	0.0086	4885		
Local Area	E	395.3	8	Modoc	194000	0.0071	1369		
Reeds Cr	W	394.0	192	Trinity	566000	0.0798	45182		
Local Area	E	392.7	16	Modoc	194000	0.0141	2739		
Red Bank Cr. nr Red Bluff	W	391.4	233	Coast	492000	0.6618	325588		
Corning Canal	W	390.9					0		
Salt Cr	E	386.4	8	Modoc	194000	0.0071	1369		
Craig Cr	E	385.3	8	Modoc	194000	0.0071	1369		
Local Area	E	383.0	28	Modoc	194000	0.0259	5021		
Antelope Cr. nr Red Bluff	E	377.6	319	Modoc	194000	0.2894	56146		
Dye Cr	E	376.6	140	Modoc	194000	0.1271	24649		
Oat Cr	W	374.8	179	Coast	492000	0.5074	249618		
Elder Cr	W	370.6	352	Coast	492000	1.0000	492000		
Mill Cr.	E	370.0	34	Modoc	194000	0.0313	6071		
Local Area	E	368.5	5	Modoc	194000	0.0047	913		
Champlin Slough	E	366.1	47	Modoc	194000	0.0424	8216		

Station Name	E/W	RK	D.A. (km^2)	Geo Unit	Sig Load (t/y)	D.A. Ratio	Mod Load (t/y)	Upstream	Divergence
McClure Cr	W	364.4	106	Coast	492000	0.3015	148324		
Thomes Cr. nr Richfield	W	362.4	736	Coast	492000	2.0882	1027412		
Toomes Cr	E	358.9	161	Modoc	194000	0.1459	28301		
Local Area	E	356.6	13	Modoc	194000	0.0118	2282		
Local Area	W	356.5	10	Coast	492000	0.0294	14471		
Deer Cr@Vina	E	353.4	544	Modoc	194000	0.4941	95859		
Kopta Slough	W	351.5	70	Coast	492000	0.1985	97676		
Local Area	W	349.2	10	Coast	492000	0.0294	14471		
Local Area	E	348.4	8	Modoc	194000	0.0071	1369		
Jewett Cr	W	346.3	39	Coast	492000	0.1103	54265		
Hoag Slough	W	343.9	16	Coast	492000	0.0441	21706		
Local Area	E	342.8	5	Modoc	194000	0.0047	913		
Local Area	W	341.2	10	Coast	492000	0.0294	14471		
Foster Island Trib	E	337.3	26	Modoc	194000	0.0235	4565		
Burch Cr	W	333.6	412	Coast	492000	1.1691	575206		
Local Area	E	331.5	5	Modoc	194000	0.0047	913		
Glen-Colusa I.D.	W	330.7					-200000		
Wilson Lndg. Trib	W	326.7	28	Coast	492000	0.0809	39794		
Sacramento @ Hamilton Cty.		320.7	28645				**3090000**	**4297489**	**-1207489**
Pine Cr	E	316.2	536	Modoc	194000	0.4871	94489		
Big Chico Cr.	E	310.6	186	Sierra	1813000	0.0903	163722		
Mud Cr	E	310.8	124	Sierra	1813000	0.0602	109148		
Stony Cr	W	305.9	1748	Coast	492000	4.9625	2441574		
Sacramento @ Butte Cty.		271.2	31274				**6650000**	**5898934**	**751066**
Moulton Weir	E	254.8					-128820		
Colusa Weir	E	235.0					-947710		
Sacramento @ Colusa		231.1	31313				**1730000**	**5573470**	**-3843470**
Butte Slough	E	222.4					-128820		
Tisdale Weir	E	191.0					-349932		
Sacramento @ Knights Lndg.		144.2	37645				**1610000**	**1251248**	**358752**
Sutter Bypass	E	133.6					537053		
Fremont Weir	W	132.9					-500765		
Feather R@Nicholaus	E	128.4	2065	Sierra	1813000	1.0000	1813000		
Sacramento Weir	W	98.2					-89000		
Diversion nr. Knights Lndg.	W						-117934		

Station Name	E/W	RK	D.A. (km^2)	Geo Unit	Sig Load (t/y)	D.A. Ratio	Mod Load (t/y	Upstream	Divergence
American R. @ Sac	E	96.9	194	Sierra	1813000	0.0939	170325		
Sacramento @ Sacramento							**4300000**	**3422679**	**877321**

APPENDIX C. ANNUAL GRAVEL BED-MATERIAL BUDGET SPREADSHEET

Annual average gravel bed-material budget spreadsheet used for assessing reaches of valley in net states of erosion and deposition. Mainstem stations are shown in bold and signature tributaries are shown in italics. The spreadsheet shows the following for each tributary and mainstem station:

Column 1: "Station Name", name of gauging station.
Column 2: "E/W", direction from which tributary enters the Sacramento (east or west).
Column 3: "RK", river kilometer counted upstream from the San Francisco Bay.
Column 4: "D.A. (km^2)", station's upstream drainage area below impoundments.
Column 5: "Geo Unit", geologic unit from which tributary rises; used to model sediment load.
Column 6: "Sig Load (t/y)", annual load of the signature station for that geologic unit.
Column 7: "D.A. Ratio", ratio of tributary drainage area to signature tributary drainage area.
Column 8: "Mod Load (t/y)", modeled sediment load.
Column 9: "Upstream", sediment load (t/y) into a reach from upstream sources (at each mainstem gauge).
Column 10: "Divergence", net sediment divergence (t/y) (at each mainstem gauge).
Column 11: "Plus", upper range of estimate (t/y) (from stochastic hydrology).
Column 12: "Minus", lower range of estimate (t/y) (from stochastic hydrology).

Station Name	E/W	RK	D.A. (km^2)	Geo Unit	Sig Load (t/y)	D.A. Ratio	Mod Load (t/y)	Upstream	Divergence	Plus	Minus
Rock Cr	W	485.9	16	Trinity	1000	0.0065	6			6	6
Middle Cr	W	484.4	10	Trinity	1000	0.0043	4			4	4
Salt Cr	W	484.1	8	Trinity	1000	0.0032	3			3	3
Local Area	W	483.6	8	Trinity	1000	0.0032	3			3	3
Local Area	E	483.4	3	Trinity	1000	0.0011	1			1	1
Jenny Cr	W	482.0	5	Trinity	1000	0.0022	2			2	2
Anderson-Cottonwood I.D.	W	479.6					0				
Sulphur Cr	E	478.9	13	Trinity	1000	0.0054	5			5	5
Local Area	E	478.0	13	Modoc	4000	0.0118	47			106	35
Local Area	W	474.0	10	Trinity	1000	0.0043	4			4	4
Canyon Hollow	W	472.5	8	Trinity	1000	0.0032	3			3	3
Oregon Gulch	W	471.7	16	Trinity	1000	0.0065	6			6	6
Local Area	E	468.3	5	Modoc	4000	0.0022	9			19	6
Local Area	W	466.7	10	Trinity	1000	0.0043	4			4	4
Olney Cr	W	465.9	36	Trinity	1000	0.0151	15			15	15
Clear Cr. nr Igo	W	465.6	591	Trinity	1000	0.2460	246			246	246
Local Area	E	462.7	16	Modoc	4000	0.0141	56			127	42
Local Area	W	461.9	3	Trinity	1000	0.0011	1			1	1
Spanish Canyon	W	459.5	28	Trinity	1000	0.0119	12			12	12
Churn Cr	E	458.0	31	Modoc	4000	0.0282	113			254	85
Clover Cr	E	454.8	21	Modoc	4000	0.0188	75			169	56
Stillwater Cr	E	452.2	174	Modoc	4000	0.1576	631			1419	473
Local Area	E	450.9	26	Modoc	4000	0.0235	94			212	71
Cow Cr	***E***	***450.8***	***1101***	***Modoc***	***4000***	***1.0000***	***4000***			***9000***	***3000***
Local Area	W	449.0	3	Trinity	1000	0.0011	1			1	1
Bear Cr	E	446.6	197	Modoc	4000	0.1788	715			1609	536
Ash Cr	E	445.9	83	Modoc	4000	0.0753	301			678	226
Local Area	W	442.7	13	Trinity	1000	0.0054	5			5	5
Buenaventura Cr	W	442.6	5	Trinity	1000	0.0022	2			2	2
Anderson Cr	W	440.6	54	Trinity	1000	0.0227	23			23	23
Local Area	E	440.2	5	Modoc	4000	0.0047	19			42	14
Cottonwood Cr	***W***	***440.0***	***2401***	***Trinity***	***1000***	***1.0000***	***1000***			***1000***	***1000***
Battle Cr	E	436.6	925	Modoc	4000	0.8400	3360			7560	2520
Local Area	E	434.5	10	Modoc	4000	0.0094	38			85	28
Frazier Cr	W	431.0	5	Trinity	1000	0.0022	2			2	2

Station Name	E/W	RK	D.A. (km^2)	Geo Unit	Sig Load (t/y)	D.A. Ratio	Mod Load (t/y)	Upstream	Divergence	Plus	Minus
Local Area	W	430.5	13	Trinity	1000	0.0054	5			5	5
Local Area	E	429.4	3	Modoc	4000	0.0024	9			21	7
Table Mtn. Trib	W	428.2	8	Trinity	1000	0.0032	3			3	3
Onks Cr	E	425.8	70	Modoc	4000	0.0635	254			572	191
Local Area	W	425.0	3	Trinity	1000	0.0011	1			1	1
E Trib No 1	E	424.1	10	Modoc	4000	0.0094	38			85	28
Local Area	E	422.5	5	Modoc	4000	0.0047	19			42	14
Sacramento @ Bend Br.		**418.9**	**23051**				**749000**	**11139**	**737861**	**666000**	**483000**
Local Area	W	416.8	16	Trinity	1000	0.0065	6			6	6
Lookout Mtn Trib	W	416.7	10	Trinity	1000	0.0043	4			4	4
Local Area	E	415.2	5	Modoc	4000	0.0047	19			42	14
Spring Cr	W	414.6	10	Trinity	1000	0.0043	4			4	4
Paynes Cr	E	407.2	241	Modoc	4000	0.2188	875			1969	656
Local Area	E	406.8	16	Modoc	4000	0.0141	56			127	42
Local Area	W	406.5	3	Trinity	1000	0.0011	1			1	1
East Trib No. 2	E	406.0	8	Modoc	4000	0.0071	28			21	7
Local Area	W	404.8	3	Trinity	1000	0.0011	1			1	1
Seven Mile Cr	E	403.6	18	Modoc	4000	0.0165	66			148	49
Blue Tent Cr	W	398.6	44	Trinity	1000	0.0183	18			18	18
Dibble Cr	W	396.9	83	Trinity	1000	0.0345	35			35	35
Local Area	W	395.3	21	Trinity	1000	0.0086	9			9	9
Local Area	E	395.3	8	Modoc	4000	0.0071	28			64	21
Reeds Cr	W	394.0	192	Trinity	1000	0.0798	80			80	80
Local Area	E	392.7	16	Modoc	4000	0.0141	56			127	42
Red Bank Cr. nr Red Bluff	W	391.4	233	Coast	1000	0.3169	317			634	317
Corning Canal	W	390.9					0				
Salt Cr	E	386.4	8	Modoc	4000	0.0071	28			64	21
Craig Cr	E	385.3	8	Modoc	4000	0.0071	28			64	21
Local Area	E	383.0	28	Modoc	4000	0.0259	104			233	78
Antelope Cr. nr Red Bluff	E	377.6	319	Modoc	4000	0.2894	1158			2605	868
Dye Cr	E	376.6	140	Modoc	4000	0.1271	508			1144	381
Oat Cr	W	374.8	179	Coast	1000	0.2430	243			486	243
Elder Cr	W	370.6	352	Coast	1000	2.1935	2194			4387	2194
Mill Cr.	E	370.0	34	Modoc	4000	0.0313	125			282	94
Local Area	E	368.5	5	Modoc	4000	0.0047	19			42	14
Champlin Slough	E	366.1	47	Modoc	4000	0.0424	169			381	127

Station Name	E/W	RK	D.A. (km^2)	Geo Unit	Sig Load (t/y)	D.A. Ratio	Mod Load (t/y)	Upstream	Divergence	Plus	Minus
McClure Cr	W	364.4	106	Coast	1000	0.1444	144			289	144
Thomes Cr. nr Richfield	***W***	***362.4***	***736***	***Coast***	***1000***	***1.0000***	***1000***			***2000***	***1000***
Toomes Cr	E	358.9	161	Modoc	4000	0.1459	584			1313	438
Local Area	E	356.6	13	Modoc	4000	0.0118	47			106	35
Local Area	W	356.5	10	Coast	1000	0.0141	14			28	14
Deer Cr@Vina	E	353.4	544	Modoc	4000	0.4941	1976			4447	1482
Kopta Slough	W	351.5	70	Coast	1000	0.0951	95			190	95
Local Area	W	349.2	10	Coast	1000	0.0141	14			28	14
Local Area	E	348.4	8	Modoc	4000	0.0071	28			64	21
Jewett Cr	W	346.3	39	Coast	1000	0.0528	53			106	53
Hoag Slough	W	343.9	16	Coast	1000	0.0211	21			42	21
Local Area	E	342.8	5	Modoc	4000	0.0047	19			42	14
Local Area	W	341.2	10	Coast	1000	0.0141	14			28	14
Foster Island Trib	E	337.3	26	Modoc	4000	0.0235	94			212	71
Burch Cr	W	333.6	412	Coast	1000	0.5599	560			1120	560
Local Area	E	331.5	5	Modoc	4000	0.0047	19			42	14
Glen-Colusa I.D.	W	330.7					0				
Wilson Lndg. Trib	W	326.7	28	Coast	1000	0.0387	39			77	39
Sacramento @ Hamilton Cty.		**320.7**	**28645**				**208000**	**759902**	**-551902**	**181000**	**192000**
Pine Cr	E	316.2	536	Modoc	4000	0.4871	1948			4384	1461
Big Chico Cr.	E	310.6	186	Sierra	0	0.0903	0			0	0
Mud Cr	E	310.8	124	Sierra	0	0.0602	0			0	0
Stony Cr	W	305.9	1748	Coast	1000	2.3764	2376			4753	2376
Sacramento @ Butte Cty.		**271.2**	**31274**				**740000**	**212325**	**527675**	**576000**	**708000**
Moulton Weir	E	254.8					0				
Colusa Weir	E	235.0					0				
Sacramento @ Colusa		**231.1**	**31313**				**149000**	**740000**	**-591000**	**98000**	**85000**
Butte Slough	E	222.4					0				
Tisdale Weir	E	191.0					0				
Sacramento @ Knights Lndg.		**144.2**	**37645**				**1627000**	**149000**	**1478000**	**1572000**	**1039000**
Sutter Bypass	E	133.6									
Fremont Weir	W	132.9					0				
Feather R@Nicholaus	***E***	***128.4***	***2065***	***Sierra***	***0***	***1.0000***	***0***			***0***	***0***
Sacramento Weir	W	98.2					0				
Diversion nr. Knights Lndg.	W						0				

Station Name	E/W	RK	D.A. (km^2)	Geo Unit	Sig Load (t/y)	D.A. Ratio	Mod Load (t/y)	Upstream	Divergence	Plus	Minus
American R. @ Sac	E	96.9	194	Sierra	0	0.0939	0			0	0
Sacramento @ Sacramento							**0**	**1627000**	**-1627000**	**1000**	**0**

APPENDIX D. ANNUAL SAND BED-MATERIAL BUDGET SPREADSHEET

Annual average sand bed-material budget spreadsheet used for assessing reaches of valley in net states of erosion and deposition. Mainstem stations are shown in bold and signature tributaries are shown in italics. The spreadsheet shows the following for each tributary and mainstem station:

Column 1: "Station Name", name of gauging station.
Column 2: "E/W", direction from which tributary enters the Sacramento (east or west).
Column 3: "RK", river kilometer counted upstream from the San Francisco Bay.
Column 4: "D.A. (km^2)", station's upstream drainage area below impoundments.
Column 5: "Geo Unit", geologic unit from which tributary rises; used to model sediment load.
Column 6: "Sig Load (t/y)", annual load of the signature station for that geologic unit.
Column 7: "D.A. Ratio", ratio of tributary drainage area to signature tributary drainage area.
Column 8: "Mod Load (t/y)", modeled sediment load.
Column 9: "Upstream", sediment load (t/y) into a reach from upstream sources (at each mainstem gauge).
Column 10: "Divergence", net sediment divergence (t/y) (at each mainstem gauge).
Column 11: "Plus", upper range of estimate (t/y) (from stochastic hydrology).
Column 12: "Minus", lower range of estimate (t/y) (from stochastic hydrology).

Station Name	E/W	RK	D.A. (km^2)	Geo Unit	Sig Load (t/y)	D.A. Ratio	Mod Load (t/y)	Upstream	Divergence	Plus	Minus
Rock Cr	W	485.9	16	Trinity	1000	0.0065	6			6	6
Middle Cr	W	484.4	10	Trinity	1000	0.0043	4			4	4
Salt Cr	W	484.1	8	Trinity	1000	0.0032	3			3	3
Local Area	W	483.6	8	Trinity	1000	0.0032	3			3	3
Local Area	E	483.4	3	Trinity	1000	0.0011	1			1	1
Jenny Cr	W	482.0	5	Trinity	1000	0.0022	2			2	2
Anderson-Cottonwood I.D.	W	479.6					0				
Sulphur Cr	E	478.9	13	Trinity	1000	0.0054	5			5	5
Local Area	E	478.0	13	Modoc	3000	0.0118	35			118	24
Local Area	W	474.0	10	Trinity	1000	0.0043	4			4	4
Canyon Hollow	W	472.5	8	Trinity	1000	0.0032	3			3	3
Oregon Gulch	W	471.7	16	Trinity	1000	0.0065	6			6	6
Local Area	E	468.3	5	Modoc	3000	0.0022	6			22	4
Local Area	W	466.7	10	Trinity	1000	0.0043	4			4	4
Olney Cr	W	465.9	36	Trinity	1000	0.0151	15			15	15
Clear Cr. nr Igo	W	465.6	591	Trinity	1000	0.2460	246			246	246
Local Area	E	462.7	16	Modoc	3000	0.0141	42			141	28
Local Area	W	461.9	3	Trinity	1000	0.0011	1			1	1
Spanish Canyon	W	459.5	28	Trinity	1000	0.0119	12			12	12
Churn Cr	E	458.0	31	Modoc	3000	0.0282	85			282	56
Clover Cr	E	454.8	21	Modoc	3000	0.0188	56			188	38
Stillwater Cr	E	452.2	174	Modoc	3000	0.1576	473			1576	315
Local Area	E	450.9	26	Modoc	3000	0.0235	71			235	47
Cow Cr	***E***	***450.8***	***1101***	***Modoc***	***3000***	***1.0000***	***3000***			***10000***	***2000***
Local Area	W	449.0	3	Trinity	1000	0.0011	1			1	1
Bear Cr	E	446.6	197	Modoc	3000	0.1788	536			1788	358
Ash Cr	E	445.9	83	Modoc	3000	0.0753	226			753	151
Local Area	W	442.7	13	Trinity	1000	0.0054	5			5	5
Buenaventura Cr	W	442.6	5	Trinity	1000	0.0022	2			2	2
Anderson Cr	W	440.6	54	Trinity	1000	0.0227	23			23	23
Local Area	E	440.2	5	Modoc	3000	0.0047	14			47	9
Cottonwood Cr	***W***	***440.0***	***2401***	***Trinity***	***1000***	***1.0000***	***1000***			***1000***	***1000***
Battle Cr	E	436.6	925	Modoc	3000	0.8400	2520			8400	1680
Local Area	E	434.5	10	Modoc	3000	0.0094	28			94	19
Frazier Cr	W	431.0	5	Trinity	1000	0.0022	2			2	2

Station Name	E/W	RK	D.A. (km^2)	Geo Unit	Sig Load (t/y)	D.A. Ratio	Mod Load (t/y)	Upstream	Divergence	Plus	Minus
Local Area	W	430.5	13	Trinity	1000	0.0054	5			5	5
Local Area	E	429.4	3	Modoc	3000	0.0024	7			24	5
Table Mtn. Trib	W	428.2	8	Trinity	1000	0.0032	3			3	3
Onks Cr	E	425.8	70	Modoc	3000	0.0635	191			635	127
Local Area	W	425.0	3	Trinity	1000	0.0011	1			1	1
E Trib No 1	E	424.1	10	Modoc	3000	0.0094	28			94	19
Local Area	E	422.5	5	Modoc	3000	0.0047	14			47	9
Sacramento @ Bend Br.		**418.9**	**23051**				**469000**	**8695**	**460305**	**417000**	**302000**
Local Area	W	416.8	16	Trinity	1000	0.0065	6			6	6
Lookout Mtn Trib	W	416.7	10	Trinity	1000	0.0043	4			4	4
Local Area	E	415.2	5	Modoc	3000	0.0047	14			47	9
Spring Cr	W	414.6	10	Trinity	1000	0.0043	4			4	4
Paynes Cr	E	407.2	241	Modoc	3000	0.2188	656			2188	438
Local Area	E	406.8	16	Modoc	3000	0.0141	42			141	28
Local Area	W	406.5	3	Trinity	1000	0.0011	1			1	1
East Trib No. 2	E	406.0	8	Modoc	3000	0.0071	21			71	14
Local Area	W	404.8	3	Trinity	1000	0.0011	1			1	1
Seven Mile Cr	E	403.6	18	Modoc	3000	0.0165	49			165	33
Blue Tent Cr	W	398.6	44	Trinity	1000	0.0183	18			18	18
Dibble Cr	W	396.9	83	Trinity	1000	0.0345	35			35	35
Local Area	W	395.3	21	Trinity	1000	0.0086	9			9	9
Local Area	E	395.3	8	Modoc	3000	0.0071	21			71	14
Reeds Cr	W	394.0	192	Trinity	1000	0.0798	80			80	80
Local Area	E	392.7	16	Modoc	3000	0.0141	42			141	28
Red Bank Cr. nr Red Bluff	W	391.4	233	Coast	1000	0.3169	317			317	317
Corning Canal	W	390.9					0				
Salt Cr	E	386.4	8	Modoc	3000	0.0071	21			71	14
Craig Cr	E	385.3	8	Modoc	3000	0.0071	21			71	14
Local Area	E	383.0	28	Modoc	3000	0.0259	78			259	52
Antelope Cr. nr Red Bluff	E	377.6	319	Modoc	3000	0.2894	868			2894	579
Dye Cr	E	376.6	140	Modoc	3000	0.1271	381			1271	254
Oat Cr	W	374.8	179	Coast	1000	0.2430	243			243	243
Elder Cr	W	370.6	352	Coast	1000	2.1935	2194			2194	2194
Mill Cr.	E	370.0	34	Modoc	3000	0.0313	94			313	63
Local Area	E	368.5	5	Modoc	3000	0.0047	14			47	9
Champlin Slough	E	366.1	47	Modoc	3000	0.0424	127			424	85

Station Name	E/W	RK	D.A. (km^2)	Geo Unit	Sig Load (t/y)	D.A. Ratio	Mod Load (t/y)	Upstream	Divergence	Plus	Minus
McClure Cr	W	364.4	106	Coast	1000	0.1444	144			144	144
Thomes Cr. nr Richfield	***W***	***362.4***	***736***	***Coast***	***1000***	***1.0000***	***1000***			***1000***	***1000***
Toomes Cr	E	358.9	161	Modoc	3000	0.1459	438			1459	292
Local Area	E	356.6	13	Modoc	3000	0.0118	35			118	24
Local Area	W	356.5	10	Coast	1000	0.0141	14			14	14
Deer Cr@Vina	E	353.4	544	Modoc	3000	0.4941	1482			4941	988
Kopta Slough	W	351.5	70	Coast	1000	0.0951	95			95	95
Local Area	W	349.2	10	Coast	1000	0.0141	14			14	14
Local Area	E	348.4	8	Modoc	3000	0.0071	21			71	14
Jewett Cr	W	346.3	39	Coast	1000	0.0528	53			53	53
Hoag Slough	W	343.9	16	Coast	1000	0.0211	21			21	21
Local Area	E	342.8	5	Modoc	3000	0.0047	14			47	9
Local Area	W	341.2	10	Coast	1000	0.0141	14			14	14
Foster Island Trib	E	337.3	26	Modoc	3000	0.0235	71			235	47
Burch Cr	W	333.6	412	Coast	1000	0.5599	560			560	560
Local Area	E	331.5	5	Modoc	3000	0.0047	14			47	9
Glen-Colusa I.D.	W	330.7					0				
Wilson Lndg. Trib	W	326.7	28	Coast	1000	0.0387	39			39	39
Sacramento @ Hamilton Cty.		**320.7**	**28645**				**206000**	**478393**	**-272393**	**179000**	**190000**
Pine Cr	E	316.2	536	Modoc	3000	0.4871	1461			4871	974
Big Chico Cr.	E	310.6	186	Sierra	12000	0.0903	1084			1896	813
Mud Cr	E	310.8	124	Sierra	12000	0.0602	722			1264	542
Stony Cr	W	305.9	1748	Coast	1000	2.3764	2376			2376	2376
Sacramento @ Butte Cty.		**271.2**	**31274**				**1724000**	**211644**	**1512356**	**1341000**	**1650000**
Moulton Weir	E	254.8					0				
Colusa Weir	E	235.0					0				
Sacramento @ Colusa		**231.1**	**31313**				**222000**	**1724000**	**-1502000**	**147000**	**126000**
Butte Slough	E	222.4					0				
Tisdale Weir	E	191.0					0				
Sacramento @ Knights Lndg.		**144.2**	**37645**				**9515000**	**222000**	**9293000**	**9191000**	**6078000**
Sutter Bypass	E	133.6									
Fremont Weir	W	132.9					0				
Feather R@Nicholaus	***E***	***128.4***	***2065***	***Sierra***	***12000***	***1.0000***	***12000***			***21000***	***9000***
Sacramento Weir	W	98.2					0				
Diversion nr. Knights Lndg.	W						0				

Station Name	E/W	RK	D.A. (km^2)	Geo Unit	Sig Load (t/y)	D.A. Ratio	Mod Load (t/y)	Upstream	Divergence	Plus	Minus
American R. @ Sac	E	96.9	194	Sierra	12000	0.0939	1127			1973	846
Sacramento @ Sacramento							**5000**	**9528127**	**-9523127**	**220000**	**4000**

APPENDIX E. ONE-DAY PEAK GRAVEL BED-MATERIAL BUDGET SPREADSHEET

Peak gravel bed-material budget spreadsheet used for assessing reaches of valley in net states of erosion and deposition. Mainstem stations are shown in bold and signature tributaries are shown in italics. The spreadsheet shows the following for each tributary and mainstem station:

Column 1: "Station Name", name of gauging station.
Column 2: "E/W", direction from which tributary enters the Sacramento (east or west).
Column 3: "RK", river kilometer counted upstream from the San Francisco Bay.
Column 4: "D.A. (km^2)", station's upstream drainage area below impoundments.
Column 5: "Geo Unit", geologic unit from which tributary rises; used to model sediment load.
Column 6: "Sig Load (t/d)", daily peak load of the signature station for that geologic unit.
Column 7: "D.A. Ratio", ratio of tributary drainage area to signature tributary drainage area.
Column 8: "Mod Load (t/d)", modeled sediment load.
Column 9: "Upstream", sediment load (t/d) into a reach from upstream sources (at each mainstem gauge).
Column 10: "Divergence", net sediment divergence (t/d) (at each mainstem gauge).
Column 11: "Plus", upper range of estimate (t/y) (from stochastic hydrology).
Column 12: "Minus", lower range of estimate (t/y) (from stochastic hydrology).

Station Name	E/W	RK	D.A. (km^2)	Geo Unit	Sig Load (t/d)	D.A. Ratio	Mod Load (t/d)	Upstream	Divergence	Plus	Minus
Rock Cr	W	485.9	16	Trinity	1000	0.0065	6			0	6
Middle Cr	W	484.4	10	Trinity	1000	0.0043	4			0	4
Salt Cr	W	484.1	8	Trinity	1000	0.0032	3			0	3
Local Area	W	483.6	8	Trinity	1000	0.0032	3			0	3
Local Area	E	483.4	3	Trinity	1000	0.0011	1			0	1
Jenny Cr	W	482.0	5	Trinity	1000	0.0022	2			0	2
Anderson-Cottonwood I.D.	W	479.6					0				
Sulphur Cr	E	478.9	13	Trinity	1000	0.0054	5			0	5
Local Area	E	478.0	13	Modoc	1000	0.0118	12			35	12
Local Area	W	474.0	10	Trinity	1000	0.0043	4			0	4
Canyon Hollow	W	472.5	8	Trinity	1000	0.0032	3			0	3
Oregon Gulch	W	471.7	16	Trinity	1000	0.0065	6			0	6
Local Area	E	468.3	5	Modoc	1000	0.0022	2			6	2
Local Area	W	466.7	10	Trinity	1000	0.0043	4			0	4
Olney Cr	W	465.9	36	Trinity	1000	0.0151	15			0	15
Clear Cr. nr Igo	W	465.6	591	Trinity	1000	0.2460	246			0	246
Local Area	E	462.7	16	Modoc	1000	0.0141	14			42	14
Local Area	W	461.9	3	Trinity	1000	0.0011	1			0	1
Spanish Canyon	W	459.5	28	Trinity	1000	0.0119	12			0	12
Churn Cr	E	458.0	31	Modoc	1000	0.0282	28			85	28
Clover Cr	E	454.8	21	Modoc	1000	0.0188	19			56	19
Stillwater Cr	E	452.2	174	Modoc	1000	0.1576	158			473	158
Local Area	E	450.9	26	Modoc	1000	0.0235	24			71	24
Cow Cr	***E***	***450.8***	***1101***	***Modoc***	***1000***	***1.0000***	***1000***			***3000***	***1000***
Local Area	W	449.0	3	Trinity	1000	0.0011	1			0	1
Bear Cr	E	446.6	197	Modoc	1000	0.1788	179			536	179
Ash Cr	E	445.9	83	Modoc	1000	0.0753	75			226	75
Local Area	W	442.7	13	Trinity	1000	0.0054	5			0	5
Buenaventura Cr	W	442.6	5	Trinity	1000	0.0022	2			0	2
Anderson Cr	W	440.6	54	Trinity	1000	0.0227	23			0	23
Local Area	E	440.2	5	Modoc	1000	0.0047	5			14	5
Cottonwood Cr	***W***	***440.0***	***2401***	***Trinity***	***1000***	***1.0000***	***1000***			***0***	***1000***
Battle Cr	E	436.6	925	Modoc	1000	0.8400	840			2520	15960
Local Area	E	434.5	10	Modoc	1000	0.0094	9			28	179
Frazier Cr	W	431.0	5	Trinity	1000	0.0022	2			0	2

Station Name	E/W	RK	D.A. (km^2)	Geo Unit	Sig Load (t/d)	D.A. Ratio	Mod Load (t/d)	Upstream	Divergence	Plus	Minus
Local Area	W	430.5	13	Trinity	1000	0.0054	5			0	5
Local Area	E	429.4	3	Modoc	1000	0.0024	2			7	2
Table Mtn. Trib	W	428.2	8	Trinity	1000	0.0032	3			0	3
Onks Cr	E	425.8	70	Modoc	1000	0.0635	64			191	64
Local Area	W	425.0	3	Trinity	1000	0.0011	1			0	1
E Trib No 1	E	424.1	10	Modoc	1000	0.0094	9			28	9
Local Area	E	422.5	5	Modoc	1000	0.0047	5			14	5
Sacramento @ Bend Br.		**418.9**	**23051**				**21000**	**3806**	**17194**	**7000**	**10000**
Local Area	W	416.8	16	Trinity	1000	0.0065	6			0	6
Lookout Mtn Trib	W	416.7	10	Trinity	1000	0.0043	4			0	4
Local Area	E	415.2	5	Modoc	1000	0.0047	5			14	5
Spring Cr	W	414.6	10	Trinity	1000	0.0043	4			0	4
Paynes Cr	E	407.2	241	Modoc	1000	0.2188	219			656	219
Local Area	E	406.8	16	Modoc	1000	0.0141	14			42	14
Local Area	W	406.5	3	Trinity	1000	0.0011	1			0	1
East Trib No. 2	E	406.0	8	Modoc	1000	0.0071	7			21	7
Local Area	W	404.8	3	Trinity	1000	0.0011	1			0	1
Seven Mile Cr	E	403.6	18	Modoc	1000	0.0165	16			49	16
Blue Tent Cr	W	398.6	44	Trinity	1000	0.0183	18			0	18
Dibble Cr	W	396.9	83	Trinity	1000	0.0345	35			0	35
Local Area	W	395.3	21	Trinity	1000	0.0086	9			0	9
Local Area	E	395.3	8	Modoc	1000	0.0071	7			21	7
Reeds Cr	W	394.0	192	Trinity	1000	0.0798	80			0	80
Local Area	E	392.7	16	Modoc	1000	0.0141	14			42	14
Red Bank Cr. nr Red Bluff	W	391.4	233	Coast	1000	0.3169	317			0	317
Corning Canal	W	390.9					0				
Salt Cr	E	386.4	8	Modoc	1000	0.0071	7			21	7
Craig Cr	E	385.3	8	Modoc	1000	0.0071	7			21	7
Local Area	E	383.0	28	Modoc	1000	0.0259	26			78	26
Antelope Cr. nr Red Bluff	E	377.6	319	Modoc	1000	0.2894	289			868	289
Dye Cr	E	376.6	140	Modoc	1000	0.1271	127			381	127
Oat Cr	W	374.8	179	Coast	1000	0.2430	243			0	243
Elder Cr	W	370.6	352	Coast	1000	2.1935	2194			0	2194
Mill Cr.	E	370.0	34	Modoc	1000	0.0313	31			94	31
Local Area	E	368.5	5	Modoc	1000	0.0047	5			14	5
Champlin Slough	E	366.1	47	Modoc	1000	0.0424	42			127	42

Station Name	E/W	RK	D.A. (km^2)	Geo Unit	Sig Load (t/d)	D.A. Ratio	Mod Load (t/d)	Upstream	Divergence	Plus	Minus
McClure Cr	W	364.4	106	Coast	1000	0.1444	144			0	144
Thomes Cr. nr Richfield	***W***	***362.4***	***736***	***Coast***	***1000***	***1.0000***	***1000***			***0***	***1000***
Toomes Cr	E	358.9	161	Modoc	1000	0.1459	146			438	146
Local Area	E	356.6	13	Modoc	1000	0.0118	12			35	12
Local Area	W	356.5	10	Coast	1000	0.0141	14			0	14
Deer Cr@Vina	E	353.4	544	Modoc	1000	0.4941	494			0	494
Kopta Slough	W	351.5	70	Coast	1000	0.0951	95			0	95
Local Area	W	349.2	10	Coast	1000	0.0141	14			0	14
Local Area	E	348.4	8	Modoc	1000	0.0071	7			21	7
Jewett Cr	W	346.3	39	Coast	1000	0.0528	53			0	53
Hoag Slough	W	343.9	16	Coast	1000	0.0211	21			0	21
Local Area	E	342.8	5	Modoc	1000	0.0047	5			14	5
Local Area	W	341.2	10	Coast	1000	0.0141	14			0	14
Foster Island Trib	E	337.3	26	Modoc	1000	0.0235	24			71	24
Burch Cr	W	333.6	412	Coast	1000	0.5599	560			0	560
Local Area	E	331.5	5	Modoc	1000	0.0047	5			14	5
Glen-Colusa I.D.	W	330.7					0				
Wilson Lndg. Trib	W	326.7	28	Coast	1000	0.0387	39			0	39
Sacramento @ Hamilton Cty.		**320.7**	**28645**				**6000**	**27375**	**-21375**	**10000**	**4000**
Pine Cr	E	316.2	536	Modoc	1000	0.4871	487			1461	487
Big Chico Cr.	E	310.6	186	Sierra	0	0.0903	0			0	0
Mud Cr	E	310.8	124	Sierra	0	0.0602	0			0	0
Stony Cr	W	305.9	1748	Coast	1000	2.3764	2376			0	2376
Sacramento @ Butte Cty.		**271.2**	**31274**				**11000**	**8863**	**2137**	**2000**	**3000**
Moulton Weir	E	254.8					0				
Colusa Weir	E	235.0					0				
Sacramento @ Colusa		**231.1**	**31313**				**6000**	**11000**	**-5000**	**4000**	**4000**
Butte Slough	E	222.4					0				
Tisdale Weir	E	191.0					0				
Sacramento @ Knights Lndg.		**144.2**	**37645**				**53000**	**6000**	**47000**	**7000**	**21000**
Sutter Bypass	E	133.6									
Fremont Weir	W	132.9					0				
Feather R@Nicholaus	***E***	***128.4***	***2065***	***Sierra***	***0***	***1.0000***	***0***			***0***	***0***
Sacramento Weir	W	98.2					0				
Diversion nr. Knights Lndg.	W						0				

Station Name	E/W	RK	D.A. (km^2)	Geo Unit	Sig Load (t/d)	D.A. Ratio	Mod Load (t/d)	Upstream	Divergence	Plus	Minus
American R. @ Sac	E	96.9	194	Sierra	0	0.0939	0			0	0
Sacramento @ Sacramento							**0**	**53000**	**-53000**	**0**	**0**

APPENDIX F. ONE-DAY PEAK SAND BED-MATERIAL BUDGET SPREADSHEET

Peak sand bed-material budget spreadsheet used for assessing reaches of valley in net states of erosion and deposition. Mainstem stations are shown in bold and signature tributaries are shown in italics. The spreadsheet shows the following for each tributary and mainstem station:

Column 1: "Station Name", name of gauging station.
Column 2: "E/W", direction from which tributary enters the Sacramento (east or west).
Column 3: "RK", river kilometer counted upstream from the San Francisco Bay.
Column 4: "D.A. (km^2)", station's upstream drainage area below impoundments.
Column 5: "Geo Unit", geologic unit from which tributary rises; used to model sediment load.
Column 6: "Sig Load (t/d)", daily peak load of the signature station for that geologic unit.
Column 7: "D.A. Ratio", ratio of tributary drainage area to signature tributary drainage area.
Column 8: "Mod Load (t/d)", modeled sediment load.
Column 9: "Upstream", sediment load (t/d) into a reach from upstream sources (at each mainstem gauge).
Column 10: "Divergence", net sediment divergence (t/d) (at each mainstem gauge).
Column 11: "Plus", upper range of estimate (t/y) (from stochastic hydrology).
Column 12: "Minus", lower range of estimate (t/y) (from stochastic hydrology).

Station Name	E/W	RK	D.A. (km^2)	Geo Unit	Sig Load (t/d)	D.A. Ratio	Mod Load (t/d)	Upstream	Divergence	Plus	Minus
Rock Cr	W	485.9	16	Trinity	1000	0.0065	6			0	6
Middle Cr	W	484.4	10	Trinity	1000	0.0043	4			0	4
Salt Cr	W	484.1	8	Trinity	1000	0.0032	3			0	3
Local Area	W	483.6	8	Trinity	1000	0.0032	3			0	3
Local Area	E	483.4	3	Trinity	1000	0.0011	1			0	1
Jenny Cr	W	482.0	5	Trinity	1000	0.0022	2			0	2
Anderson-Cottonwood I.D.	W	479.6					0				
Sulphur Cr	E	478.9	13	Trinity	1000	0.0054	5			0	5
Local Area	E	478.0	13	Modoc	1000	0.0118	12			35	12
Local Area	W	474.0	10	Trinity	1000	0.0043	4			0	4
Canyon Hollow	W	472.5	8	Trinity	1000	0.0032	3			0	3
Oregon Gulch	W	471.7	16	Trinity	1000	0.0065	6			0	6
Local Area	E	468.3	5	Modoc	1000	0.0022	2			6	2
Local Area	W	466.7	10	Trinity	1000	0.0043	4			0	4
Olney Cr	W	465.9	36	Trinity	1000	0.0151	15			0	15
Clear Cr. nr Igo	W	465.6	591	Trinity	1000	0.2460	246			0	246
Local Area	E	462.7	16	Modoc	1000	0.0141	14			42	14
Local Area	W	461.9	3	Trinity	1000	0.0011	1			0	1
Spanish Canyon	W	459.5	28	Trinity	1000	0.0119	12			0	12
Churn Cr	E	458.0	31	Modoc	1000	0.0282	28			85	28
Clover Cr	E	454.8	21	Modoc	1000	0.0188	19			56	19
Stillwater Cr	E	452.2	174	Modoc	1000	0.1576	158			473	158
Local Area	E	450.9	26	Modoc	1000	0.0235	24			71	24
Cow Cr	***E***	***450.8***	***1101***	***Modoc***	***1000***	***1.0000***	***1000***			***3000***	***1000***
Local Area	W	449.0	3	Trinity	1000	0.0011	1			0	1
Bear Cr	E	446.6	197	Modoc	1000	0.1788	179			536	179
Ash Cr	E	445.9	83	Modoc	1000	0.0753	75			226	75
Local Area	W	442.7	13	Trinity	1000	0.0054	5			0	5
Buenaventura Cr	W	442.6	5	Trinity	1000	0.0022	2			0	2
Anderson Cr	W	440.6	54	Trinity	1000	0.0227	23			0	23
Local Area	E	440.2	5	Modoc	1000	0.0047	5			14	5
Cottonwood Cr	***W***	***440.0***	***2401***	***Trinity***	***1000***	***1.0000***	***1000***			***0***	***1000***
Battle Cr	E	436.6	925	Modoc	1000	0.8400	840			2520	840
Local Area	E	434.5	10	Modoc	1000	0.0094	9			28	9
Frazier Cr	W	431.0	5	Trinity	1000	0.0022	2			0	2

Station Name	E/W	RK	D.A. (km^2)	Geo Unit	Sig Load (t/d)	D.A. Ratio	Mod Load (t/d)	Upstream	Divergence	Plus	Minus
Local Area	W	430.5	13	Trinity	1000	0.0054	5			0	5
Local Area	E	429.4	3	Modoc	1000	0.0024	2			7	2
Table Mtn. Trib	W	428.2	8	Trinity	1000	0.0032	3			0	3
Onks Cr	E	425.8	70	Modoc	1000	0.0635	64			191	64
Local Area	W	425.0	3	Trinity	1000	0.0011	1			0	1
E Trib No 1	E	424.1	10	Modoc	1000	0.0094	9			28	9
Local Area	E	422.5	5	Modoc	1000	0.0047	5			14	5
Sacramento @ Bend Br.		**418.9**	**23051**				**13000**	**3806**	**9194**	**5000**	**6000**
Local Area	W	416.8	16	Trinity	1000	0.0065	6			0	6
Lookout Mtn Trib	W	416.7	10	Trinity	1000	0.0043	4			0	4
Local Area	E	415.2	5	Modoc	1000	0.0047	5			14	5
Spring Cr	W	414.6	10	Trinity	1000	0.0043	4			0	4
Paynes Cr	E	407.2	241	Modoc	1000	0.2188	219			656	219
Local Area	E	406.8	16	Modoc	1000	0.0141	14			42	14
Local Area	W	406.5	3	Trinity	1000	0.0011	1			0	1
East Trib No. 2	E	406.0	8	Modoc	1000	0.0071	7			21	7
Local Area	W	404.8	3	Trinity	1000	0.0011	1			0	1
Seven Mile Cr	E	403.6	18	Modoc	1000	0.0165	16			49	16
Blue Tent Cr	W	398.6	44	Trinity	1000	0.0183	18			0	18
Dibble Cr	W	396.9	83	Trinity	1000	0.0345	35			0	35
Local Area	W	395.3	21	Trinity	1000	0.0086	9			0	9
Local Area	E	395.3	8	Modoc	1000	0.0071	7			21	7
Reeds Cr	W	394.0	192	Trinity	1000	0.0798	80			0	80
Local Area	E	392.7	16	Modoc	1000	0.0141	14			42	14
Red Bank Cr. nr Red Bluff	W	391.4	233	Coast	1000	0.3169	317			0	317
Corning Canal	W	390.9					0				
Salt Cr	E	386.4	8	Modoc	1000	0.0071	7			21	7
Craig Cr	E	385.3	8	Modoc	1000	0.0071	7			21	7
Local Area	E	383.0	28	Modoc	1000	0.0259	26			78	26
Antelope Cr. nr Red Bluff	E	377.6	319	Modoc	1000	0.2894	289			868	289
Dye Cr	E	376.6	140	Modoc	1000	0.1271	127			381	127
Oat Cr	W	374.8	179	Coast	1000	0.2430	243			0	243
Elder Cr	W	370.6	352	Coast	1000	2.1935	2194			0	2194
Mill Cr.	E	370.0	34	Modoc	1000	0.0313	31			94	31
Local Area	E	368.5	5	Modoc	1000	0.0047	5			14	5
Champlin Slough	E	366.1	47	Modoc	1000	0.0424	42			127	42

Station Name	E/W	RK	D.A. (km^2)	Geo Unit	Sig Load (t/d)	D.A. Ratio	Mod Load (t/d)	Upstream	Divergence	Plus	Minus
McClure Cr	W	364.4	106	Coast	1000	0.1444	144			0	144
Thomes Cr. nr Richfield	***W***	***362.4***	***736***	***Coast***	***1000***	***1.0000***	***1000***			***0***	***1000***
Toomes Cr	E	358.9	161	Modoc	1000	0.1459	146			438	146
Local Area	E	356.6	13	Modoc	1000	0.0118	12			35	12
Local Area	W	356.5	10	Coast	1000	0.0141	14			0	14
Deer Cr@Vina	E	353.4	544	Modoc	1000	0.4941	494			1482	494
Kopta Slough	W	351.5	70	Coast	1000	0.0951	95			0	95
Local Area	W	349.2	10	Coast	1000	0.0141	14			0	14
Local Area	E	348.4	8	Modoc	1000	0.0071	7			21	7
Jewett Cr	W	346.3	39	Coast	1000	0.0528	53			0	53
Hoag Slough	W	343.9	16	Coast	1000	0.0211	21			0	21
Local Area	E	342.8	5	Modoc	1000	0.0047	5			14	5
Local Area	W	341.2	10	Coast	1000	0.0141	14			0	14
Foster Island Trib	E	337.3	26	Modoc	1000	0.0235	24			71	24
Burch Cr	W	333.6	412	Coast	1000	0.5599	560			0	560
Local Area	E	331.5	5	Modoc	1000	0.0047	5			14	5
Glen-Colusa I.D.	W	330.7					0				
Wilson Lndg. Trib	W	326.7	28	Coast	1000	0.0387	39			0	39
Sacramento @ Hamilton Cty.		**320.7**	**28645**				**6000**	**19375**	**-13375**	**10000**	**4000**
Pine Cr	E	316.2	536	Modoc	1000	0.4871	487			1461	487
Big Chico Cr.	E	310.6	186	Sierra	1000	0.0903	90			0	90
Mud Cr	E	310.8	124	Sierra	1000	0.0602	60			0	60
Stony Cr	W	305.9	1748	Coast	1000	2.3764	2376			0	2376
Sacramento @ Butte Cty.		**271.2**	**31274**				**26000**	**9014**	**16986**	**4000**	**7000**
Moulton Weir	E	254.8					0				
Colusa Weir	E	235.0					0				
Sacramento @ Colusa		**231.1**	**31313**				**9000**	**26000**	**-17000**	**5000**	**6000**
Butte Slough	E	222.4					0				
Tisdale Weir	E	191.0					0				
Sacramento @ Knights Lndg.		**144.2**	**37645**				**312000**	**9000**	**303000**	**45000**	**125000**
Sutter Bypass	E	133.6									
Fremont Weir	W	132.9					0				
Feather R@Nicholaus	***E***	***128.4***	***2065***	***Sierra***	***1000***	***1.0000***	***1000***			***0***	***1000***
Sacramento Weir	W	98.2					0				
Diversion nr. Knights Lndg.	W						0				

Station Name	E/W	RK	D.A. (km^2)	Geo Unit	Sig Load (t/d)	D.A. Ratio	Mod Load (t/d)	Upstream	Divergence	Plus	Minus
American R. @ Sac	E	96.9	194	Sierra	1000	0.0939	94			0	94
Sacramento @ Sacramento							**1000**	**313094**	**-312094**	**5000**	**0**